The role of the endocannabinoid receptor CB2 in a mouse model of Alzheimer's disease

Dissertation

zur

Erlangung des Doktorgrades (Dr. rer. nat.)

der

Mathematisch-Naturwissenschaftlichen Fakultät

der

Rheinischen Friedrich-Wilhelms Universität Bonn

vorgelegt von

Ramona Lundt, geb. Göhrs

Bonn

März 2018

Angefertigt mit Genehmigung der Mathematisch-Naturwissenschaftlichen Fakultät der Rheinischen Friedrich-Wilhelms-Universität Bonn

1. Gutachter: Professor Dr. rer. nat. Andreas Zimmer
2. Gutachter: Professor Dr. rer. nat. Waldemar Kolanus

Tag der mündlichen Prüfung: 11.07.2018

Erscheinungsjahr: 2018

Disclosure statement:

I hereby declare that I prepared this thesis entitled: "The role of the endocannabinoid receptor CB2 in a mouse model of Alzheimer's disease" entirely by myself except where otherwise stated. All text passages that are literally or correspondingly taken from published or unpublished papers are indicated as such. All materials or services provided by other people are equally indicated.

Parts of this thesis are published as follows:

AC Schmöle, R Lundt, S Ternes, Ö Albayram, T Ulas, JL Schultze, D Bano, P Nicotera, J Alferink, A Zimmer. Cannabinoid receptor 2 deficiency results in reduced neuroinflammation in an Alzheimer's disease mouse model. *Neurobiol Aging*, Feb;36(2):710-9, 2015

AC Schmöle, R Lundt, G Toporowski, JN Hansen, E Beins, A Halle, A Zimmer. Cannabinoid Receptor 2-Deficiency Ameliorates Disease Symptoms in a Mouse Model with Alzheimer's Disease-Like Pathology. *J Alzheimers Dis*, 64(2):379-392, 2018

Bonn, March, 1st 2018

Ramona Lundt

Abbrevations

2-AG	2-Arachidonoylglycerol
AA	Amino acid
ABHD	Aβ-hydrolase
AD	Alzheimer's disease
ADAM	A disintegrin and metalloproteinase
AEA	*N*-arachidonoylethanolamine, anandamide
AGER	Advanced glycation end products receptor
AICD	APP intracellular domain
AMPA	α-amino-3-hydroxy-5-methyl-4-isoxazolepropionic acid
ANOVA	Analysis of variance
APC	Allophycocyanin
APH	Anterior pharynx-defective
APOE	Apolipoprotein E
APP	Amyloid precursor protein
ARA	Arachidonic acid
Arg1	Arginase 1
ATP	Adenosine triphosphate
Aβ	Amyloid-β
BACE1	β-site APP cleaving enzyme 1
BBB	Blood brain barrier
BCA	Bicinchoninic acid
BCP	1-bromo-3-chloropropane
BMdM	Bone marrow-derived macrophages
BSA	Bovine serum albumin
CA	Cornu Ammonis
CB	Cannabinoid receptor [protein]
CD	Cluster of differentiation
cDNA	Complementary deoxyribonucleic acid
cnr	Cannabinoid receptor [gene]
CNS	Central nervous system
CP	Crossing point

Cy3	Cyanine 3
DAG	Diacylglycerol
DAGL	Diacylglycerol lipase
DAPI	4',6-Diamino-2-phenylindole
DC	Dendritic cell
DG	Dentate gyrus
DMEM	Dulbeccos's modified eagle medium
DNA	Deoxyribonucleic acid
DS	Down syndrome
DSE	Depolarisation induced suppression of excitation
DSI	Depolarisation induced suppression of inhibition
EAE	Experimental autoimmune encephalitis
EC	Endothelial cells
ECS	Endocannabinoid system
EDTA	Ethylenediaminetetraacetate
ELISA	Enzyme-linked immunosorbent assay
FAAH	Fatty acid amide hydrolase
FACS	Fluorescence activated cell sorter
FAD	Familial Alzheimer's disease
FCS	Foetal calf serum
FIZZ1	Found in inflammatory zone 1
FRET	Fluorescence resonance energy transfer
GABA	γ-aminobutyric acid
GAPDH	Glyceraldehyde 3-phosphate dehydrogenase
gMFI	Geometric mean fluorescence intensity
GPCR	G-protein-coupled receptor
h	Hour
hAPP	Humanised amyloid precursor protein
HBSS	Hank's buffered salt solution
HSC	Haematopoietic stem cell
Iba1	Ionized calcium-binding adapter molecule 1
ICAM	Intercellular adhesion molecule
ICL	Intracerebral leukocytes

IDE	Insulin degrading enzyme
IFN	Interferon
IL	Interleukin
iNOS	Inducible nitric oxide synthase
JNK	Jun amino-terminal kinases
JWH	John William Huffman
LPS	Lipopolysaccharide
MAGL	Monoacylglycerol lipase
MARCO	Macrophage receptor with collagenous structure
M-CSF	Macrophage colony-stimulating factor
MEM	Minimum essential medium
MFI	Mean fluorescence intensity
mM	Millimolar (millimol/l)
mGlu	Metabotropic glutamate receptors
MMP9	Matrix metalloproteinase-9
MMR	Macrophage mannose receptor
MWM	Morris water maze
NAGly	N-Arachidonyl glycine
NAPE	N-acylphosphatidylethanolamine
NAPE-PLD	N-acylphosphatidylethanolamine phospholipase D
NEP	Neprilysin
NeuN	Neuronal nuclei
NFT	Neurofibrillary tangles
NMDA	N-methyl-D-aspartate
NSAID	Non-steroidal anti-inflammatory drug
Parv	Parvalbumin
PBS	Phosphate buffered saline
PCR	Polymerase chain reaction
PDGF-β	platelet derived growth factor-β chain
PE	Phycoerythrin
PEA	N-Palmitoylethanolamide
PerCP-Cy5.5	Peridinin-chlorophyll-cyanine 5.5
PET	Positron-emission tomography

PFA	Paraformaldehyde
PGK	Phosphoglycerate kinase
PLC	Phospholipase C
PrP	Prion protein
PS1, PSEN1	Presenilin-1
PVM	Perivascular macrophage
qRT-PCR	quantitative real-time PCR
RAGE	Receptor for advanced glycation end products
RIPA	Radioimmunoprecipitation assay
RNA	Ribonucleic acid
RPM	Rounds per minute
RPMI	Roswell Park Memorial Institute
RT	Room temperature
SAPK	Stress-activated protein kinases
aAPP	Soluble APP
SDS	Sodium dodecyl sulfate
SEM	Standard error of the mean
TAE	TRIS acetate EDTA
TE	TRIS EDTA
tg	Transgenic
TGF	Transforming growth factor
Th	T-helper
THC	Tetrahydrocannabinol
TLR4	Toll-like receptor 4
TMB	3,3',5,5'-Tetramethylbenzidine
TNF	Tumor necrosis factor
TREM2	triggering receptor expressed on myeloid cells 2
TRIS	Tris(hydroxymethyl)aminomethane
TRPV-1	transient receptor potential vanilloid type-1
WT	Wildtype

Summary

Over the past years, an important role of the cannabinoid receptor 2 (CB2) has been implicated in several neurological and immunological conditions, such as experimental autoimmune encephalitis, stroke, memory, neuropathic pain or Alzheimer's disease (AD).

In AD transgenic mouse models, AD-associated neuroinflammatory processes were shown to decrease by the pharmacological stimulation with agonists of the endocannabinoid system (ECS), while age- and AD-associated cognitive deficits were diminished. However, the exact mechanism by which CB2 might be involved in these processes still remains elusive.

Therefore, the current study was designed to analyse the effects of CB2 signalling on the one hand in microglia polarisation using *in vitro* cell-culture models. On the other hand, neuroinflammatory and neurodegenerative processes as well as changes in cognitive performances were evaluated in the AD transgenic mouse model APPswe/PS1dE9 (APP/PS1) and in mice lacking functional CB2 receptor expression ($CB2^{-/-}$).

We demonstrate here that neonatal microglia derived from $CB2^{-/-}$ mice were less responsive to pro-inflammatory stimuli when compared to microglia derived from wildtype mice. These findings were based on the cell surface marker expression of the intercellular adhesion molecule 1 (ICAM) and cluster of differentiation (CD) 40 as well as the release of the cytokines interleukin (IL) -6 and tumor necrosis factor (TNF) -α and the chemokine CCL2. Furthermore, we found a reduced amyloid-β (Aβ) plaque load in hippocampal and cortical regions, a reduced microgliosis, diminished markers of neuroinflammation as well as a decreased neurodegeneration in aged APP/PS1$*CB2^{-/-}$ mice when compared to samples of age-matched APP/PS1 mice. Finally, we could demonstrate that spatial learning and memory deficits were rescued in aged APP/PS1$*CB2^{-/-}$ mice.

These data suggest that microglia polarisation is alternatively altered in the absence of CB2 signalling and positively influenced AD-associated neuroinflammation in the present mouse model.

Contents

1 Introduction

1.1 Alzheimer's Disease

Among chronic neurodegenerative diseases, Alzheimer's disease (AD) is one of the most prevailing neurological diseases in western countries, affecting up to 70% of the more than 35 million people suffering from dementia [63, 204]. So far, no preventive treatment is available, thus an increasing prevalence of AD is expected due to demographic changes, affecting approximately 115 million people by the year 2015 [204]. In 1907, the German psychiatrist Alois Alzheimer first described unique structures in the cerebral cortex in a case study publication of a 55-year-old woman with progressive dementia [251]. In his article ("Über eine eigenartige Erkrankung der Hirnrinde") he delineated disorientation, memory impairments as well as problems in reading, spelling and speaking of his patient Auguste Deter. He related these deficits with post-mortem diagnosed changes of neurofibrils, which he identified using Bielschowsky's silver method. Additionally, he described "miliary foci", which were later referred to as amyloid-β (Aβ) plaques, in an evenly atrophic brain. Today, the pre-clinical phase of AD possesses deficits in learning and short-term memory. With progression of the disease, patients unlearn well-known skills and are more and more unable to recognize friends and family members as well as trivial objects. Furthermore, behavioural problems, such as hallucination and agitation up to loss of body functions are described. These behavioural changes are accompanied by shrinkage of the cerebral cortex, entorhinal cortex and the hippocampus from moderate to extreme, while ventricles enlarge with progressing disease (Fig. 1.1, A). Up to now, AD is mainly characterised by two histopathological hallmarks: deposition of extracellular Aβ plaques (Fig. 1.1, B) and intracellular neurofibrillary tangles (NFT; Fig. 1.1, C). Production of Aβ is a result of proteolytic cleavage of the amyloid precursor protein (APP).

NFT are composed of hyperphosphorylated microtubule-associated binding protein tau (τ) [145]. In healthy neurons, τ is an essential component of microtubules, which acts as an internal support structure providing axonal transport for nutrients, vesicles and mitochondria. In AD, τ proteins are hyperphosphorylated and form tangled treads, which leads to a dysregulated axonal transport [81, 32]. These pathological hallmarks are further accompanied by increasing loss of synapses and neurons, firstly affecting in the entorhinal cortex, followed by neuronal loss in the hippocampus, amygdala and neocortical areas [82].

1.1.1 APP processing

Although the physiological function of APP in the adult brain is poorly understood, extensive research on this complex molecule and its numerous cleavage products revealed an important function of in central nervous system (CNS) development and cell differentiation [149].
In the healthy brain, the cleavage pathway of the type I transmembrane protein APP is referred

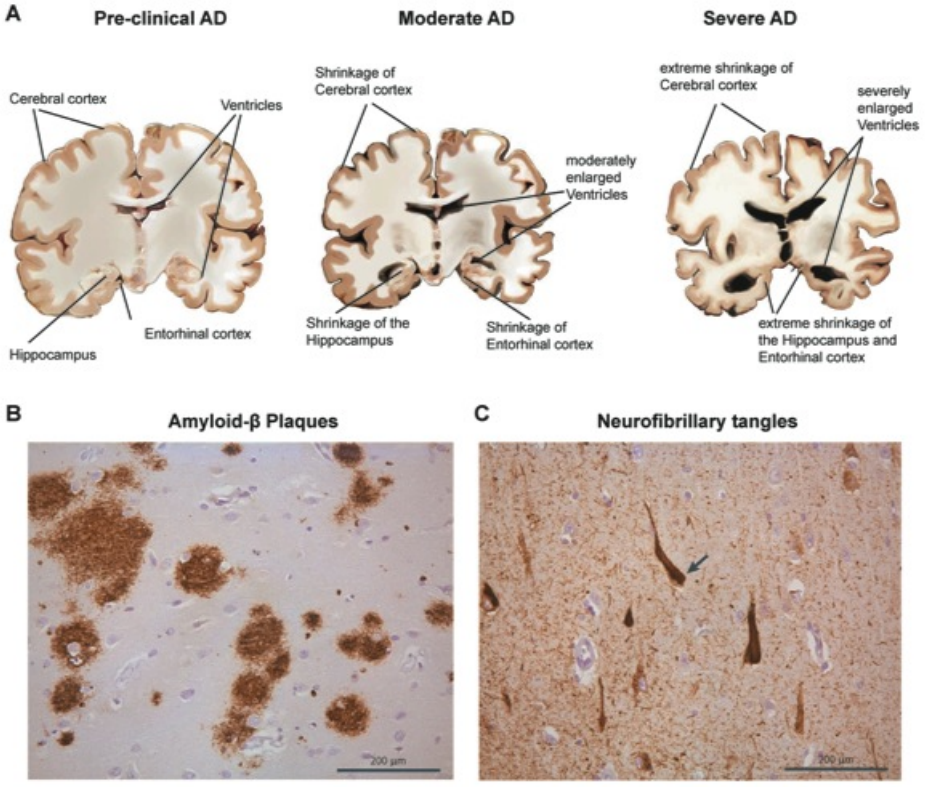

Figure 1.1: Histopathological hallmarks of Alzheimer's disease A) Representative illustrations of atrophic brain regions in AD. With disease progression, shrinkage of the hippocampus, cerebral cortex and entorhinal cortex and enlargement of ventricles are described. Histopathological hallmarks are amyloid-β plaques (B) and neurofibrillary tangles (NFT). Image A adapted from [219], images B and C adapted from [3].
AD = Alzheimer's disease

to as the non-amyloidogenic pathway (Fig. 1.2). Thereby, APP is initially cleaved by an extracellular α-secretase (a disintegrin and metalloproteinase domain-containing protein, short ADAM), ADAM10 or ADAM17, liberating the extracellular soluble APP (sAPP) fragment sAPPα. This APP cleavage product shows neurotrophic properties, identified by enhanced survival of cells and neurite outgrowth in cortical and hippocampal neurons [9, 191]. Furthermore, neurotrophic as well as regulatory functions of sAPPα regarding cell excitability and synaptic plasticity were demonstrated (reviewed by [263]). In a second step, the remaining APP fragment is cut within the transmembrane region by the so-called γ-secretase, liberating the APP intracellular domain (AICD) and a small residual peptide. The γ-secretase is composed of at least four different proteins: presenilin 1 or 2 (PSEN1 or PSEN2), nicastrin, anterior pharynx-defective (APH) 1 and presenilin-enhancer 2. In mammalian cells, two homologues of APH-1, APH-1a and APH-1b, were identified [86, 66]. Furthermore, APH-1a exists in two different splice forms, APH-1aS and APH-1aL, resulting in at least six different possible γ-secretase complexes [245].

In brains of AD patients, APP is primarily cleaved by an aspartyl protease, known as the β-

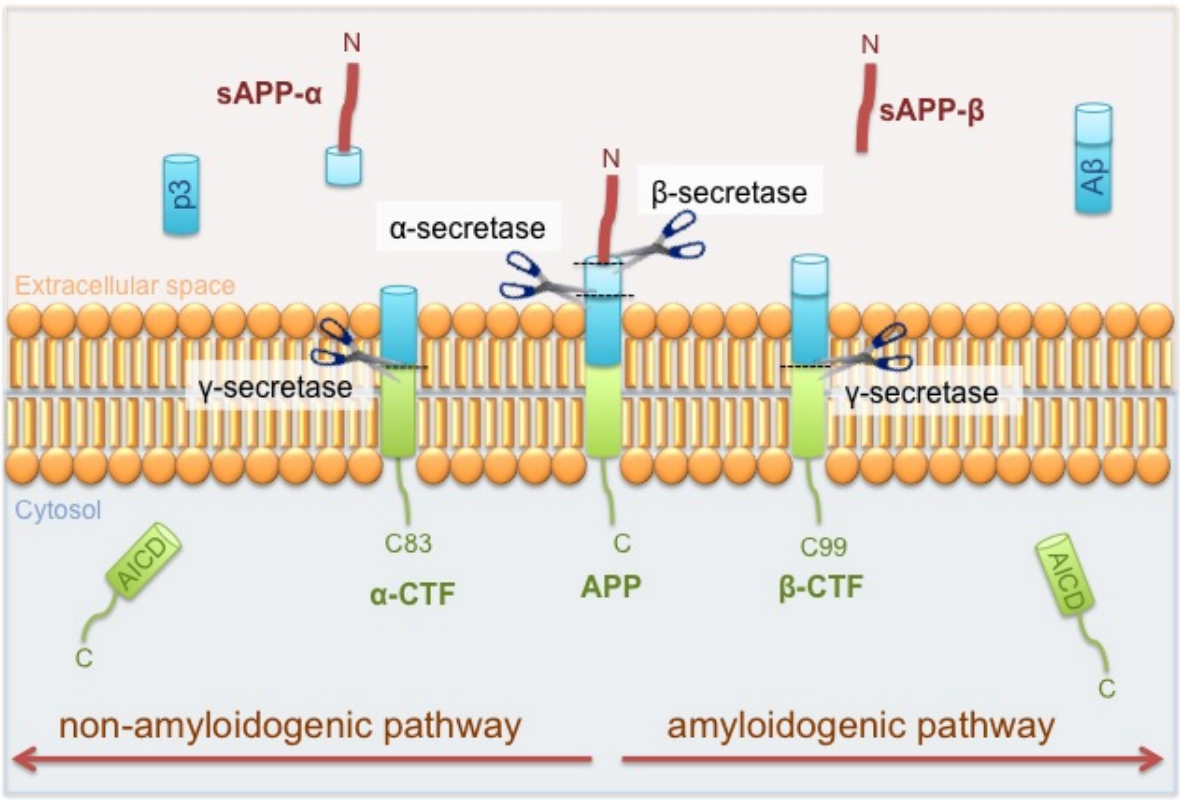

Figure 1.2: Cleavage pathways of the amyloid precursor protein. In the non-amyloidognic pathway, APP is initially cleaved by an α-secretase, followed by cleavage through the integral membrane γ-secretase. This results in the release of cytoplasmic soluble sAPPα and the small p3 peptide as well as the release of AICD. The role of sAPPα In patients with AD, the amyloidogenic pathway takes place. Thereby, APP is sequentially cut by β-secretase followed by γ-secretase cleavage, resulting in the release of toxic Aβ peptides. Image adapted from [16].
AICD = APP intracellular domain; APP = amyloid precursor protein; CTF = c-terminal fragment; Aβ = amyloid-β; P3 = P3 peptide.

secretase (beta-site amyloid precursor protein cleaving enzyme 1 [BACE1]), followed by cleavage through the γ-secretase. The small fragment, 40 to 42 amino acids (AA), remaining between the β- and γ-cleavage site, is known as the Aβ peptide. These small fragments are able to aggregate extracellularly, forming oligomers and ultimately cluster to macroscopic plaques (Fig 1.2). Additionally to Aβ, sAPPβ is released from the cell membrane. sAPPβ shares the same AA sequence as sAPPα, apart from the last 16 carboxy-terminal AA. However, neuroprotective effects of sAPPβ against excitotoxicity or glucose deprivation were 50- to 100-fold less potent than effects observed after treatment with sAPPα [69].

1.1.2 Forms of AD: early onset, late onset and familiar AD

The main risk factor for the development of AD is ageing. Far more than 90% of all patients are diagnosed after the age of 65. This form of AD is generally termed as sporadic or idiopathic AD. Earlier disease onset is usually associated with dominant genetic mutations and referred to as familiar AD (FAD). Only rare cases of early onset AD are not associated with genetic predispositions. Gene mutations of at least three proteins were shown to be causative of FAD: PSEN1, PSEN2 and

APP (for review see [24]).

Mutations in the *Psen1* gene on chromosome 14 are the most common cause of early onset FAD; affecting 362 families and a disease onset between 35 and 50 years [243]. However, at least two of the identified 166 pathogenic mutations in the *Psen1* gene have been associated with late onset FAD. Patients are clinically characterised by early onset memory impairment and rapid global cognitive decline. Mutations in *Psen2* gene on chromosome 1 are causative for only a small group of families (18 affected families) [220, 142]. Disease onset lies between the age 45 to 88 and patients show similarities with patients affected with sporadic late-onset AD. Mutations of the *App* gene on chromosome 21 account for about 78 families worldwide. Here, the disease onset lies between 40 and 65 years and patients develop an aggressive form of dementia [80].

In recent years, over a dozen genes have been found to increase the lifetime risk for developing sporadic AD by using genome-wide association studies [23, 24]. The most important polymorphism was found in the gene encoding for apolipoprotein E (APOE) [46]. In the brain, ApoE is mainly expressed by astrocytes and microglia and functions in lipoprotein metabolism [124]. The human apoe gene is polymorphic, containing several single nucleotide polymorphism (SNPs)[186]. One of the most common SNPs is resulting in the APOε4 isoform and was discovered as the strongest genetic risk factor for AD [46]. Individuals with one ε4 allele show a 2-3 fold increased risk for AD, while in individuals with two ε4 alleles the risk is about 12-fold increased as compared to individuals with no ε4 alleles [225]. Furthermore, an earlier onset of AD is also associated with expression of the APOε4 allele [225].

1.2 Cause of AD

1.2.1 The amyloid cascade hypothesis

Up to know, the main cause of AD remains still unknown and the general view on disease progression based on the "Amyloid cascade hypothesis" [238, 93] is controversially discussed. This hypothesis states Aβ as the causative agent for both familiar and sporadic AD. Hence, NFT, neuronal loss, vascular damage and dementia are seen as a direct result of plaque deposition. The amyloid hypothesis was further supported by findings of FAD mutations, all of which affect properties or production of Aβ [91, 187]. Additionally, virtually all patients suffering from Down syndrome (DS), a heterogeneous disorder caused by the presence of an extra copy of human chromosome 21 (trisomie 21), also develop AD neuropathology [280]. However, not all DS patients also develop dementia [134]. The "Amyloid cascade hypothesis" could be confirmed by two tests: firstly, adding Aβ to healthy individuals should result in the development of AD. Secondly, removing Aβ from patients suffering from AD should ameliorate disease progression. Studies using life imaging with positron-emission tomography (PET) ligands clearly showed the existence of a group of individuals

carrying substantial amyloid burdens in their brains, however without being cognitively impaired [4]. Therefore, we can be sure, that the existence of amyloid plaques is not sufficient to cause AD [100].

Several studies have linked AD progression to a number of different cellular imbalances: malfunction in autophagy [190], lysosomal malfunction [189], imbalance in calcium homoeostasis [25, 49], loss of mitochondria function [256, 255, 287] or oxidative damage of deoxyribonucleic acid (DNA) [135, 292]. In summary, the cause of AD has not clearly been identified and could therefore result from a number of different physiological malfunctions, environmental and genetic conditions.

1.2.2 Neuroinflammatory processes in Alzeimer's disease

Emerging evidence suggests that chronic inflammation plays a pivotal role in disease pathogenesis [44, 98, 278, 289]. The initial connection of AD and inflammation was established in arthritis patients, which were chronically medicated with non-steroidal anti-inflammatory drugs (NSAIDs). In these patients, the risk for developing AD was approximately 50% reduced [166, 221]. Nowadays, a neuroinflammatory component of AD is well established and an increasing number of classic immune molecules are associated with AD, especially in and around AD-defining Aβ plaques and NFT (Table 1.1).

Table 1.1: List of inflammatory molecules associated with AD

Inflammatory mediators	**Function**	**Reference**
Complement components	Aβ can bind and activate the classical complement cytolytic pathway in vitro	[222]
Interleukin-1	IL-1 is upregulated in brains of AD patients	[89, 177, 242, 241]
Interleukin-6	IL-6 exerts dichotomic functions in the CNS	[17, 151, 249]
Macrophage colony-stimulating factor (M-CSF)	M-CSF expression is increased in the CNS, cerebrospinal fluid and in plasma levels of AD patients. M-CSF activates microglia and triggers chomotaxis, proliferation and phagocytosis.	[55, 138]
Transforming growth factor (TGF)	Might be involved in plaque formation	[265, 256]
Reactive oxygen species	Produced by microglia, enhances Aβ neurotoxicity	[8, 212, 234, 199]
Reactive nitrogen species	Might contribute to lipid oxidation in AD brains	[277, 10]

1.3 Microglia: Cellular mediators of neuroinflammation

A characteristic histological sign of chronic CNS inflammation is gliosis, characterised as an increased number of astrocytes and microglia, the brain resident immune cells [7, 99]. Reactive glia

cells have been found in close vicinity to plaques and tangles in AD [239] and are known to produce multiple inflammatory mediators. The following section will discuss the origin of microglia, which was the matter of debate for a long time, different activation profiles of microglia and the role of resident microglia and invading macrophages in AD.

1.3.1 Origin of Microglia

Microglia cells, initially discovered by Cajal and his student Rio-Hortega, represent the brains' resident innate immune cells. In the healthy brain, microglia account for 5-20% of the total glia population [200] and continuously control the brain parenchyma to protect and support neuronal functions [188, 262].

Origin of murine microglia was a long and controversial debate . For a long time it was assumed that bone-marrow derived monocytes enter the CNS via blood circulation and subsequently differentiate into tissue-macrophage. However, this view has changed dramatically due to recent fate-mapping studies. Nowadays, there is growing evidence of two independent waves of erythro-myeloid progenitors, which give rise to microglia and macrophages [104]. The so-called primitive haematopoiesis gives rise to microglia, which arise from erythromyeloid precursors in extra-embryonic yolk sac blood islands in early embryonic development (E7.5-E8.0) [121]. After establishment of the blood circulating system, these progenitors migrate into various tissues, including the brain, where they differentiate into primitive macrophages as early as embryonic day 9.5 [78, 79] (Fig 1.3).

A second wave of haematopoietic progenitors arises within the haemogenic endothelium of the embryo proper, starting in the aorta-gonad-mesonephros region. The definite haematopoiesis gives rise to immature and mature haematopoietic stem cells (HSC), seeding the foetal liver at around E12.5. Via the blood stream, foetal liver monocytes subsequently spread to all tissues and differentiate into tissue macrophages. This is true for all tissues except for the brain, which is isolated by the blood brain barrier (BBB). Establishment of the BBB occurs approximately E13.5. During neuroinflammatory, neurodegenerative and neurooncological diseases non-parenchymal macrophages, such as perivascular, choroid plexus and meningeal macrophages, also play a pivotal role as critical effectors and regulators of immune responses at CNS borders. Therefore, their origin was also critically discussed in recent years and is nowadays believed to arise from HSC, as reviewed by by Prinz and Priller [208].

Previously established primitive macrophages are consequently replaced by these fetal monocyte-derived macrophages. In certain tissues, such as the liver, replacing macrophages maintain their self-renewal capacity throughout adulthood [105]. Differences in primitive and definite haematopoiesis were further confirmed by findings showing that the latter is dependent on the expression of c-Myb, a transcription factor required for the expansion and differentiation of haematopoietic cell lineages

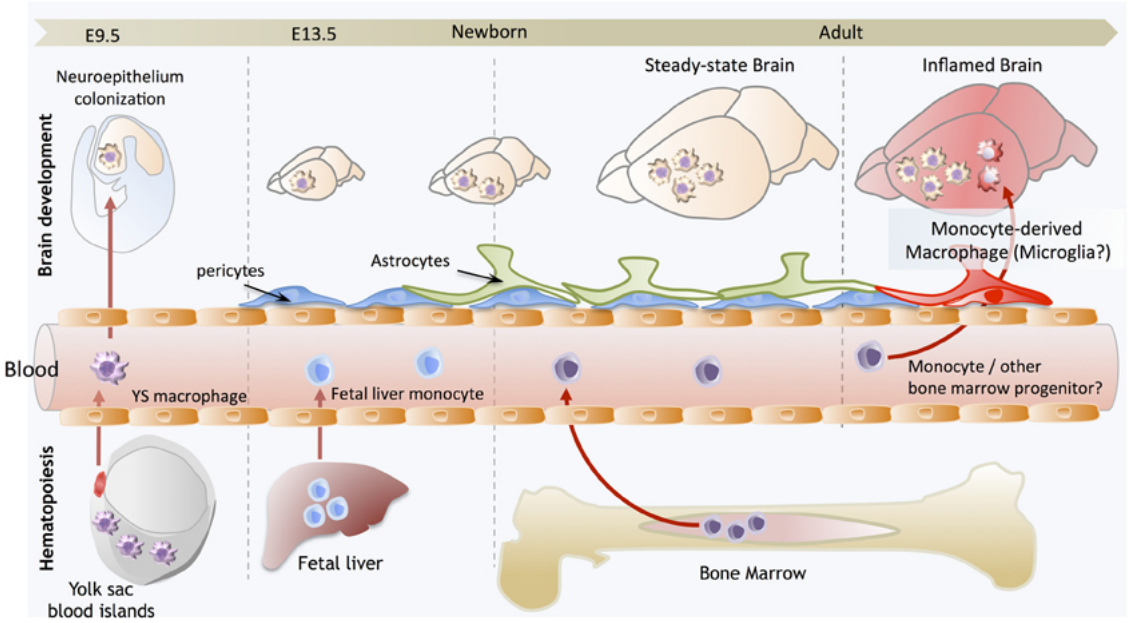

Figure 1.3: Microglia arise from yolk sac progenitors. Primitive macrophages, which arise from yolk sac blood islands, enter the brain neuroepithelium at the onset of blood circulation from E9.5 and give rise to microglia. Development of the BBB starts from E13.5 and thus permit entry of foetal liver macrophages. After birth, embryonic microglia expand and colonize the whole CNS until adulthood. In the steady-state brain, microglia maintain themselves via proliferation. However, upon inflammatory conditions and a disruption of BBB, resident microglia can be supplemented with recruited monocytes or bone-marrow derived precursors. Figure adapted from [79].
BBB = blood brain barrier; CNS = central nervous system

[216]. In contrast, microglia arise from a Myb-independent [237, 85] but Pu.1- and interferon regulatory factor 8 (Irf8) dependent pathway [121]. Thus, microglia and monocyte-derived macrophages represent two ontogenetically distinct populations and fulfil different functions [209].

1.3.2 Microglia polarisation

Under homoeostatic conditions, microglia are the first line of defence against invading pathogens or apoptotic cells. Therefore, they constantly screen the brain parenchyma with their motile processes for pathological alterations [188]. In the healthy brain, activation of microglia is tightly regulated by various neuronal signalling molecules, the so-called "on and off signals" [26]. Under physiological conditions, neurons constitutively release "off signals", e.g. cluster of differentiation (CD) 200 or CX3CL1 (also known as fractalkine), to dampen microglia activation (Fig 1.4). Disappearance of "off signals" in turn directly causes *per se* a microglial response [266]. "On signals" on the other hand are produced on demand to initiate a defined microglia polarisation to an either more anti- or pro-inflammatory state [266]. Potential "On signals" released by endangered neurons are e.g. the chemokines CCL21 [217, 47] and CXCL10 [129], which induce microglia migration *in vitro*. Damaged neurons also release purines, e.g. adenosine triphosphate (ATP), which can bind to specific microglial $P2Y_{12}R$ or $P2Y_6$ receptors and induce various types of activation [131].

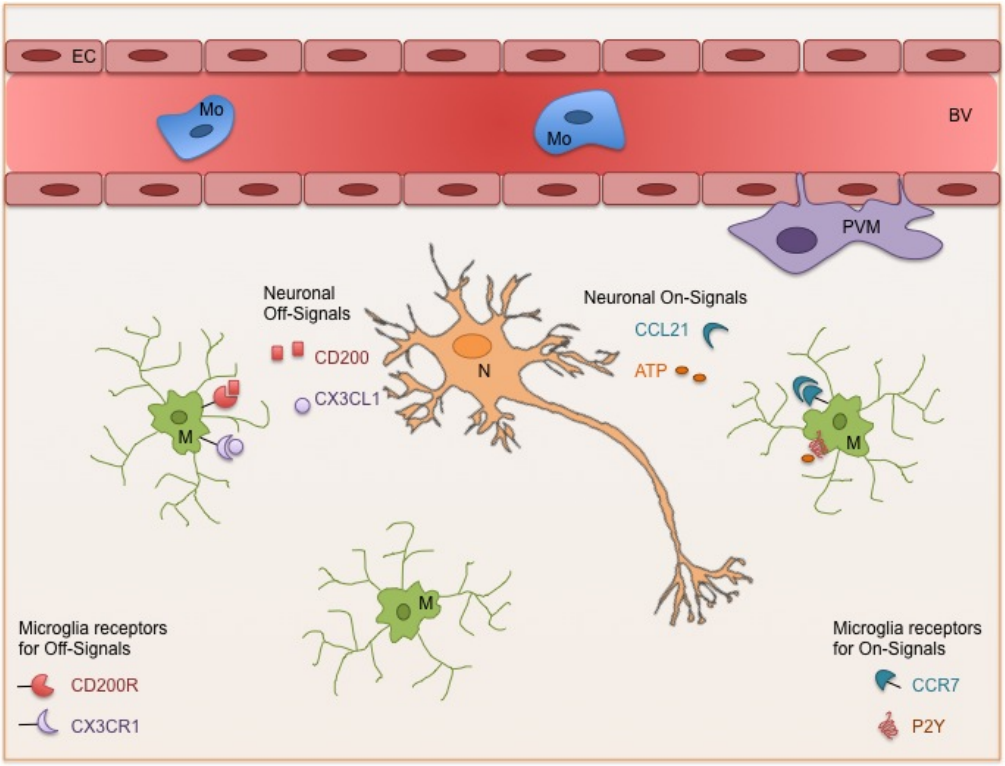

Figure 1.4: Innate immunity profile in the healthy brain. The healthy brain is protected by an intact BBB, formed by firmly connected endothelial cells (EC). This restricts entry on pathogens or toxins from the circulating blood vessel (BV) to the brain parenchyma. Neurons (N) tightly regulate microglial (M) functions by the release of various "on and off signals". Widely studied "off-signals" CD200 and CX3CL1 (fractalkine) bind to microglial receptors, CD200R and CX3CR1 (fractalkine receptor), respectively, and dampen microglial activation. In contrast "on-Signals" trigger a specific microglia activation profile, e.g. CCL21 binding to its specific receptor CCR7 and ATP binding to microglial P2Y receptors. Figure adapted from [258].
ATP = adenosine triphosphate; BBB = blood brain barrier; BV = blood vessel; CD = cluster of differentiation; EC = endothelial cells; M = microglia; Mo = monocyte, N = neuron; PVM = perivascular macrophage

Complementary to macrophages in the periphery, microglia can polarize into various activation states upon detection of different signals [43]. This allows a rapid migration to sites of lesion and inflammation [120]. The ability of peripheral macrophages to polarize into different activation states has been studied intensively in the last decades [155, 160, 122, 37, 246, 185, 53]. Mirroring the Th1/Th2 nomenclature of T-helper cells (Th-cells), at least two different activation states in macrophages have been recognised already in the early 1990s [250] and various terminologies were used since then: the pro-inflammatory or anti-inflammatory [250], M1 or M2 polarisation [175], followed by a subdivision of different M2 polarisation states into M2a, M2b and M2c [29].

Th1 cytokines, such as interferon (IFN) -γ or the bacterial lipopolysaccharide (LPS) are able to polarize macrophages into the pro-inflammatory M1 phenotype. These activated macrophages release pro-inflammatory cytokines, such as interleukin- (IL) 12, IL23, and tumor necrosis factor- (TNF) α as well as the chemokines CXCL9 and CXCL10 to recruit Th1 cells. Furthermore, they show an increased capacity of antigen presentation and are able to generate reactive oxygen and nitrogen species though the activation of inducible nitric oxide synthase (iNOS) [101]. In com-

parison, the Th2 cytokine IL-4 induces M2 polarisation. IL-4 stimulated macrophages secret anti-inflammatory cytokines, such as IL-10, and show an increased phagocytic activity. Additionally, tissue remodelling and repair is supported by M2 macrophages through an upregulation of arginase 1 (Arg1) expression [101].

However, M1 and M2 polarisations are just the extremes of a continuum of functional states, assessed by transcriptome-based network analysis [283]. Therefore, a new terminology of macrophage activation was recommended, which adopts a nomenclature linked to the stimulation condition, i.e., M(IL-4), M(IL-10), M(IFN-γ), M(LPS), and so on [182].

Similar to polarisation in macrophages, divergent microglia activation states have been described [172, 6] and polarisation of microglia with divergent stimuli was the focus of several research groups in the past years. In accordance with macrophages, murine microglial M1 and M2 phenotypes are clearly distinguishable by the expression of a specific pattern of cell surface markers and cytokines [160]. The pro-inflammatory activation state M1 is mostly correlated with an increased expression of CD16/32 (Fc receptor), CD86, IL-1β, IL-6, IL-12, IL-23, TNFα, iNOS, and CCL5. In contrast, alternatively activated microglia show enhanced expression of Arg1, macrophage mannose receptor (MMR or CD206), insulin-like growth factor 1, triggering receptor expressed on myeloid cells 2 (TREM2), chitinase 3-like 3 (also known as YM-1), resistin-like-α (also known as 'found in inflammatory zone 1' [FIZZ1]) and IL-10 [141, 195]. MMR is a transmembrane glycoprotein that specifically binds to mannosylated molecules, which are expressed on the surface of several pathogens, such as bacteria, fungi, parasites and viruses [61, 67]. By endocytosis of divergent pathogens, MMR serves as an important factor in homoeostasis and immune responses.

Hence, microglia can exert divergent functions, varying from beneficial and neuroprotective to neurotoxic properties. In the past, these activation states have been correlated with microglial morphology. So-called resting microglia were correlated with a highly ramified morphology with small cell bodies. In response to pathogenic stimuli, ramified microglia retract their processes and acquire a morphology, which was referred to as "activated microglia" displaying an amoeboid shape with a larger cell body. Additionally, "activated" microglia were shown to express harmful substances. This led to the assumption that amoeboid shaped or "activated" microglia are detrimental and mostly neurotoxic, whereas ramified microglia remain in a resting state monitoring the brain parenchyma. However, this concept of "microglial activation" has changed lately, as recent publications clearly demonstrated that highly ramified microglia in the healthy brain are active as well [272, 2, 92, 96, 95].

1.3.3 Resident Microglia and peripheral monocytes in AD

In the healthy brain, microglia can be easily identified using specific antibodies against the ionized calcium binding protein 1 (Iba1) or CD11b. However, under pathological conditions, in which the

BBB integrity is disrupted [19], circulating monocytes can enter the CNS and differentiate into bone marrow-derived macrophages (BMdM) [174] (Fig. 1.5).

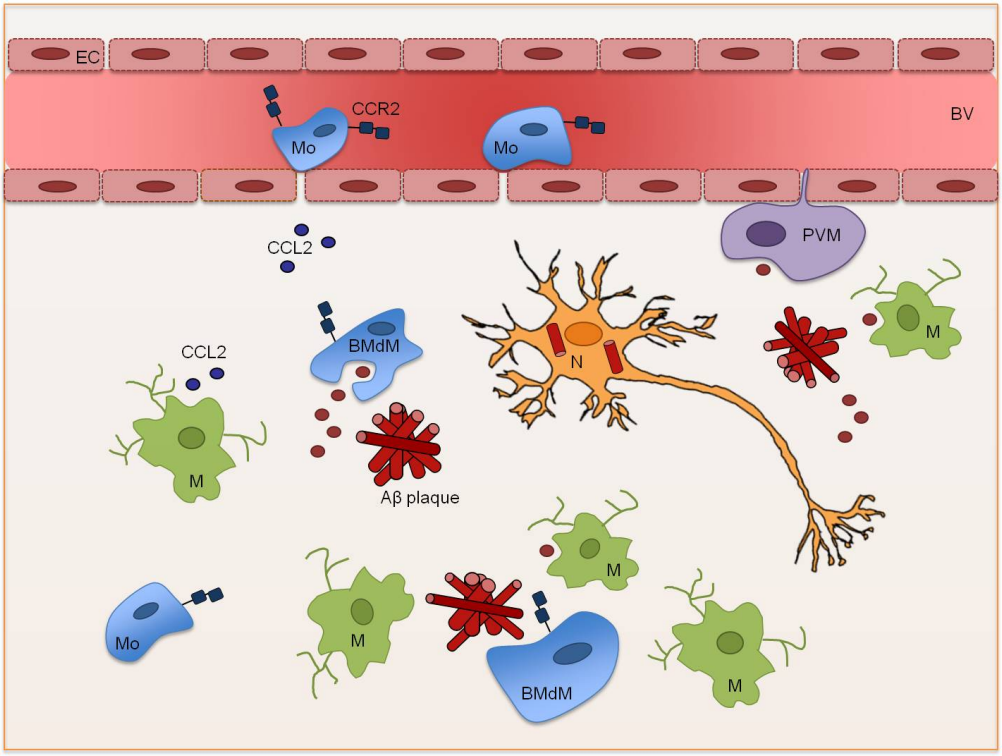

Figure 1.5: Innate immunity in Alzheimer's diseased brain. Under pathological conditions, integrity of the BBB is compromised due to deregulation of endothelial cell (EC) tight junctions. Amyloid depositions (Aβ plaques) induce activation of resident microglia (M), which in turn release pro-inflammatory cytokines and chemokines, including monocyte-chemoattractant protein CCL2 (or MCP-1). This triggers the entry of blood-derived circulating monocytes (Mo) into the inflamed perivascular space and brain parenchyma through CCR2. Infiltrated monocytes subsequently differentiate into BMdM. Together with perivascular macrophages (PVM), BMdM contribute to uptake and phagocytosis of Aβ deposits. Furthermore, the release of pro-inflammatory mediators (e.g. reactive oxygen species) and a disturbed microenvironment can directly harm neuronal functions and lead to cellular death. Figure adapted from [258].
Aβ = amyloid β, BBB = blood brain barrier; BMdM = bone marrow-derived macrophage; BV = blood vessel; CD = cluster of differentiation; EC = endothelial cells; M = microglia; Mo = monocyte, N = neuron; PVM = perivascular macrophage

Although microglia and peripheral monocytes have different ontogeny [208], they share many properties and are not easily distinguishable. There is growing evidence from transgenic (tg) mouse models and experiments using bone-marrow chimeras that myeloid infiltration is highly dependent on the expression of the chemokine (C-C motif) receptor 2 (CCR2) [103]. Expression of CCR2 is regarded as a marker for peripheral monocytes [174, 207, 206]. Another way to discriminate between resident microglia and infiltrated monocytes is the expression of CD45 and CD11b using flow cytometry. [218, 87]. Although both cell types express CD45, resident microglia display only a dim expression, while blood derived macrophages show enhanced expression of this common leukocyte antigen [84]. Several studies pointed out an important role for infiltrated monocytes in terms of Aβ clearance, demonstrating that invading BMdM display a greater potential to phagocytose and clear Aβ deposits [247]. This finding suggests that resident microglia and BMdM display not only

a different ontogeny but also fulfil non-redundant functions in the AD brain [173]. Additionally, another type of myeloid cells, namely perivascular macrophages (PVM), have been observed in Aβ clearance. These cells are regularly replenished by infiltrated and differentiated monocytes in the perivascular space and seem to assist in plaque elimination [94].

The role of microglia in Aβ clearance and AD pathology is still under debate. Recent genome-wide association studies have linked rare microglial gene variants to an increased risk for AD, implicating an important function of microglia in AD pathogenesis. Variances in the gene encoding for CD33, a transmembrane receptor of the innate immune system expressed on the surface of microglia and peripheral monocytes, have been linked to amyloid pathology and disease progression [106, 184, 88]. Similarly, variances in the gene encoding for TREM2 have also been associated with an increased risk for developing late-onset AD [116, 90, 65]. With disease progression, murine microglia are functionally impaired in plaque clearance and display deficits in process motility and phagocytosis [133].

Conclusively, the balance of activated microglia being harmful to the microenvironment and microglial activation being necessary for the repair and neurogenesis functions seems to be disturbed in AD pathogenesis. Therefore, the interplay between microglia and peripherally derived monocytes has to be further clarified in future studies.

1.4 Mouse models of Alzheimer's Disease

With demographic change and subsequently elevated incidence and prevalence rates of dementia, AD research as well as the development of therapies is of increasing importance. To study and manipulate different aspects of AD, several mouse models reflecting AD pathogenesis have been established in the last decades. These mouse models are based on autosomal dominant mutations, which account only for the relatively few FAD cases. Up to now, many humanised APP (hAPP) tg mouse lines exists, all of which generally develop a robust amyloid pathology and memory impairments. Differences between hAPP lines lie in the driving promoters, the hAPP isoforms and mutations as well as in the background strain used. Most commonly used promoters for the generation of hAPP mice are the platelet derived growth factor-β chain (PDGF-β), the thymocyte differentiation antigen 1 (Thy-1) and the prion protein (PrP) promoter. The strongest, but less selective expression levels are driven by the PrP promoter. Due to alternative splicing, three APP isoforms exist, named by the number of remaining AA: APP695, APP751 and APP770. Most tg mouse lines were generated with the APP695 isoform. The first AD mouse model, which was developed in 1995, expresses the so-called human Indiana-mutation of APP (valine717phenylalanine: V717F) under control of the PDGF-β promoter [74]. These mice resemble the main pathological hallmarks of AD: numerous amyloid deposits, synaptic loss, astrocytosis and microgliosis. Additionally, Dodart and colleagues described a reduction in the size of hippocampus, fornix and corpus

callosum in this mouse model, which correlated to working and reference memory impairments [54]. Shortly after, the Tg2576 AD mouse model was reported [108]. Human APP_{695} containing the double mutation lysin670asparagine and methionine671leucine (K670N and M671L) was inserted into a hamster prion protein cosmid vector. Compared to non-tg littermates, tg mice express about 5.5-fold higher levels of endogenous murine APP and plaque-like deposits in 11-month-old mice across the frontal, temporal and entorhinal cortices, hippocampus, presubiculum, subiculum and cerebellum, similar to the expression pattern observed in PDAPP mice. Furthermore, microgliosis and astrocytosis as well as hyperphosphorylated tau were found [260]. However these mice did not develop measurable synaptic loss as compared to PDAPP mice [125].

Mutations in *Psen1* have also been used for the generation of tg AD mice. However, mice expressing merely a mutation in the *Psen1* gene do not develop cognitive deficits or AD pathology [110], although increased levels of Aβ42 are generated. The reason for this is likely due to differences in the AA sequence of human and murine APP [114]. Nowadays, double-tg AD mice are most commonly used. These mice are developed by a co-injection of *Psen* and *hApp* transgenes. Borchelt and colleagues developed a tg mouse line, that combines hAPP containing the Swedish mutation and PSEN1 containing the ΔE9 mutation, namely the APPswe/PSdE9 (further on referred to as APP/PS1) mouse model [31, 30]. Similar to AD patients, these mice develop Aβ plaques in the hippocampus and cerebral cortex with increasing age [109]. Furthermore, memory decline, anxiety-like behaviour, hippocampal atrophy as well as neuronal and synapse protein loss have been demonstrated in aged APP/PS1 mice [109]. Therefore, these mice represent a useful research tool to study Aβ-related pathogenesis.

Nevertheless, it is of importance to emphasize that no existing tg mouse line models all features of the disease, even though several different mouse models for the analysis of AD pathology have been developed in the past two decades. Even though most models show amyloid pathology and cognitive deficits, tau pathology is only seen when human tau is expressed. However, due to the fact that until now all clinical trials evaluating the effectiveness of newly designed drugs, such as bapineuzumab, solanezumab, ganteneruman and crenezumab, to treat patients with AD or mild cognitive impairments did not show any statistically significant slowing in cognitive decline compared to patients treated with placebo [228]. Therefore, further basic research is needed to investigate AD development and pathogenesis as well as AD associated neuroinflammation.

1.5 The Endocannabinoid system

Usage of the plant marijuana (*Cannabis sativa*) dates back over 10000 years and was initially grown for fibre and grain [236]. First archaeological evidence for the medicinal purposes of cannabis was found in a 2700-year old tomb in north-western China [226]. The Irish physician Sir William B. O'Shaughnessy publicised the therapeutic value of cannabis for the first time in the western countries in the early 19th century [196]. Since then, medicinal properties of cannabis were assessed clinically and the so-called cannabis research started.

Based on pioneering work from Thomas Wood and colleagues, who firstly isolated cannabinol, Lord Alan Tood simultaneously with Roger Adams completed the elucidation of its chemical structure in 1940 [112]. However, the discovery of the main psychoactive component was not before 1964, when Yehiel Gaoni und Raphael Mechoulam isolated and synthesised tetrahydrocannabinol (THC) [76]. This was the starting point for the intensively studied cannabinoid research. However, it took more than two decades until the corresponding receptor for THC, termed cannabinoid-receptor (CB) 1, was identified from several previously cloned 'orphan' G-protein-coupled receptors (GPCRs) [163]. Three years later, the second receptor was identified and named CB2 [181].
The first endocannabonoid, arachidonoylethanolamide (AEA), later named anandamide, was identified in the early 1990s by Mechoulams group and others [51]. Three years later, the second and more abundant endocannabinoid, 2-arachidonoylglycerol (2-AG), was identified by two research groups [171, 253]. Both compounds are derived from lipid precursors, are produced on demand and are rapidly released into the synaptic cleft. Here they act on pre-synaptic cannabinoid receptors as retrograde signalling molecules. These findings gave rise to the now widely known field of endocannabinoid research, which is comprised of cannabinoid receptors, their corresponding ligands as well as synthesising and degrading enzymes.

Due to increasing functional investigation of the endocannabinoid system (ECS), there is a wide and unanimous consensus for a distinct expression pattern of the two - primarily $G_{i/o}$-protein coupled - cannabinoid receptors. CB1, encoded by the gene *Cnr1*, is generously expressed in the CNS on different neuronal cell types. In the hippocampus, CB1 receptors are more abundantly expressed on inhibitory γ-aminobutyric acid (GABA)-ergic terminals than on glutamatergic principal neurons [158, 119, 264]. Furthermore, CB1 receptor expression has also been detected in peripheral tissues, such as thymus, prostate, heart, bone-marrow, lung and tonsils [71]. In contrast, CB2, encoded by the gene *Cnr2*, is primarily expressed on immune cells, such as B-cells, T-cells, macrophages, dendritic cells (DCs) and microglia [197].

Expression of functional CB2 receptors in the healthy CNS, especially a neuronal expression of CB2, is still controversially discussed and was the content of different publications in the recent years [193, 290, 233, 143]. This controversy is due to poor availability of specific antibodies for

CB2 protein detection in murine tissue and missing controls, such as CB2 knockout tissues, in the past. While CB2 expression on CNS resident microglia is nowadays being accepted more widely [34, 13], the expression of CB2 on neuronal subtypes is still a matter of debate. However, just recently it was demonstrated that CB2 receptors are indeed expressed in hippocampal principal neurons, where they mediate a cell-type specific plasticity in pyramidal cells of the hippocampal *Cornu Ammonis* (CA) regions CA3 and CA2 [252].

In the past decades, other receptors, like the orphan G-protein coupled receptor 18 [130, 45] and 55 [139, 227] as well as the transient receptor potential vanilloid type-1 (TRPV-1) have been discussed as non CB1 / CB2 cannabinoid receptors [293]. Nevertheless, both, the immune system and cognitive functions are affected by cannabinoid signalling. Thus, the ECS has been implicated in diverse diseases, such as malaria, multiple sclerosis, amyotrophic lateral sclerosis, Huntington's disease, pain, addiction, depression and schizophrenia.

1.5.1 ECS mediated retrograde signalling

Communication between neurons is mediated through synaptic transmission (depicted in Fig. 1.6). In response to an action potential, calcium influx into the pre-synaptic bouton is induced. This directly activates the release of glutamate to the synaptic cleft through exocytosis of neurotransmitter-filled vesicles with the membrane. Under normal conditions, released glutamate binds to post-synaptic N-methyl-D-aspartate receptors (NMDA) or the ionotropic α-amino-3-hydroxy-5-methyl-4-isoxazolepropionic acid (AMPA) receptor.

This basal communication does not activate the ECS. However, upon high frequency stimulation of the pre-synaptic neuron, dramatically increased levels of released glutamate also bind to post-synaptic type 1 metabotropic glutamate receptors (mGlu) 1/5. Thereby, coupled G-proteins become activated, leading to the production of diacylglycerol (DAG) by phospholipase C (PLC). Activation of the diacylglycerol lipase (DAGL) in turn hydrolyses DAG into the monoacylglycerol 2-AG and fatty acid [205, 253]. 2-AG is released into the synaptic cleft, where it binds to pre-synaptic CB1 receptors. Similar to other G_i-coupled receptors, the activation of CB1 typically blocks the activation of adenylyl cyclase, preventing signalling through cyclic AMP. Subsequently, inhibition of voltage-gated calcium channels reduce neurotransmitter release from the pre-synapse. This phenomenon is also known as depolarisation induced suppression of excitation (DSE), when mediated via excitatory glutamatergic synapses and depolarisation induced suppression of inhibition (DSI), when mediated via inhibitory GABA-ergic synapses.

CB2 receptors are also coupled to $G_{i/o}$ proteins, whereby adenylyl cyclase is inhibited and the mitogen-activated protein (MAP) kinase cascade is induced [254].

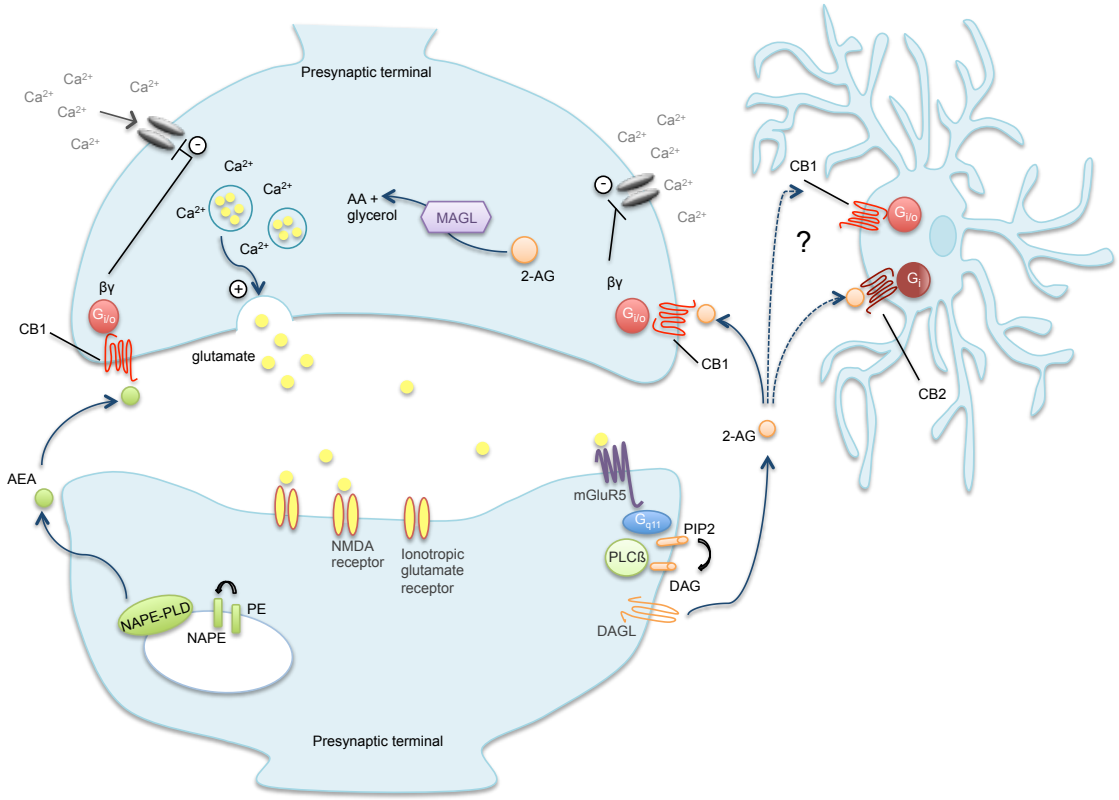

Figure 1.6: ECS mediated retrograde signalling illustrated exemplary for a glutamatergic synapse. Incoming action potential induce the influx of extracellular calcium into the pre-synaptic bouton. This triggers the fusion of transmitter-filled vesicles with the synaptic membrane and releases neurotransmitters (in this example glutamate) into the synaptic cleft. Glutamate in turn binds to post-synaptic NMDA or AMPA receptors, which will transmit the signal. However, upon excessive stimulation of the pre-synapse, increased amounts of glutamate are released and, additionally to AMPA and NMDA receptors, bind to mGlu. Consequently, coupled G-proteins trigger the production of DAG by PLC, which in turn activates the enzyme DAGL. This mediates the hydrolysis of DAG to 2-AG. Released 2-AG binds pre-synaptic G_i-coupled CB1 receptors and thereby activation of the adenylate cyclase is blocked and further calcium influx prevented. Same effects can be induced by AEA, which is produced by the enzyme NAPE-PLD. How the activation of microglial CB2 in close vicinity to synapses is regulated and the exact molecular mechanism of communication between these cell types, still remains a matter of future research.
2-AG = 2-Arachidonoylglycerol; AEA = N-arachidonoylethanolamine; AMPA = α-amino-3-hydroxy- 5-methyl-4-isoxazolepropionic acid; CB = cannabinoid receptor; DAG = diacylglycerol; DAGL = diacylglycerol lipase; ECS = endocannabinoid system; mGlu = metabotropic glutamate receptors; NAPE-PLD = N-acylphosphatidylethanolamine phospholipase D; NMDA = N-methyl-D-aspartate; PLC = phospholipase C

1.5.2 Synthesis and hydrolysis of endocannabinoids

As mentioned above, endocannabinoids cannot be stored and thus have to be synthesised on demand due to their lipophilic nature. Biosynthesis of AEA is not yet fully elucidated, however, synthesis is devided into in two-steps. Firstly, the plasma membrane constituent phosphatidylethanolamine is acetylated by the membrane-bound enzyme N-acetyltransferase to generate N-acylphosphatidylethanolamine (NAPE). In a second step, NAPE hydrolysing phospholipase D (NAPE-PLD) converts NAPE to AEA in a calcium sensitive manner. Hydrolysis of AEA is mediated through fatty acid amide hydrolase (FAAH), which leads to the production of arachidonic acid (ARA) and ethanolamine. 2-AG synthesis is also generated in two steps. Hydrolysis of the

membrane phospholipid phosphatidylinositol through the PLC provides the ARA-containing precursor DAG. Subsequently, DAGL hydrolyses DAG into the monoacylglycerol 2-AG and fatty acid. Hydrolysis of 2-AG is mostly mediated via monoacylglycerol lipase (MAGL) (up to 85%). However, also the two Aβ-hydrolases (ABHD) 6 and ABHD12 have been shown to play a role in 2-AG signalling termination (for review see [231]). Together these three serine hydrolases account for approximately 99% of 2-AG hydrolysing activity.

1.5.3 The endocannabinoid system in Alzeimer's disease

Increasing evidence suggests that the ECS plays an important regulatory role in AD-associated neuroinflammation. Using *in vitro* receptor autoradiography and *in situ* hybridization, it was shown that CB1 binding density was reduced in brains of AD patients, but expression of CB1 was not altered [276]. In contrast, independent findings by Ramirez and Solas revealed a significant decrease in CB1 receptor levels as well as CB1 protein nitration in areas of microglial activation in AD brains [215, 248]. Increased CB1 receptor activity at early stages of the disease were recently shown to decrease with age and disease progression, indicating an attempt to compensate for early synaptic impairments [156]. However, this compensatory mechanism seems to weaken over time. Correspondingly, in mouse models of AD, a decreased CB1 protein expression was found when compared to age-matched control mice [18, 117].

In contrast to the CB1 receptor, the relationship between CB2 and AD was intensively investigated in the past years. In brains of AD patients, CB2 and FAAH were selectively overexpressed in neuritic plaque-associated microglia [20]. Furthermore, increased CB2 receptor expression in AD brains was correlated with two relevant molecular markers of AD, Aβ levels and senile plaque score [248]. Apart from human studies, AD-associated mouse models also revealed an overexpression of CB2 in Aβ-affected brain areas [107, 233]. Likewise, rats and rat astroglioma cells showed an up-regulation of CB2 receptors and an increase in 2-AG concentration after treatment with Aβ [60].

Since chronic neuroinflammation is one of the hallmarks of AD, anti-inflammatory strategies have been proposed as an attractive approach to cope with disease progression. The ECS displays important anti-inflammatory and neuroprotective properties and is therefore intensively studied as a therapeutic target. The role of CB2 receptor activation in AD pathogenesis was investigated by independent researchers over the past years. Most of the initial reports were investigated in *in vitro* models of Aβ induced neuronal toxicity and later followed up in AD tg or Aβ-injected animals.

Using pharmacological activation with synthetic CB2 ligands, a modulation of disease progression in different mouse models of AD was reported. Administration of the specific CB2 agonist JWH-133 (named after the chemist John William Huffman [JWH]), into double-tg APP/PS1 mice improved cognitive performance, decreased microglial reactivity and the expression of pro-inflammatory cy-

tokines IL-1β, IL-6, TNFα and IFNγ [11]. Furthermore, JWH-133 reduced the expression of active p38 and stress-activated protein kinases (SAPK)/Jun amino-terminal kinases (JNK) and increased the expression of inactive glycogen synthase kinase 3 β [11]. In rats, injected with Aβ1-40 fibrils, the treatment with the novel CB2 receptor agonist 1-((3-benzyl-3-methyl-2,3-dihydro-1-benzofuran-6-yl) carbonyl) piperidine (MDA7) decreased the secretion of IL-1β and expression of CB2 receptors. Additionally, Aβ clearance was promoted and synaptic plasticity, cognition and memory was restored after daily MDA7 treatment for 14 days [281]. Only few reports do not support the beneficial effects of cannabinoids on AD pathology. Chronic administration of the synthetic cannabinoid agonist HU-210 did not improve performance of AβPP23/PS45 mice in the Morris water maze paradigm or in contextual fear conditioning, as reported by Chen and colleagues [38].

Nevertheless, the exact molecular mechanism of reported beneficial effects after CB2 receptor stimulation in AD pathogenesis remains still unknown and further research is needed to evaluate the role of CB2 and other cannabinoid receptor stimulation in the modulation of the disease.

2 Aim of this Study

Alzheimer's disease, one of the most prevailing neurological diseases in western countries and affects the majority of the more than 35 million people suffering from dementia. To date, no preventive treatment is available, thus, an increasing prevalence of AD is expected due to demographic changes. An inflammatory process is nowadays discussed as a fundamental component of AD, therefore, various research groups have studied alterations of neuroinflammatory processes in AD mouse models.

The ECS - especially CB2 receptors - have been discussed as a therapeutic target for the treatment of AD. It has been demonstrated that CB2 is upregulated in plaque-associated microglia. Furthermore, the pharmacological stimulation of CB2 receptors in AD-associated mouse models or cell-culture systems revealed beneficial effects on neuroinflammation, A-β load as well as cognitive deficits. However, the exact role of CB2 signalling on these events remains elusive.

Therefore, the current study was designed to evaluate the influence of CB2 signalling on AD associated expression of inflammatory markers, Aβ deposition as well as on learning and memory. Thus, mice lacking functional CB2 receptor expression ($CB2^{-/-}$) were crossed with the AD mouse model APP/PS1 to compare the AD-associated pathology in APP/PS1$*$$CB2^{-/-}$ mice with age-matched AD and control mice. In the first part, we investigated the effect of conditional CB2 receptor deletion on microglial polarisation *in vitro*. In the second part, components of the ECS were analysed in APP/PS1$*$$CB2^{-/-}$ and control mice. Finally, we investigated AD-associated plaque deposition, microgliosis, neuroinflammation, neurodegenration and cognitive performance.

3 Materials

3.1 Equipment

Analytical balance	Sartorius BP 2100, Elk Grove, IL, USA
Apotome	ApoTome2, Zeiss, Jena, Germany
CCD camera	Axiocam MRm, Zeiss, Jena, Germany
Cell count chamber	Neubauer, CarlRoth GmbH, Karlsruhe, Germany
Cell culture dishes	Greiner Bio-one, Frickenhausen, Germany
Centrifuge	Fresco17 Zentrifuge, Heraeus and Multifuge 3SR, Heraeus, Thermo Scientific, Langenselbold, Germany
Cryostate	CM3050 S, Leica, Wetzlar, Germany
Electrophoresis apparatus	PowerPac supply, BioRad, Muenchen, Germany
Flow cytometer	FACS-Canto II, BD Bioscience, Heidelberg, Germany
Homogenizers	Precellys® 24, Bertin Technologies, Erlangen, Germany Ultra-Turrex®, IKA Werke, Staufen, Germany Ultrasound homogenizer, Bandelin Sonoplus, Berlin, Germany
Incubator	CB210, Binder, Tuttlingen, Germany
Magnetic stirrer	MR3001, Heidolph, Schwabach, Germany
Microscope	Axioplan 2, Zeiss, Jena, Germany
PCR Cycler	7900 HAT Fast Real-Time PCR System, Applied Biosystem, Carlsbad, CA, USA
Photometer	NanoDrop ND-1000 Spectraphotometer, Wilmington, DE, USA
Petri dishes	Greiner, Bio-one, Frickenhausen, Germany
Polyamide mesh (40 μm)	VWR International, Darmstadt, Germany
Polypropylene vials (15, 50 ml)	BD Bioscience, Pharmingen, San Diego, CA, USA
Polystyrene vials (5 ml)	BD Bioscience, Pharmingen, San Diego, CA, USA
Safe-lock vials (0.5, 1.5, 2 ml)	Eppendorf, Hamburg, Germany
SlideA-Lyzer mini dialysis cassette (3.5 kD)	Pierce, ThermoFisher Scientific, Rockford, IL, USA
Superfrost Plus® slides	Menzel-Glaeser, Braunschweig, Germany

Thermo mixer	Eppendorf, Hamburg, Germany
Thermo cycler	ICycler, BioRAD, Muenchen, Germany
Tissue culture hood	HERsafe, Thermo Scientific, Langenselbold, Germany
Plate photometer	MRX TC II, Dynex Technologies, Denkendorf, Germany
24-well-plate	BD Bioscience, Pharmingen, San Diego, CA, USA
96-well-plate for cell-culture	Greiner, Bio-one, Frickenhausen, Germany
96-well-plate for ELISA	eBioscience, San Diego, CA, USA
384-well-plate	Applied Biosystems, Carlsbad, CA, USA

3.2 Antibodies and Primers

Table 3.1: List of Primary Antibodies used in this study: Abcam, Cambridge, UK; AbD Serotec, Düsseldorf, Germany; BD Pharmingen, San Diego, IL, USA; Biozol, Eching, Germany; eBioscience, Frankfurt, Germany; Invitrogen, Darmstadt, Germany; Millipore, Schwalbach, Germany; Santa Cruz Biotechnol., Heidelberg, Germany; SIGMA-Aldrich, Steinheim, Germany; Signet Laboratories, Dedham, MA; USA; Wako Chemicals GmbH, Neuss, Germany

1st Antibody	Species	Host	Conjugation	Dilution	Company
amyloid-β 6E10	human	mouse	-	1:1000	Signet Laboratories
β-actin	mouse	mouse	-	1:2000	SIGMA-Aldrich
CD11b	mouse	rat	APC	1:200	eBioscience
CD11b	mouse	rat	Biotin	1:200	BD Pharmingen
CD11b	mouse	rat	eFluor450	1:200	eBioscience
CD11b	mouse	rat	FITC	1:200	Biozol
CD11b	mouse	rat	PE	1:200	BD Pharmingen
CD16/32	mouse	rat	-	1:300	Biozol
CD40	mouse	rat	PE	1:200	eBioscience
CD45	mouse	rat	eFluor450	1:200	eBioscience
CD54 (ICAM)	mouse	rat	FITC	1:200	eBioscience
F4/80	mouse	rat	Biotin	1:200	eBioscience
F4/80	mouse	rat	FITC	1:200	Biozol
Iba1	mouse	rabbit	-	1:500	WAKO
NeuN	mouse	rabbit	-	1:500	Sigma
Parv	mouse	rabbit	-	1:1000	Abcam

Table 3.2: List of secondary Antibodies used in this study:

2nd Antibody	Species	Host	Conjugation	Dilution	Company
anti-goat	goat	rabbit	AlexaFluor647	1:500	Invitrogen
anti-rabbit	rabbit	goat	Biotin	1:500	Invitrogen
anti-rabbit	rabbit	goat	Cy3	1:500	Invitrogen
Streptavidin	-	-	APC	1:300	Biozol
Streptavidin	-	-	Cy3	1:300	Invitrogen
Streptavidin	-	-	PerCP-Cy5.5	1:300	BD Pharmingen

Table 3.3: Cell culture stimulants and according concentrations: Peptide Specialty Companies, Heidelberg, Germany; Roche, Grenzach, Germany; R&D systems, Wiesbaden-Nordenstadt, Germany; SIGMA-ALDRICH, Steinheim, Germany

Stimulant	concentration or dilution	company
Amyloid-β peptide	515 nM	Peptide Speciality Companies
IFNγ	20 ng/ml	R&D Systems
LPS	100 ng/ml	SIGMA-Aldrich
Proteinase K	0.6% (v/v)	Roche

Table 3.4: Assays and ELISA Kits: eBioscience, Frankfurt, Germany; Invitrogen, Darmstadt, Germany; Linaris, Dossenheim, Germany; PerkinElmer, Rodgau, Germany; ThermoFisher, Rockford, IL, USA

Kit	Company
Human Aβ $_{40}$ ELISA Kit	Invitrogen
Human Aβ $_{42}$ ELISA Kit	Invitrogen
Mouse CCL2 (MCP-1) ELISA Ready-SET-Go!®	eBioscience
mouse IL-6 ELISA Ready-SET-Go!®	eBioscience
mouse IL-10 ELISA Ready-SET-Go!®	eBioscience
mouse TNFα ELISA Ready-SET-Go!®	eBioscience
Peptide labeling Kit	Thermo Fisher
BCA Assay	Thermo Fisher
TSA Enhancer Kit	Perkin Elmer
VectaShield DAPI	Linaris

Table 3.5: Primer sequences for PCR: All primers for polymerase chain reactions (PCR) were purchased from TIBMolBiol, Berlin, Germany

Primer	Sequence
PSEN-1 (forward)	GGT CCA CTT CGT ATG CTG
PSEN-1 (reverse)	AAA CAA GCC CAA AGG TGA T
CB2 common	GTC GAC TCC AAC GCT ATC TTC
CB2 wild-type	GTG CTG GGC AGC AGA GCG AAT C
CB2 knock-out	AGC GCA TGC AGA CTG CCT

Table 3.6: List of TaqMan gene assays: All Taqman primer were purchased from Applied Biostystems, Carlsbad, CA, USA

Target gene	Assay ID
adam10	Mm00545742_m1
adam17	Mm00456428_m1
ager	Mm01134790_g1
arg1	Mm00475988_m1
app	Mm01344172_m1*
bace1	Mm00478664_m1
ccl2	Mm00441242_m1*
ccr2	Mm00438270_m1
cnr1	Mm01212171_s1*
cnr2	Mm00438286_m1
cxcr3	Mm99999054_s1*
daglα	Mm00813830_m1*
fos	Mm00487425_m1*
gapdh	Mm9999991_g1
gpr18	Mm01224541_m1
il-1β	Mm01336189_m1
marco	Mm00440265_m1*
magl	Mm00449274_m1*
mmp9	Mm00442991_m1*
nape-pld	Mm00724596_m1*
nep	Mm00485028_m1*
tlr4	Mm00445273_m1
tnfα	Mm00443258_m1

3.3 Chemicals

The following chemicals, presented in alphabetical order, were used according to manufacturer protocols or standard operating protocols in the current study.

Agarose	Invitrogen
β-mercaptoethanol	GIBCO®
Collagenase	Roche
Dulbeccos's modified eagle medium (DMEM) (4500 mg/l glucose)	GIBCO®
DNase	Roche
Ethylene diamine tetraacetic acid (EDTA)	Sigma-Aldrich
Ethanol, absolut (C_2H_5OH; M 46.07 g/mol)	Merck
Ethidiumbromide	Promega
Foetal calf serum (FCS)	PAA
GoTaq® Green Master Mix (2x)	Promega
Hanks balanced salt solution (HBSS)	GIBCO®
IGEPAL® CA-630	Sigma-Aldrich
Isopentan (methylbutan)	VWR
Ketamine hydrochrloride	Sigma-Aldrich
Lipopolysachharide (LPS)	Sigma-Aldrich
Roti®-phenol / chlorophorm / isoamylalcohol	Roth
Paraformaldehyde (PFA)	Sigma-Aldrich
Phosphate buffered saline (PBS)	GIBCO®
Penicillin / streptomycin	GIBCO®
Percoll	VWR
Poly-L-lysin	Sigma-Aldrich
Proteinase K	Roche
Sodium dodecyl sulfate (SDS)	Fluka
Tris(hydroxymethyl)aminomethane (TRIS)	Carl Roth GmbH + Co. KG
Trypsin / EDTA	GIBCO®
TWEEN® 20	Roth
Vectashield® mounting medium (DAPI)	Vector Laboratories, Linaris
Xylazine	Sigma-Aldrich

3.4 Buffers and solutions

All reagents used were purchased from Carl Roth (Karlsruhe, Germany), Invitrogen (Darmstadt, Germany), Merck (Darmstadt, Germany), or SIGMA-Aldrich (Steinheim, Germany). Exceptions are noted separately.

cell culture medium	DMEM (4.5 g/l glucose) 10% (v/v) FCS (heat-inactivated)
digestion solutions for CNS	0.1 mg/ml collagenase (in cell culture medium) or 0.1 mg/ml DNase (in cell culture medium)
ELISA washing buffer	1x PBS 0.05% (v/v) TWEEN® 20
ELISA stop solution	1 M H_3PO_4
FACS buffer	1x PBS (pH = 7.2) 2% (v/v) FCS (heat-inactivated)
macrophage culture medium	RPMI 1640 15% (v/v) M-CSF 10% (v/v) FCS (heat-inactivated) 1% (v/v) penicillin / streptomycin 0.1% (v/v) β-mercaptoethanol
microglia culture medium	DMEM (4.5 g/l glucose) 10% (v/v) FCS (heat-inactivated) 1% (v/v) penicillin / streptomycin 1% (v/v) minimum essential medium (MEM) 0.1% (v/v) β-mercaptoethanol
lysis buffer	450 μl TNE buffer 50 μl 10% (w/v) SDS 3 μl (v/v) proteinase K
narcotic solution	1 ml ketamine (100 mg/ml) 0.5 ml xylazine (20 mg/ml) 8.5 ml saline (sterile, isotonic)
percoll gradient solutions	70% (v/v) percoll (in cell culture medium) 30% (v/v) percoll (in FACS buffer)
radioimmunoprecipitation assay (RIPA) buffer	100 millimolar (mM) TRIS (pH = 8) 150 mM NaCl 0.5% (w/v) IGEPAL® 0.2% (w/v) SDS (prior to use: 1 tablet complete mini protease inhibitor per 10 ml buffer)
10% SDS	100g SDS per 1 l pH = 7.2

TRIS acetate EDTA (TAE) buffer	40 mM TRIS acetate 1 mM EDTA
TRIS EDTA (TE) buffer	10 mM TRIS-HCl 1 mM EDTA pH = 7.6
TNE buffer	10 ml 1 M TRIS (pH 8.0) 20 ml 5 M NaCl 2 ml 0.5 M EDTA make up to 1 l with H_2O_{milliQ}

4 Methods

4.1 Mouse strains and animal housing

$CB2^{-/-}$ mice were generated by Buckley and colleagues [33]. Thereby, the 3'region of the *Cnr2* coding exon was replaced through homologous recombination by the phosphoglycerate kinase (PGK)-neomycin sequence. Consequently, this mutation resulted in the elimination of a part of the intracellular loop 3, the transmembrane domains 6 and 7 and the carboxy terminus. APP/PS1 mice were purchased from Charles River Laboratories (B6.Cg-Tg (APPswe(K594N/M595L)/,PSEN1dE9) 85Dbo/J; Charles River Laboratories, Germany GmbH) and crossed with $CB2^{-/-}$ mice.
APP/PS1$*CB2^{+/-}$ mice were then crossed with $CB2^{-/-}$ mice. All animals were bred and housed in a specific pathogen-free animal facility under standard animal housing conditions in a 12 hour (h) dark-light cycle with access to food and water *ad libitum* according to German guidelines for animal care (Tierschutzgesetz v 18.5.2006 BGBI. I S. 1206, 1313). Mice were weaned and ear-tagged 3 weeks after birth and generally group-housed with up to six animals per cage. As APP/PS1*$CB2^{-/-}$ pups were not obtained with the expected Mendelian frequency, APP/PS1* $CB2^{-/-}$ mice were bred with $CB2^{-/-}$ mice. The experiments were carried out with mice at the age of 9 and 14 months from both breeding strategies. Mice were genotyped by PCR using DNA from tail biopsies. For cell culture experiments, C57BL/6J (JAX^{TM} mice strain) mice were used as controls. C57BL/6J, further on referred to as wildtype (WT or $CB2^{+/+}$) mice, were initially purchased from Charles River Laboratories and bred in-house for the current study.

4.1.1 APP/PS1 and CB2 genotyping

Tail biopsies were obtained from 3-4 weeks old mice and incubated in 500 μl lysis buffer at 37°C overnight. DNA extraction was conducted using the phenol/chloroform/isoamylalcohol (25:24:1) method. Thereby, lysed biopsies were incubated with phenol/chloroform/isoamylalcohol and thoroughly mixed. After centrifugation at 13,000 rounds per minute (rpm) for 5 min, the supernatant was taken and the DNA was precipitated by adding 900 μl $ethanol_{abs}$. After centrifugation at 13,000 rpm for 5 min, the supernatant was discarded and the pellet was washed with 500 μl 70% (v/v) ethanol and dried for 20 min. The pellet was re-suspended in 200 μl TE buffer. DNA concentration was measured at $\lambda_{nm} = 260$ nm using a NanoDrop spectrophotometer. Purity of the DNA samples was given by a ratio of $A_{260/280nm} = 1.8$ and a ratio of $A_{260/230nm} = 2.0$.
For APP/PS1 genotyping, purified DNA samples were diluted with DNase/RNase free water to obtain a concentration of 50-100 ng$*\mu l^{-1}$.

For each sample, the following concentrations were used:

1 μl sample

8 μl H_2O

10 μl 2x GoTaq Green Master Mix

0.5 μl primer PSEN forward

0.5 μl primer PSEN reverse

APP/PS1-PCR reaction mixtures were run under the following conditions:

1 x:	denaturation (1x):	95°C, 5 min
40 x:	I. denaturation:	95°C, 1 min
	II. annealing:	63°C, 1 min
	III. elongation:	72°C, 1 min
1 x:	final denaturation:	72°C, 10 min
		4°C, ∞

For CB2 genotyping, two PCR reaction mixtures (CB2 WT and knockout) were prepared:

1 μl sample

8 μl H_2O

10 μl 2x GoTaq Green Master Mix

0.5 μl primer CB2 common

0.5 μl primer CB2 WT or knockout, respectively

Both CB2-PCR reaction mixtures were run using the following cycling parameters:

1 x:	denaturation (1x):	95°C, 5 min
40 x:	I. denaturation:	95°C, 30 sec
	II. annealing:	60°C, 45 sec
	III. elongation:	72°C, 1 min
1 x:	final denaturation:	72°C, 7 min
		4°C, ∞

The samples were loaded on a 1% (w/v) agarose gel, run with 120 V for 50 min, and incubated in a 0.16% (w/v) EtBr bath for 20 min.

4.2 Cell culture experiments

4.2.1 Generation of bone marrow-derived macrophages

For the generation of BMdM, $CB2^{+/+}$ and $CB2^{-/-}$ mice were killed by cervical dislocation and the skin was removed from both hind limbs. Femur and tibia were isolated and remaining tissue was removed by using scalpel blades. Tissue-free bones were opened by cutting off the epiphyses under cell-culture sterile conditions, before flushing out the bone-marrow with ice-cold PBS using a 10 ml-syringe. Bone-marrow from femur and tibia from each mouse was collected in a 10 cm^2 Petri dish and re-suspended until a single-cell suspension was achieved by using a glass pipette. This suspension was filtered into a 50 ml tube though a 100 μm filter and cells were washed with ice-cold PBS to a final volume of 50 ml. Cells were counted, adjusted to a cell number of 1,5 x 10^5 cells / ml and seeded in a total volume of 10 ml in fresh macrophage medium in uncoated Petri dishes. Cells were incubated for 6 days at 37°C and 5% CO_2. On day 3, 5 ml of freshly prepared medium was added. On day 6, cells were harvested for phagocytosis assays.

4.2.2 Isolation of primary microglia cells

Primary mouse microglia cells were isolated from $CB2^{+/+}$ and $CB2^{-/-}$ mice at postnatal day 1-4. After cervical dislocation, whole brains were isolated from the skull. Isolated cortices were mechanically minced to a single-cell suspension using a pipette. Cortices of up to 70 mice per genotype were pooled in ice-cold Hanks buffered salt solution (HBSS). For sedimentation of insoluble fragments, brain homogenates were kept on ice for 5 min. Supernatant was transferred into a fresh tube and centrifuged at 1200 *g* for 5 min. Cell pellets were re-suspended in pre-warmed microglia medium. Cortices of 2-3 pups of the same genotype were plated onto poly-L-lysine coated cell-culture flasks at 37°C and 5% CO_2. Medium was changed after 24 h and subsequently twice per week for approximately 21 days, or until mixed glia cultures reached confluency.

4.2.3 Harvesting and re-plating of primary microglia cells

Microglia cells were harvested by mild trypsination according to Saura et al. [230]. To enrich microglia cells, confluent mixed glia cultures were first subjected to 0.25% trypsin/ethylenediaminetetraacetic acid (EDTA) (1/2) diluted 1/4 in microglia medium without serum for 15-20 min at 37°C and 8% CO_2. After detachment of the upper cell layer, trypsin digestion was stopped by adding the same volume of complete media containing FCS. Remaining cells were harvested by an incubation with undiluted 0.25% trypsin/EDTA (1/2) for 5 min. Detached cells were spun down (1200 *g*, 5 min) and re-plated into 24 well plates at a density of $1.5 - 2$ x 10^5 cells per ml.

4.2.4 Phagocytosis assay

Microglia cells were incubated with fluorescently labelled Aβ (AlexaFlour 649) for 1 h at room temperature (RT), or at 4°C as a negative control to exclude unspecific binding. Labelling of Aβ was performed by using DyLight^{TM}649 Microscale Antibody Labelling Kit (ThermoScientific, Waltham, MA). Purification of Aβ-DyLight649 (4.5 kDa) from unlabelled peptide was conducted using the Slide-A-Lyzer mini dialysis cassette for peptides $<$ 3.5 kDa. The Aβ-DyLight649 solution was incubated in the dialysis cassette for 2 h in HBSS on a stirrer (RT, dark). Purified Aβ-DyLight649 solution was aliquoted and stored at -20°C before usage. After washing, cells were subjected to flow cytometric analyses and stained with CD11b antibodies.

4.2.5 Stimulation assay

Stimulation of primary microglia cells was conducted 24 h after harvesting and re-plating cells (4.2.3). Stimulation substances were diluted adequately in microglia medium and added to the medium. For aggregation, monomeric Aβ peptides were incubated at RT for 1 h and a subsequent stimulation with aggregated Aβ was conducted for 24 h. LPS and IFNγ were applied for approximately 16 h, while unstimulated cells served as controls. After stimulation, each supernatant was collected separately, shock-frozen in liquid nitrogen and stored at -20°C for further usage. Subsequently, cells were harvested for flow cytometric staining. All cell culture experiments were carried out in triplicates.

4.3 Organ withdrawal and isolation methods

4.3.1 Brain removal for protein isolation and immunohistochemistry

Prior to surgery, mice were injected intraperitoneally with a ketamine/xylazine combination cocktail (0.1 ml volume of cocktail was administered to mouse per 10 g body weight). Once the animal had reached a surgical plane of anaesthesia, it was fixed backwards on a polystyrene plate. Abdomen and thorax were opened, and each mouse was perfused transcardially with 20 ml ice-cold PBS. Next, the skull was opened, the brain was removed carefully and divided into the two hemispheres. For protein isolation, the left hemisphere was immediately snap-frozen in $N_{2(liq.)}$ and stored at -80°C. The right hemisphere was fixed in 4% (w/v) PFA overnight at 4°C, followed by an incubation in 20% (w/v) sucrose, embedded in TissueTek® and stored at -80°C.

4.3.2 Isolation of cortex and hippocampus

For isolation of different brain areas, mice were sacrificed by cervical dislocation and the skull was opened. Using micro forceps, cortex and hippocampus of each hemisphere were isolated and frozen in pre-cooled tubes on dry ice. Samples were stored at -80°C.

4.3.3 Isolation of intracerebral leucocytes

For the analysis of intracerebral leucocytes (ICL), mice were anaesthetised and perfused as described above (4.3.1). Brains were removed, placed in 5 cm^2 Petri dishes (one brain per dish), and cut into small pieces. For digestion, 1 ml of collagenase digestion solution was added to each dish and brain pieces were further minced by pipetting up and down with a syringe containing 4 ml cell culture medium. The brains were incubated at 37°C and 5% CO_2 for 45 minutes. Thereafter, 1 ml of DNase digestion solution was added per dish and the brains were incubated again for 45 min (37°C, 5% CO_2). After digestion, the single cell suspension was filtered through a 100 μm mesh, and the digestion was stopped by adding cell culture medium up to 50 ml. The cell suspension was spun down (1,500 rpm for 7 min at 4°C) and the cell pellet was dissolved in 20 ml of 70% (v/v) percoll solution. To achieve a two-phase density gradient system, the 70% percoll solution was carefully overlaid with a 30% (v/v) percoll solution. The samples were spun down again (2,100 rpm for 25 min at RT, without brake). Intracerebral mononuclear cells, which were identified as a white ring between the two phases, were collected at the interface of the two phases. 10 ml of the cell containing interphase were placed into a fresh tube and combined with 40 ml of cell culture medium. After centrifugation (1,800 rpm for 10 min at 4°C), the cell pellet was dissolved in 1 ml fluorescence-activated cell sorting (FACS) buffer for flow cytometric analysis.

4.4 Flow cytometry

BMdM(4.2.1), primary microglia cells (4.2.2) as well as isolated ICL (4.3.3) were washed in 1 ml FACS buffer by centrifuging with 4,500 rpm for 5 min at 4°C. The cell pellet was re-suspended in 45 μl blocking buffer (CD16/32; 1:300) and incubated for 15 min on ice. Cells were washed with 500 μl FACS buffer and spun down (4,500 rpm for 5 min at 4°C). Afterwards, cells were incubated in 45 μl mixed primary antibody solution (1:200) and stained for cell surface markers for 15 min in the dark on ice. After a washing step, cells were incubated in 45 μl secondary antibody solution (1:200) for 15 min on ice in the dark. After a last washing step, cells were re-suspended in 300 μl (intracerebral mononuclear cells) or 200 μl (primary microglia or BMdM) FACS buffer. Immediately before flow cytometric analyses, cell suspensions were filtered through a 40 μm mesh of gauze (for the removal of aggregated cells) into FACS tubes and measured with a FACS Canto II (BD Bioscience). Data analysis was performed using FlowJo software, versions 887 and X 10.0.7r2 (Tree Star Inc.).

4.5 Biomolecular and biochemical methods

4.5.1 Protein isolation

For protein isolation, frozen brain hemispheres were weighted and 1 ml radioimmunoprecipitation assay (RIPA) buffer with proteinase inhibitor was added per 150 mg brain. Brains were homogenised by sonication (first step: 1 x 20 s, 30% cycles, 100% power; second step: 1 x 20 s, 60% cycles, 100% power) and chilled on ice for 20 min. Afterwards, samples were spun down (13,300 g for 30 min at 4°C) and the supernatant was portioned in 200 μl aliquots and stored at -80°C.

4.5.2 Protein quantification by BCA assay

To determine the total level of proteins, the commercially available bicinchoninic acid (BCA) kit was used. The assay makes use of the ability of proteins to react with Cu^{2+} to a Cu^{1+} coloured protein chelat complex under alkaline conditions (biuret reaction). In a second step, BCA reacts with the reduced (cuprous) cation that was formed in the first step and exhibits a colour-intense stable complex with a linear absorption at $\lambda_{nm} = 562$ nm, increasing with protein concentrations. Samples were diluted 1:50 and the total protein concentration was measured following manufacturer's instructions.

4.5.3 Enzyme-linked immunosorbent assays (ELISA)

ELISA kits were used to quantify protein concentrations in cell culture supernatant of stimulated primary microglia cells and human amyloid-β (h$A\beta$42, h$A\beta$40) in mouse brain homogenates. The so-called sandwich assays are based on the principle of antibody-mediated detection of a specific protein. In summary, 96-well plates are coated with a specific antibody against the target antigen. After application of the sample, the target antigens binds to the specific antibody and unbound proteins are discarded and washed, to exclude false-positive reactions. Subsequently, a secondary antibody, specific for the target antigen, is added. As this antibody is coupled to the enzyme horse radish peroxidase and can catalyse oxidation of the chromogenic substrate 3,3',5,5'-tetramethylbenzidine (TMB), resulting in a directly proportional light-sensitive detection signal. This specific colour shift was detected using a plate reader at $\lambda_{nm} = 450$ nm. For the determination of cytokines or chemokines concentrations, the samples were diluted individually for each target protein and concentrations were determined according to the manufacturers instructions.

4.5.4 RNA isolation

Ribonucleic acid (RNA) from hippocampal tissue was isolated using TRIzol® protocol. Therefore, frozen tissue samples were transferred to 2 ml tubes containing 1.4 mm zirconium oxide beads and homogenised in TRIzol® (800 μl TRIzol®) by vigorous shaking (2 x 30 sec with 5,000 rpm) in the

Precellys® tissue homogenizer. Homogenised tissue was transferred to a new tube and spun down (12,000 *g*, 10 min, 4°C), to exclude bigger tissue aggregations. After transferring the supernatant to another fresh tube, 1-bromo-3-chloropropane (BCP) (1:5) was added and the samples were mixed thoroughly for 30 sec. After a 10 min incubation at RT, samples were spun down (12,000 *g*, 10 min, 4°C). Subsequently, the RNA-containing upper phase (aqueous) was transferred into a new tube and precipitated with 400 μl isopropyl alcohol. After two washing steps with 75% ethanol, dried RNA pellets were dissolved in 20 μl RNase-free water. Samples were stored at -80°C.
RNA concentration of each sample was measured using NanoDrop spectrophotometer. RNA shows an absorption maximum at $\lambda_{nm} = 260$ nm (A_{260}) and the ratio of A_{260} and A_{280} is used to assess RNA purity of each sample preparation. The absorption of 1 unit at 260 nm is equivalent to a RNA concentration of 40 μl/ml. Protein or phenol impurities can influence this ratio due to different absorption maxima.

4.5.5 cDNA synthesis

For complementary DNA (cDNA) synthesis, 400 ng RNA were incubated for 5 min at 65°C and then reversely transcribed at 42°C for 50 minutes. For each sample, cDNA synthesis was performed using the following master mix reaction and an intermittent cycling program:

master mix per sample (8 μl)	
5x first strand buffer	5 μl
DTT (0.1 M)	2 μl
dNTPs (10 mM)	1 μl

cycling parameters for 1 μl RNA + 1 μl Oligo (dt) primer:	
70°C	10 min
4°C	3 min
add 8 μl master mix per sample	
42°C	2 min
4°C	3 min
add 1 μl reverse transcriptase per sample	
42°C	60 min
70°C	15 min
4 °C	10 min

cDNA samples were adjusted to a final concentration of 10 ng/μl and stored at -20°C.

4.5.6 Quantitative real-time PCR

Quantitative real-time PCR (qRT-PCR) was conducted to quantify gene expression levels in animals dependent on age and genotype. This method offers the possibility to track DNA amplification in real-time by making use of the fluorescence resonance energy transfer (FRET). A gene-specific oligonucleotide probe, fluorescently labeled at the 5' end (6-carboxyfluorescein, acronym: FAM) and quenched at the 3' end with a non-fluorescent tag (tetramethylrhodamine, acrony: TAMRA), is added to the cDNA sample together with an unlabelled pair of primers. During the annealing phase, the probe hybridises with the complementary target sequence and the 5'→ 3' exonuclease activity of the Taq polymerase allows degradation of the probe. Thereby, the fluorochrome is released from the quencher, while fluorescence intensity increases which each cycle. This is proportional to the amount of cDNA template available in the sample. To determine the relative expression, the difference (Δ) between the crossing points (CP) of a target gene and a constitutively expressed reference gene is measured (ΔCP) [148]. Each sample was run in triplicates; for each gene one water control was used as a negative control to account for possible contaminations.

PCR setup for TaqMan gene expression analysis:	
cDNA (= 10 ng/μl)	4 μl
RNase-free water	0.5 μl
2x Taqman Gene Expression Master Mix	5 μl
20x Taqman Gene Expression Assay	0.5 μl

Cycling parameters:		
1 x	95°C	10 min
40-45 x	95°C	15 sec
	60°C	60 sec

ΔCP values were calculated by subtracting the CP values of the internal reference gene glyceraldehyde 3-phosphate dehydrogenase (GAPDH). Afterwards, $2^{-\Delta CP}$ values were calculated.

4.6 Immuno-histochemical methods

4.6.1 Cryo sectioning

TissueTek-embedded frozen brains were sliced sagitally or coronally into 12 or 14 μm slices, respectively. Sagittal slices were taken starting from a lateral depth of 1.92 mm to a lateral depth of 0.24 mm (for hippocampus). Coronal slices were taken from bregma -0.94 mm to -3.08 mm (for hippocampus and cortex). Every second slice was taken on Superfrost^{TM} microscope slides (three slices per slide) and slides were stored at -20°C until staining.

4.6.2 Thioflavine T staining

The AD mouse model, APP/PS1, develops Aβ aggregates with increasing age. These aggregates contain β-sheet-rich structures, which can be specifically detected by benzothiazol dyes, such as thioflavin T or thioflavin S. These compounds display a dramatic shift of the excitation maximum (from 385 nm to 450 nm) and the emission maximum (from 445 nm to 482 nm), and are therefore widely used chemical compounds to specifically stain Aβ plaques in mouse models of AD. Brain slices were thawed for 5 min at 4°C, washed for 5 min in PBS, and incubated in 280 ml of 0.025% (w/v) thioflavine T solution (1:2 EtOH/PBS). Slices were washed twice with PBS for 5 min and subsequently embedded with Fluoromount^{TM} aqueous mounting medium. Cover slips were fixed with nail polish. For quantification, numbers of Aβ plaques were counted in 1 mm^2 in 4 to 9 sections per animal by using a self-established makro for ImageJ (1.50i, Wayne Rasband, National Institute of Health, USA).

4.6.3 Iba1, NeuN and Parv immunostaining

Brain slices from all genotypes were prepared as described above (4.6.1). Slices were thawed at 37°C for 30 min, washed with PBS and subsequently permeabilised with 0.2% (v/v) Triton^{TM} X-100 for 20 min. After washing with PBS for 10 min, slices were blocked in 3% (w/v) bovine serum albumin (BSA) for 20 min at RT. After blocking, the primary antibody (see table 3.1) was diluted in 0.5% BSA (w/v) and directly applied onto the slices. Incubation was conducted in a moist chamber at 4°C over night (for dilutions of antibodies see table 3.1). The following day, slices were washed 3 times followed by the incubation with the secondary antibody, diluted in 0.5% BSA (w/v), for 1 h at RT. Finally, slices were washed again and mounted in 4',6-diamidino-2-phenylindole (DAPI) Fluoromount^{TM}. To avoid drying-out, cover slips were sealed using nail polish.

4.7 Behavioral phenotyping

The Morris water maze (MWM) task, developed by Richard Morris in the early 1980's [176], is one of the most widely used methods to examine cognitive performances in tg AD mice. Using this task, spatial learning and memory can be assessed. Thereby, mice are trained to find a hidden platform in large pool of milky water using visual keys. Learning ability of the mouse is given by the escape latency, the time to find the hidden platform. As a second parameter, memory strength can be measured. Thereby, the platform is removed after the acquisition phase and the time spent in each quadrant is measured. In the current study, mice were trained to find the hidden platform over five consecutive days with four trails per day. To assess small genotype differences in the acquisition phase, the intertrial time was set to 1 h.

4.8 Statistical analyses

To determine differences between genotype- and treatment- or age-groups, two-way analysis of variance (ANOVA) and Tukey's multiple comparisons test were used, except if stated otherwise. For statistical analysis within one age-group, one-way ANOVA followed by Tukey's multiple comparisons test was used. To detect genotype differences in the Morris water maze learning paradigm over the training period, two-way ANOVA followed by Sidak's multiple comparisons test was used. Data are given as mean ± standard error of the mean (SEM). All tests were performed with GraphPad Prism 5 software (GraphPad Software, San Diego, USA) and $p \leq 0.05$ was considered significant.

4.9 Integrated projects and cooperation partners

Within my PhD thesis, a side project was overtaken by a medical PhD student. Immunohistochemical experiments involving staining for the marker neuronal nuclei (NeuN) and parvalbumin (Parv) were performed by Gregor Toporowski in the context of his medical thesis. Stimulation experiments of primary microglia cells were done in cooperation with Dr. Anne Schmoele from the German centre of neurological diseases (DZNE), Bonn, Germany. Analyses of endocannabinoids and related lipids in cortical and hippocampal tissue of 9- and 14-month-old mice was conducted in a cooperation with the lipidomic group of Prof. Dr. Beat Lutz and Dr. Laura Bindila from the Institute of physiological chemistry of the University Medical Center Mainz, Germany.

5 Results

5.1 Role of microglial CB2 receptor signalling in vitro

5.1.1 Microglia derived from CB2$^{-/-}$ mice are less responsive to pro-inflammatory stimuli

To examine the role of CB2 signalling on microglia polarisation, primary neonatal microglia cells derived from CB2$^{+/+}$ and CB2$^{-/-}$ mice were stimulated with LPS and IFNγ to induce a pro-inflammatory activation state. Cell surface marker expression, analysed as mean fluorescence intensity (MFI) via flow cytometry, was compared. After stimulation, mean expression of the intercellular adhesion molecule (ICAM) was significantly increased in microglia derived from both, CB2$^{+/+}$ (mean ICAM-MFI: 709 vs. 4944; $p < 0.0001$) and CB2$^{-/-}$ (mean ICAM-MFI: 694 vs. 1409; $p = 0.0016$) mice as compared to each unstimulated control (Fig. 5.1, A). However, even though CB2$^{-/-}$ microglia responded with an upregulation of ICAM upon LPS/IFNγ stimulation, this increase was markedly reduced in comparison to stimulation-induced ICAM-upregulation in CB2$^{+/+}$ microglia (2-way ANOVA, genotype effect $F_{1,12} = 273.3$, $p < 0.0001$).

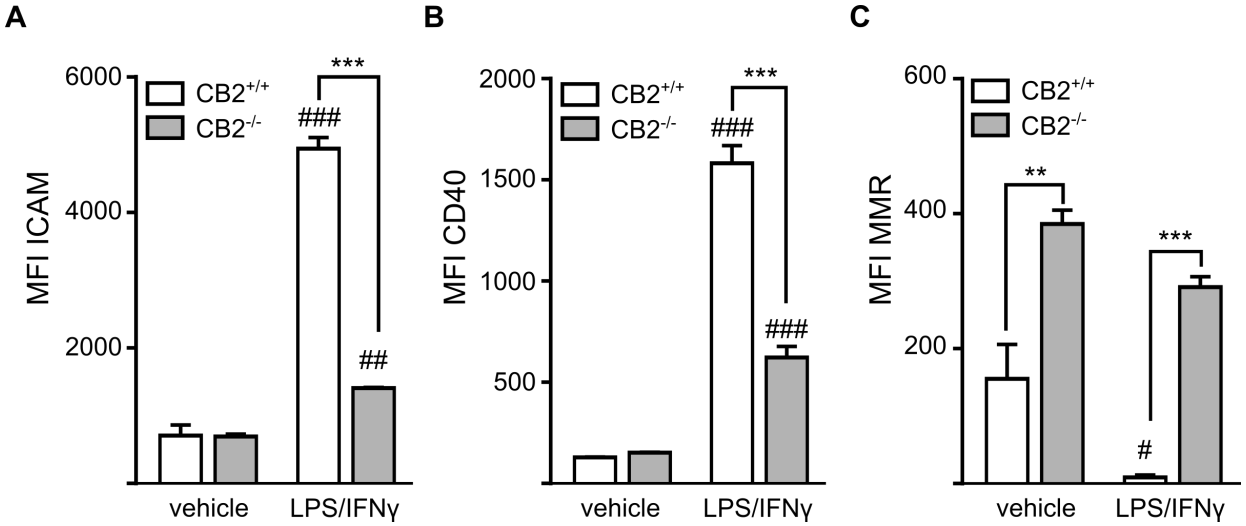

Figure 5.1: Expression levels of cell-surface marker in CB2$^{+/+}$ and CB2$^{-/-}$ primary microglia. Upon stimulation with LPS/IFNγ, expression of cell-surface marker ICAM (A), CD40 (B) and MMR (C) was compared to unstimulated controls (vehicle). In CB2$^{-/-}$ microglia (light gray bars), ICAM and CD40 expression was significantly reduced when compared to corresponding CB2$^{+/+}$ microglia (white bars), while MMR expression was increased under basal and stimulatory conditions in CB2$^{-/-}$ microglia. N = 3; samples were run in triplicates. Data were analysed by 2-way ANOVA, followed by Tukey's multiple comparisons test, $*p < 0.05$, $**p < 0.01$, $***p < 0.001$; # significance to unstimulated corresponding genotype control.

A similar expression pattern and a highly significant genotype effect (2-way ANOVA, genotype effect $F_{1,10} = 62.25$, $p < 0.0001$) was observed for expression levels of the co-stimulatory molecule CD40 (Fig. 5.1, B). Upon LPS/IFNγ challenge, CD40 expression was 12-fold increased in cultures of $CB2^{+/+}$ microglia (mean CD40-MFI: 130 vs. 1583; $p < 0.0001$) as compared to a four-fold increase in $CB2^{-/-}$ microglia cultures (mean CD40-MFI: 153 vs. 622; $p = 0.0004$). Finally, expression levels of the anti-inflammatory marker MMR was investigated (Fig. 5.1, C). Under basal conditions, $CB2^{-/-}$ microglia showed increased expression levels of MMR as compared to cultures derived from $CB2^{+/+}$ ($p = 0.0016$). Upon LPS/IFNγ stimulation, expression levels of MMR were significantly reduced in $CB2^{+/+}$ cells ($p = 0.0419$), whereas expression levels in $CB2^{-/-}$ microglia remained constant ($p = 0.2996$; Fig. 5.1, C) in comparison to basal expression levels. Conclusively, $CB2^{+/+}$ and $CB2^{-/-}$ microglia showed highly significant cell surface marker expression of MMR upon pro-inflammatory stimulation (2-way ANOVA, genotype effect $F_{1,12} = 31.56$, $p = 0.0001$; followed by Tukey's multiple comparisons test: $p = 0.0003$).

Following analyses of cell surface marker expression, the secretion of cytokines and chemokines upon pro-inflammatory stimulation was analysed as an indicator of microglial activation. Via ELISA measurements, levels of secreted TNFα, IL-6, CCL2 and IL-10 were analysed in cell culture supernatants of unstimulated (vehicle) and stimulated microglia derived from $CB2^{+/+}$ and $CB2^{-/-}$ mice. Similar to the expression profile of cell-surface marker, secretion of the pro-inflammatory cytokine TNFα was significantly induced after challenge with LPS/IFNγ in both groups (2-way ANOVA, stimulation effect $F_{2,12} = 1437$, $p < 0.0001$; Fig. 5.2, A). However, microglia derived from $CB2^{-/-}$ mice secreted significantly less TNFα than microglia derived from $CB2^{+/+}$ mice (2-way ANOVA, genotype effect $F_{1,12} = 33.40$, $p < 0.0001$; followed by Tukey's multiple comparisons test: $p < 0.0001$). A highly significant stimulation and genotype effect was also observed for the levels of secreted IL-6 (2-way ANOVA, stimulation effect $F_{2,11} = 165.1$, $p < 0.0001$; genotype effect $F_{1,11} = 121.7$, $p < 0.0001$; Fig. 5.2, A). In $CB2^{+/+}$ microglia, IL-6 secretion was significantly induced by LPS/IFNγ challenge ($p < 0.0001$), while IL-6 levels in stimulated $CB2^{-/-}$ microglia were significantly reduced as compared to levels of $CB2^{+/+}$ microglia ($p < 0.0001$; Fig 5.2, B). Secretion of the monocytic migratory chemokine CCL2 was highly upregulated in LPS/IFNγ challenged microglia derived from $CB2^{+/+}$ mice ($p < 0.0001$; Fig. 5.2, C). In contrast, $CB2^{-/-}$ microglia did not upregulate CCL2 secretion after pro-inflammatory stimulation ($p > 0.9999$), thus a highly significant genotype difference was detected (2-way ANOVA, genotype effect $F_{1,12} = 144.2$, $p < 0.0001$; followed by Tukey's multiple comparisons test: $p < 0.0001$; Fig. 5.2, C). Furthermore, secretion of the anti-inflammatory cytokine IL-10 was analysed. Under basal conditions, IL-10 secretion was not detectable in cell cultures derived from $CB2^{+/+}$ nor from $CB2^{-/-}$ mice (Fig. 5.2, D). However, LPS/IFNγ treatment significantly induced the secretion of IL-10 in cell cultures obtained from mice of both genotypes (2-way ANOVA, stimulation effect $F_{2,12} = 1313$, $p < 0.0001$;

Fig. 5.2, C). Interestingly, a LPS/IFNγ-initiated upregulation of IL-10 was significantly more pronounced in samples of $CB2^{-/-}$ than in samples of $CB2^{+/+}$ microglia (2-way ANOVA, genotype effect $F_{1,12} = 255.7$, $p < 0.0001$; followed by Tukey's multiple comparisons test: $p < 0.0001$; Fig. 5.2, D). In general, microglia derived from $CB2^{-/-}$ mice seemed to be less responsive in terms of an induced expression of pro-inflammatory cell-surface marker or the secretion of pro-inflammatory cytokines and chemokines upon inflammatory conditions. On the contrary, expression or secretion of anti-inflammatory markers, such as MMR and IL-10, respectively, was significantly enhanced in $CB2^{-/-}$ microglia as compared to $CB2^{+/+}$ controls.

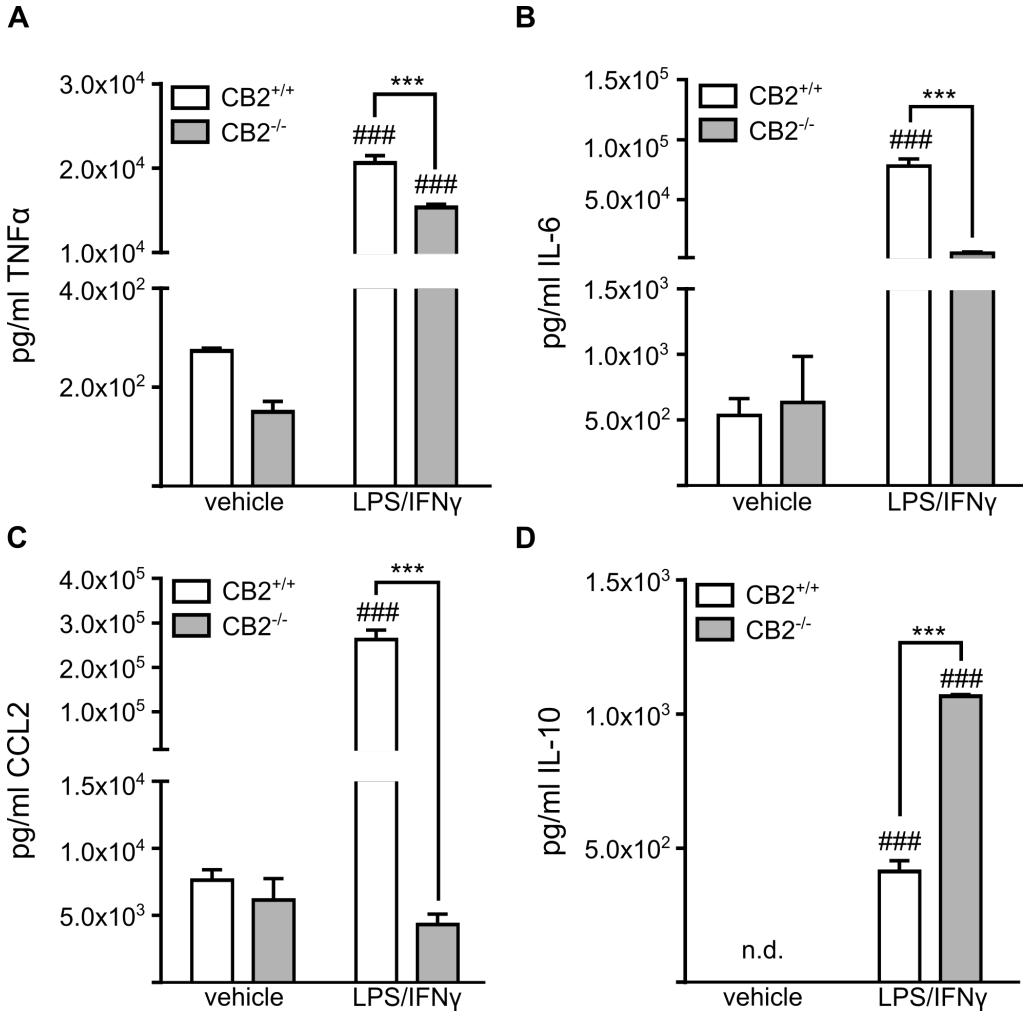

Figure 5.2: Measurement of cytokine and chemokine release in supernatants of $CB2^{+/+}$ and $CB2^{-/-}$ primary microglia. After stimulation with LPS/IFNγ, secretion of TNFα (A), IL-6 (B), CCL2 (C) and IL-10 (D) was quantified in microglia from $CB2^{+/+}$ (white bars) and $CB2^{-/-}$ (light gray bars) and compared to unstimulated controls (vehicle). Microglia from $CB2^{-/-}$ displayed a markedly reduced secretion of TNFα IL-6 and CCL2 in comparison to microglia derived from $CB2^{+/+}$ mice, while secretion of IL-10 was increased in $CB2^{-/-}$ upon LPS/IFNγ stimulation. N = 3; samples were run in triplicates. Data were analysed by 2-way ANOVA, followed by Tukey's multiple comparisons test, $*p < 0.05$, $**p < 0.01$, $***p < 0.001$; # significance to corresponding unstimulated genotype control.

5.1.2 Microglia and macrophages derived from CB2$^{-/-}$ mice show equal phagocytic capacities compared to cultures from CB2$^{+/+}$ mice

We next determined whether the reduced pro-inflammatory activation profile observed in CB2$^{-/-}$ microglia was also associated with changes in the phagocytic efficacy of microglia. Therefore, the uptake of fluorescently labelled Aβ by neonatal microglia and BMdM derived from CB2$^{+/+}$ and CB2$^{-/-}$ mice was analysed. Cells were incubated with DyLight647®-labelled Aβ for 1 h at 37°C to analyse their phagocytic activity. A control experiment was conducted simultaneously at 4°C to account for unspecific binding. Using flow cytometric analysis, living cells were gated for their expression of CD11b to determine the proportion of microglia. Subsequently, CD11b^{+} cells were gated for their expression of DyLight647® to analyse the proportion of cells that phagocytosed Aβ.

Via dot plot analysis, we identified a proportion of approximately 50% CD11b^{+} microglia, that took up DyLight647®-labelled Aβ at 37°C when compared to the control group at 4°C (Fig. 5.3, A; upper right quadrant). Quantification revealed an equivalent percentage of CB2$^{+/+}$ and CB2$^{-/-}$ microglia that phagocytosed Aβ, thus a genotype specific difference regarding the phagocytic activity was absent (Fig. 5.3, B). Similarly, histograms of DyLight647®-labelled Aβ fluorescence intensity were comparable between both genotypes (representatively shown in Fig. 5.3, C).

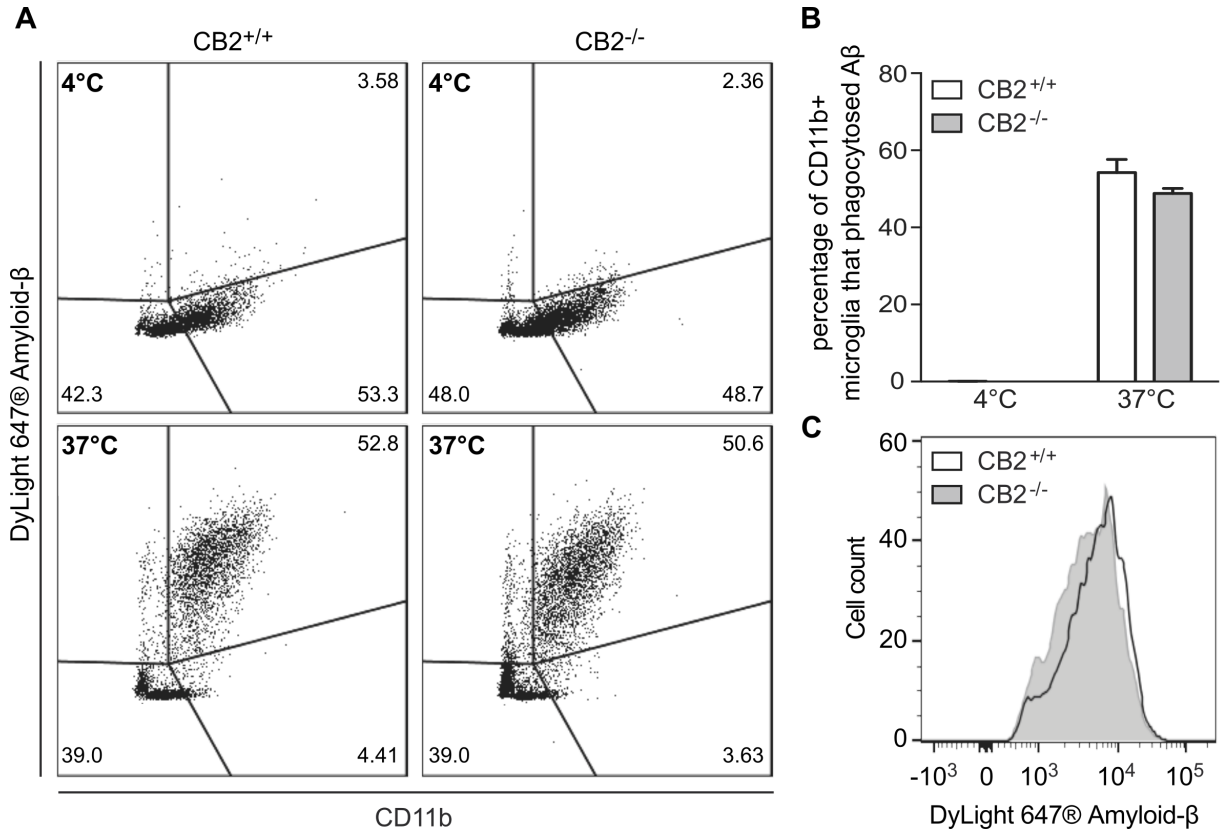

Figure 5.3: Phagocytosis of fluorescently labelled Aβ by primary neonatal microglia. Representative dotplots of Aβ uptake by CB2$^{+/+}$ and CB2$^{-/-}$ microglia analysed by flow cytometry (A). Quantification of the percentage of cells, that phagocytosed labelled Aβ (B). Representative histogram of Aβ fluorescence intensity labelled with DyLight647® and cell count of CB2$^{+/+}$ and CB2$^{-/-}$ microglia (C).

As infiltrating macrophages have been discussed as better phagocytes [150], we next analysed BMdM for their ability to take up fluorescently-labelled Aβ. Analogous to microglia, their phagocytic activity was evaluated via flow cytometry and quantified as the proportion of macrophages (CD11b$^+$), which took up fluorescently labelled Aβ (Fig. 5.4, A). After quantification, a comparable proportion of BMdM phagocytosed Aβ within both genotypes (Fig. 5.4, B). Similar to neonatal microglia, also the fluorescence intensity of DyLight647®-labelled Aβ remained comparable between both genotypes (Fig. 5.4, C). These data demonstrate that the presence or absence of CB2 signalling did not affect the efficiency of Aβ phagocytosis in primary neonatal microglia or BMdM.

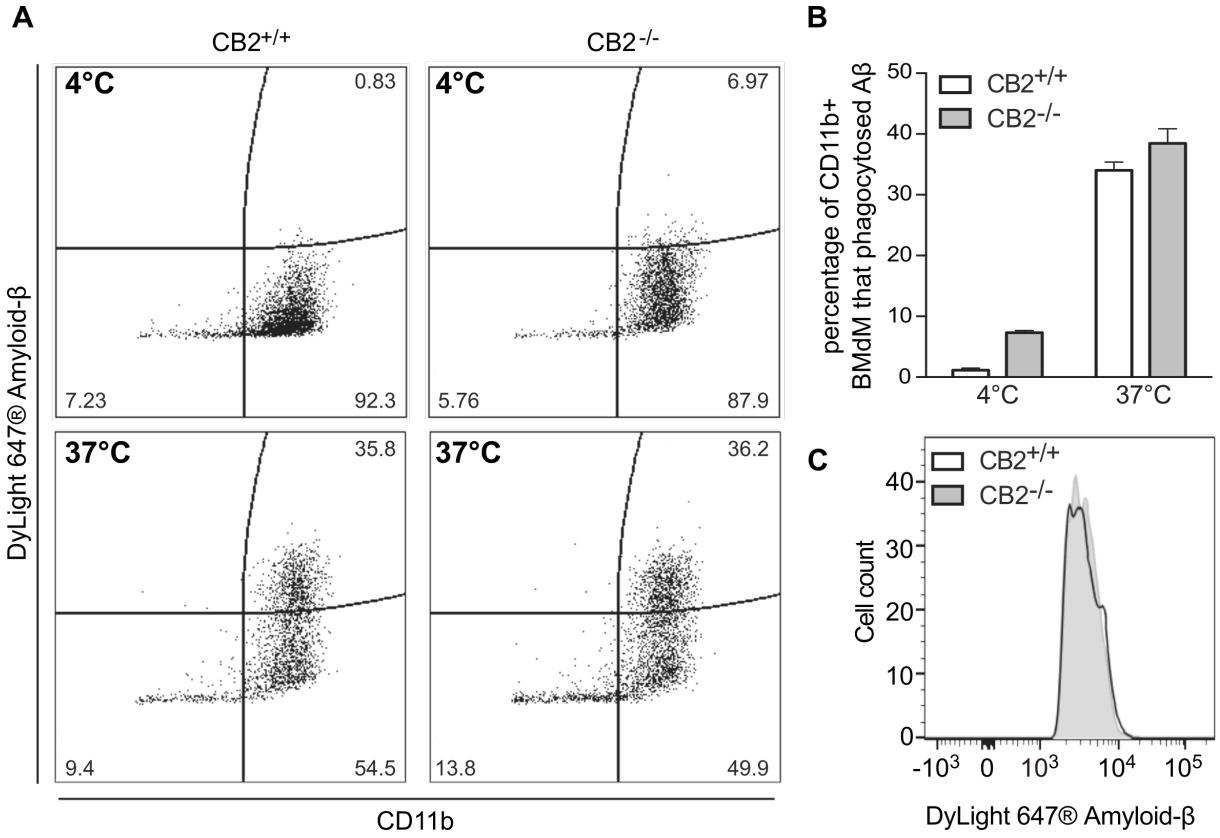

Figure 5.4: Phagocytosis of fluorescently labelled Aβ by BMdM. Representative dotplots of Aβ uptake by bone-marrow derived CB2$^{+/+}$ and CB2$^{-/-}$ macrophages analysed by flow cytometry (A). Quantification of the percentage of cells, that phagocytosed labelled Aβ (B). Representative histogram of Aβ fluorescence intensity labelled with DyLight647® and cell count of CB2$^{+/+}$ and CB2$^{-/-}$ BMdM (C).

5.2 Role of CB2 signalling on expression of ECS components

5.2.1 mRNA expression of ECS receptors is altered in APP/PS1∗CB2$^{-/-}$

ECS components are known to change with age and disease progression in humans. Therefore, we examined whether the expression of humanised APP and mutated presenilin also influenced expression levels of cannabinoid receptors, endocannabinoid-producing enzymes or the levels of the main endocannabinoids and cannabinoid-related lipids in 9- and 14-month-old tg and control mice. Hippocampal tissue of 9- and 14-month-old mice was subjected to qRT-PCR and target gene expression levels were compared to expression levels of the internal reference gene GAPDH (Fig. 5.5).

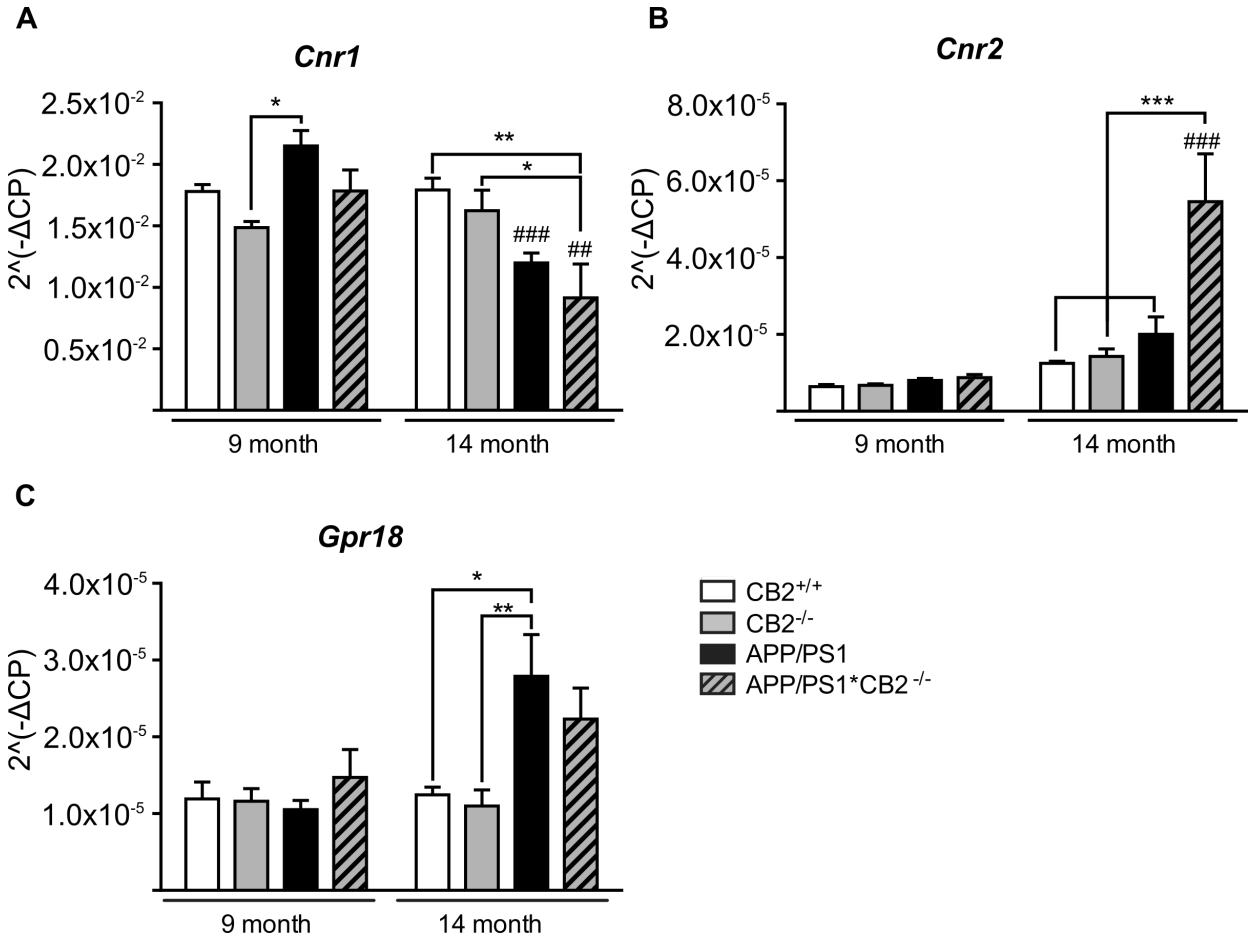

Figure 5.5: Expression levels of endocannabinoid system receptors. Shown are expression levels of the cannabinoid receptor 1 (*Cnr1*, A), *Cnr2* (B) and the orphan cannabinoid receptor *Gpr18* (C). n = 5-8; samples were run in triplicates. Data were analysed by 2-way ANOVA followed by Tukey's multiple comparisons test, $*p < 0.05$, $**p < 0.01$, $***p < 0.001$; # significance to corresponding 9-month-old group.

Overall, cannabinoid receptor 1 (*Cnr1*) mRNA expression levels were significantly altered by age ($F_{1,53} = 15957$, $p = 0.0002$), genotype ($F_{3,53} = 3.096$, $p = 0.0345$) and interaction ($F_{3,53} = 7.572$, $p = 0.0003$; Fig. 5.5, A). Specifically, *Cnr1* mRNA levels were age-dependently decreased in APP/PS1 ($p = 0.0003$) and APP/PS1∗CB2$^{+/+}$ mice ($p = 0.0031$) in comparison to the corresponding 9-month-old group. In samples of 9-month-old APP/PS1 mice, *Cnr1* mRNA expression levels

were slightly upregulated compared to CB2$^{-/-}$ mice ($p = 0.0292$), while expression levels in CB2$^{+/+}$ and APP/PS1$*$CB2$^{-/-}$ were comparable (Fig. 5.5, A). In 14-month-old mice, a significant decrease in *Cnr1* mRNA levels was found in samples of APP/PS1$*$CB2$^{-/-}$ mice when compared to expression levels in CB2$^{+/+}$ ($p = 0.0027$) or CB2$^{-/-}$ ($p = 0.0285$) hippocampal tissue (Fig. 5.5, A).

As an increased expression of CB2 receptors has been associated with AD pathology in recent years, we also investigated *Cnr2* expression levels in both age groups. In 9-month-old mice, *Cnr2* expression was comparable between the four groups, even in CB2$^{-/-}$ mice (Fig. 5.5, B). The expression of *Cnr2* in tissue samples of CB2$^{-/-}$ mice is due to the expression of a truncated CB2 receptor, because the strategy used to generate CB2 knockout mice was by replacing a part of the coding exon with a neomycin resistance cassette. This resulted in the deletion of part of the intracellular loop 3, the transmembrane domains 6 and 7 as well as the carboxy terminus. Even though ligand receptor binding studies were used to confirm the loss of CB2 receptor function [33], the remaining N-terminus is still expressed. Therefore, currently available antibodies targeting this N-terminus still lead to the detection of a truncated CB2 receptor.

Nevertheless, we detected a significantly increased *Cnr2* expression in samples of 14-month-old APP/PS1$*$CB2$^{-/-}$ mice when compared to 9-month-old APP/PS1$*$CB2$^{+/+}$ mice ($p < 0.0001$) and in comparison to age-matched CB2$^{+/+}$ ($p < 0.0001$), CB2$^{-/-}$ ($p < 0.0001$) and APP/PS1 ($p < 0.0001$), suggesting a compensatory effect.

Gene expression of the recently discovered orphan cannabinoid receptor *Gpr18* remained stable in hippocampal tissue of all four 9-month-old groups (Fig. 5.5, C). However, in 14-month-old mice, *Gpr18* expression was significantly altered with age ($F_{1,54} = 6.641$, $p = 0.0127$) and genotype ($F_{3,54} = 2.954$, $p = 0.0405$). In detail, *Gpr18* gene expression was remarkably upregulated in APP/PS1 mice as compared to CB2$^{+/+}$ ($p = 0.0209$) and CB2$^{-/-}$ ($p = 0.0053$) mice, as analysed by Tukey's multiple comparisons test.

5.2.2 mRNA expression of ECS enzymes is altered with age

Subsequent to expression analyses of the main endocannabinoid receptors, expression levels of the main enzymes responsible for endocannabinoid synthesis and degradation were analysed. Statistical analysis of *Dagl*α gene expression in hippocampal tissue of 9- and 14-month-old mice showed a significant interaction ($F_{3,51} = 4.459$, $p = 0.0074$), age ($F_{1,51} = 18.64$, $p < 0.0001$) and genotype effect ($F_{3,51} = 3.204$, $p = 0.0308$). Interestingly, *Dagl*α gene expression was exclusively upregulated in tissue of 14-month-old APP/PS1$*$CB2$^{-/-}$ mice as compared to age-matched control groups ($p = 0.0032$ vs CB2$^{+/+}$, $p = 0.0017$ vs CB2$^{-/-}$, $p = 0.0469$ vs APP/PS1) or expression levels in hippocampal tissue of 9-month-old mice APP/PS1$*$CB2$^{-/-}$ ($p = 0.0002$; Fig. 5.6, A). In all other groups, *Dagl*α gene expression was unaltered.

While gene expression levels of *Magl* remained comparable in hippocampal tissue samples of

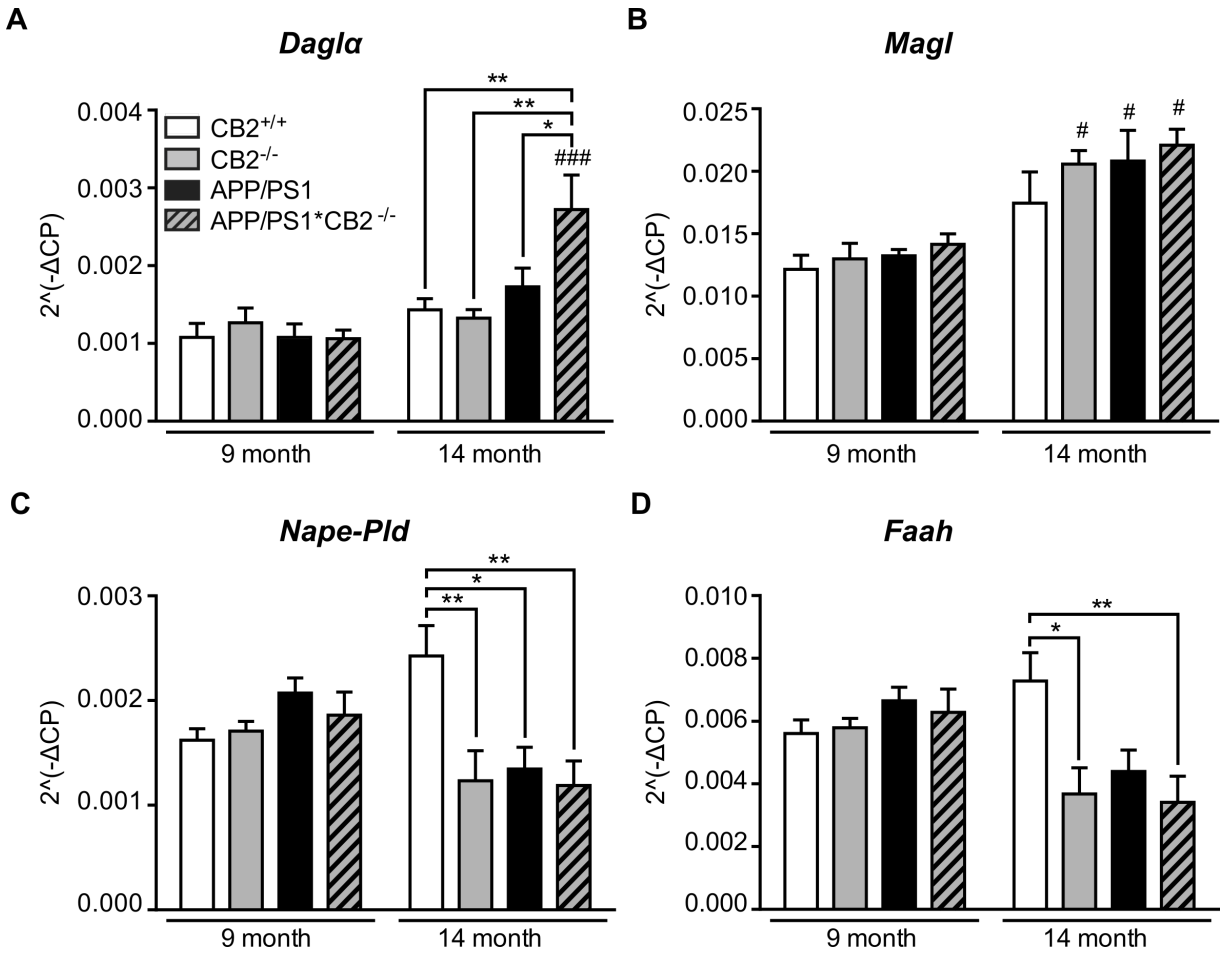

Figure 5.6: Expression levels of endocannabinoid system synthesizing and degrading enzymes. Shown are expression levels of 2-AG synthesizing and degrading enzymes *Daglα* (A) and *Magl* (B), AEA synthesizing and degrading enzymes *Faah* (C) and *Nape-Pld* (D). n = 5-8; samples were run in triplicates. Data were analysed by 2-way ANOVA followed by Tukey's multiple comparisons test, $*p < 0.05$, $**p < 0.01$, $***p < 0.001$; # significance to corresponding 9-month-old group.

9-month-old animals, *Magl* mRNA expression levels were significantly upregulated in hippocampal tissue of 14-month-old $CB2^{-/-}$ ($p = 0.0401$), APP/PS1 ($p = 0.0219$) and APP/PS1$*$$CB2^{-/-}$ ($p = 0.0393$; Fig. 5.6, B) mice, respectively. This finding was accompanied by a highly significant age effect (2-way ANOVA, $F_{1,51} = 38.44$, $p < 0.0001$).

Similar to *Daglα* and *Magl*, gene expression of *Nape-Pld*, the main enzyme responsible for the biosynthesis of AEA, was not altered in hippocampal tissue of 9-month-old mice (Fig. 5.6, C). However, a highly significant interaction effect ($F_{3,52} = 5.977$, $p = 0.0014$) and a significant genotype effect ($F_{3,52} = 2.826$, $p = 0.0475$) was detected. In detail, *Nape-Pld* expression levels were significantly decreased in tissue samples of 14-month-old $CB2^{-/-}$ ($p = 0.0049$), APP/PS1 ($p = 0.0106$) and APP/PS1$*$$CB2^{-/-}$ ($p = 0.0031$) mice when compared expression levels of age-matched $CB2^{+/+}$ mice.

The expression pattern of the enzyme responsible for AEA degradation, *Faah*, was comparable with the expression pattern of *Nape-Pld* (Fig. 5.6, D). In 9-month-old animals, *Faah* gene expression levels were almost equal, while gene expression levels were significantly reduced in samples of aged

$CB2^{-/-}$ and APP/PS1∗$CB2^{-/-}$ as compared to 14-month-old $CB2^{+/+}$ littermates ($p = 0.0126$ and $p = 0.0037$, respectively). These findings were further confirmed by a significant interaction ($F_{3,53} = 4.536$, $p = 0.0067$) and age effect ($F_{1,53} = 8.638$, $p = 0.0049$; Fig. 5.6, D).

5.2.3 Endocannabinoid level in cortex and hippocampus

Subsequent to gene expression analyses of cannabinoid receptors as well as synthesizing and hydrolysing enzymes, secretion of the main endocannabinoids 2-AG and AEA was evaluated. Additionally, secretion levels of ARA, a polyunsaturated fatty acid present in diacylgylcerol, and N-palmitoylethanolamine (PEA), an anti-inflammatory and analgesic mediator, were analysed. Lipid extraction of hippocampal and cortical tissue samples and measurements of endocannabinoid levels were conducted in a collaboration with Prof. Dr. Beat Lutz and Dr. Laura Bindila from the institute of physiological chemistry, University Medical Center Mainz, Germany.
In cortical tissue of 9- and 14-month-old mice, we were not able to detect significant differences in the secretion of AEA between the four individual groups, however a significant interaction effect was observed ($F_{3,40} = 4.036$, $p = 0.0134$; Fig. 5.7, A).

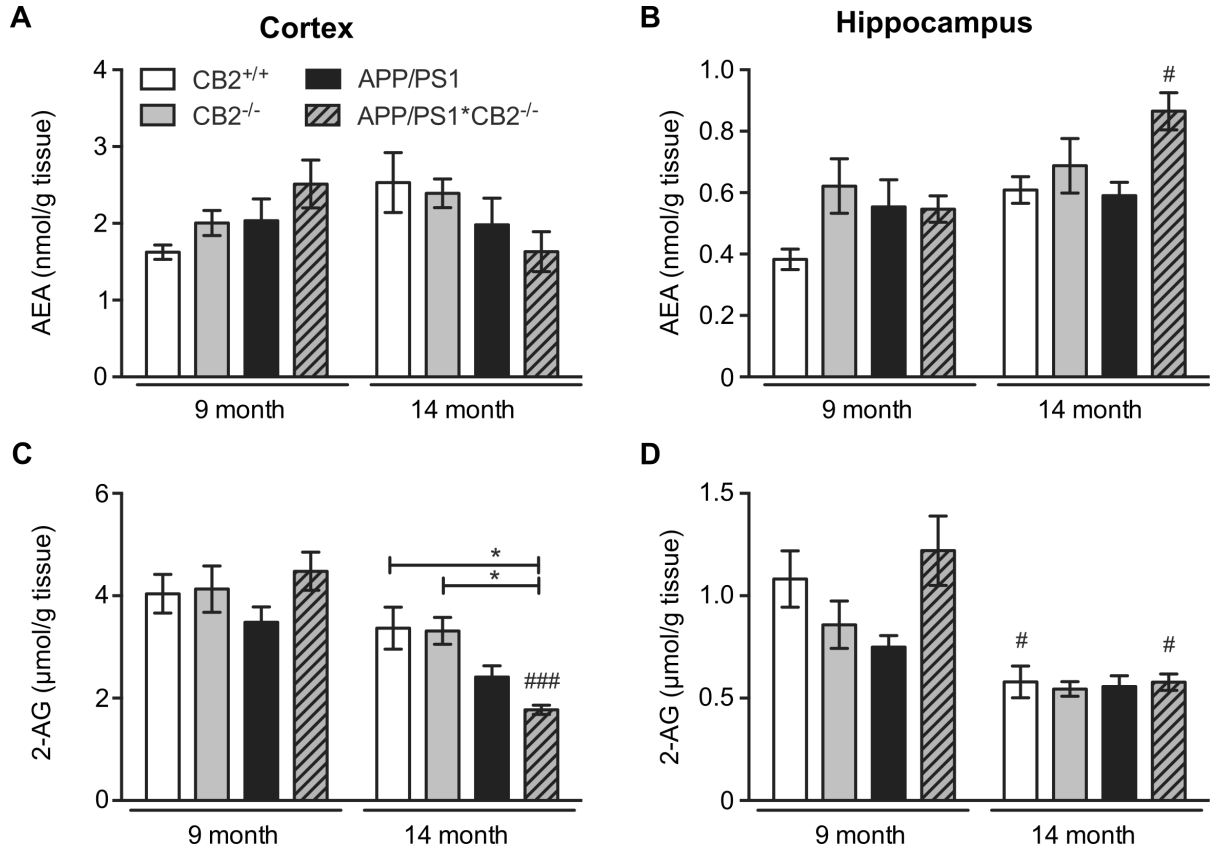

Figure 5.7: Secretion of AEA and 2-AG in cortical and hippocampal tissue of 9- and 14-month-old mice. Quantification of AEA (A, B) and 2-AG (C, D) secretion in cortical and hippocampal tissue of 9- and 14-month-old mice. n = 5-8; Data were analysed by 2-way ANOVA followed by Tukey's multiple comparisons test, $*p < 0.05$, $**p < 0.01$, $***p < 0.001$; # significance to corresponding 9-month-old group.

In comparison to cortical tissue, AEA measurements in hippocampal tissue were age- and genotype-dependently regulated (age effect $F_{1,40} = 12.61$, $p = 0.0010$ and genotype effect $F_{3,40} = 4.041$, $p = 0.0134$; Fig. 5.7, B). In detail, secretion levels of AEA were significantly increased in 14-month-old APP/PS1$*$CB2$^{-/-}$ as compared to levels of 9-month-old APP/PS1$*$CB2$^{-/-}$ mice ($p < 0.0139$), as analysed by Tukey's multiple comparisons test. In all other mouse groups, significant alterations regarding AEA secretion were not detected. At the age of 9 months, 2-AG secretion of cortical tissue was comparable between the four groups (Fig. 5.7, C). However, at the age of 14 months, 2-AG secretion was significantly reduced in APP/PS1$*$CB2$^{-/-}$ when compared to 9-month-old APP/PS1$*$CB2$^{-/-}$ ($p < 0.0001$) as well as in comparison to age-matched CB2$^{+/+}$ ($p = 0.0414$) and CB2$^{-/-}$ mice ($p = 0.0370$). These findings were further accompanied by significant interaction ($F_{3,40} = 4.089$, $p = 0.0127$), age ($F_{1,40} = 31.65$, $p < 0.0001$) and genotype ($F_{3,40} = 2.883$, $p = 0.0476$) effects (Fig. 5.7, C). In hippocampal tissue, the secretion of 2-AG was age-dependently reduced in CB2$^{+/+}$ ($p = 0.0395$) and APP/PS1$*$CB2$^{-/-}$ mice ($p = 0.0016$) when compared to corresponding secretion levels of 9-month-old mice. These results were also reflected by a highly significant age effect ($F_{1,41} = 30.14$, $p < 0.0001$). In contrast, 2-AG secretion in tissue samples of CB2$^{-/-}$ and APP/PS1$*$CB2$^{+/+}$ mice remained constant between both age groups (Fig. 5.7, D).

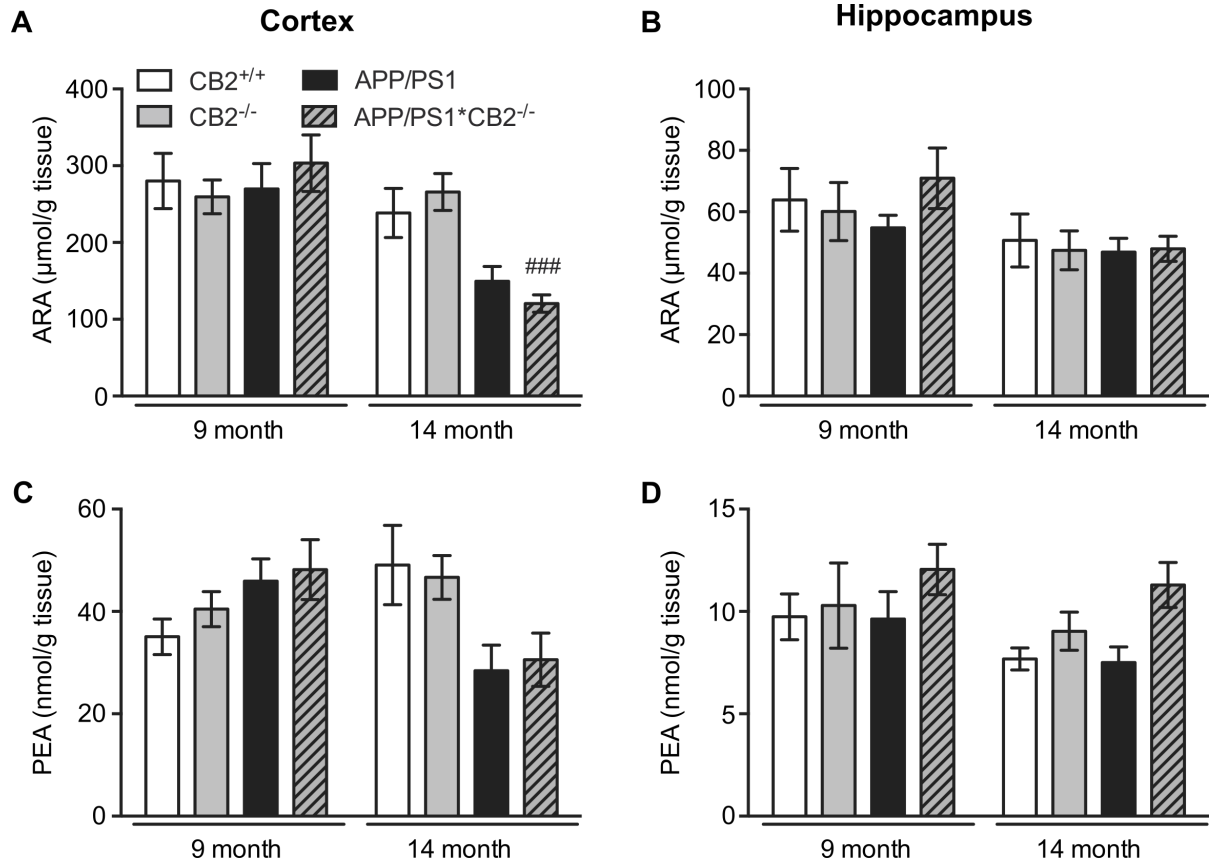

Figure 5.8: Secretion of ARA and PEA in cortical and hippocampal tissue of 9- and 14-month-old mice. Quantification of ARA (A, B) and PEA (G, H) secretion in cortical and hippocampal tissue of 9- and 14-month-old mice. n = 5-8; Data were analysed by 2-way ANOVA followed by Tukey's multiple comparisons test, $*p < 0.05$, $**p < 0.01$, $***p < 0.001$; # significance to corresponding 9-month-old group.

Secretion of ARA in cortical tissue of 9-month-old mice was not altered within the four groups (Fig. 5.8, A). However, in tissue samples of aged mice, a significantly reduced secretion of ARA was observed in samples of APP/PS1∗CB2$^{-/-}$ mice when compared to secretion levels of 9-month-old mice ($p = 0.0009$). In general, significant interaction ($F_{3,40} = 4.462$, $p = 0.0085$) and age ($F_{1,40} = 17.98$, $p = 0.0001$) effects were observed (Fig. 5.8, A). In hippocampal tissue, ARA secretion remained comparable within the four genotypes, however a significant age effect ($F_{1,41} = 6.413$, $p = 0.0153$; Fig. 5.8, B) was detected, indicating reduced secretion levels in cortical tissue samples of 14-month-old mice. Finally, the secretion of PEA in cortical tissue was analysed and revealed a significant interaction effect ($F_{3,40} = 5.325$, $p = 0.0035$), due to an increased secretion of PEA in tissue samples of CB2$^{+/+}$ and CB2$^{-/-}$ mice and decreased secretion levels of PEA in tissue samples of APP/PS1 and APP/PS1∗CB2$^{-/-}$ mice (Fig. 5.8, C). In hippocampal tissue, secretion levels of PEA were neither age- and nor genotype-dependently affected, thus, PEA secretion was comparable between all groups (Fig. 5.8, D). In summary, expression levels of AEA, 2-AG, ARA and PEA tended to decrease with age, especially in APP/PS1∗CB2$^{-/-}$ mice and expression in hippocampal tissue seemed to be more stable regarding age and genotype differences.

5.3 Role of CB2 signalling in APP processing and plaque formation

5.3.1 Reduced Aβ plaque load in APP/PS1$*$CB2$^{-/-}$ mice

Most AD animals models are reflecting the Aβ-plaque-component of the disease, which is believed to be the main reason for AD associated neuronal dysfunction. Due to the fact that the mouse model used in the present study also expresses a mutated form of APP, the Aβ-plaque load in different brain regions of 9- and 14-month-old mice was analysed. Therefore, the benzothiazole salt thioflavin T was used to visualize and quantify the presence of misfolded APP-derived aggregates. By binding to β-sheet-rich structures, the dye displays an enhanced fluorescence intensity as well as a characteristic red shift of its emission spectrum.

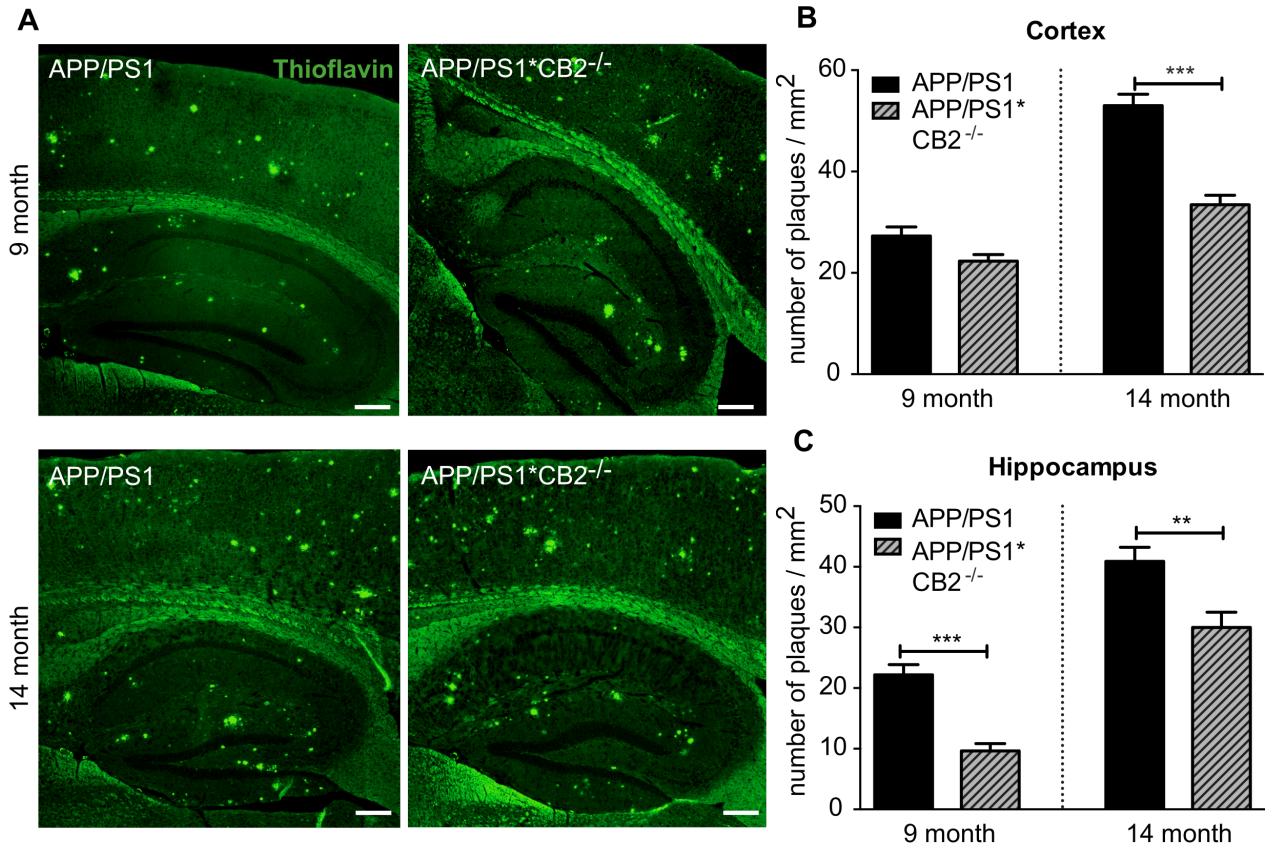

Figure 5.9: Plaque deposition in 9- and 14-month-old AD transgenic mice. Representative images of thioflavin t stained tissue of 9- and 14-month-old mice (A). Quantification of the number of plaques in each group in cortical sections (B) and hippocampal sections (C). scale bar 50 μ; n = 5-8; Data were analysed by 2-way ANOVA, followed by Tukey's multiple comparisons test, $*p < 0.05$, $**p < 0.01$, $***p < 0.001$; # significance to corresponding 9-month-old group.

After thioflavin T staining in brain slices of AD tg mice, APP-derived aggregates were clearly visible (Fig. 5.9, A), while stained brain slices of control mice were absent of any plaques (data not shown). Furthermore, increased numbers of thioflavin T stained plaques were detectable between brain slices of 9- and 14-month-old mice (Fig. 5.9, B and C). After quantification of thioflavin T stained Aβ plaques in cortical brain regions, significant interaction ($F_{1,71} = 14.35$, $p = 0.0003$), age ($F_{1,71} = 91.65$, $p < 0.0001$) and genotype effects ($F_{1,71} = 40.58$, $p < 0.0001$) were found. In 9-

month-old mice, the numbers of Aβ plaques per mm^2 in cortical areas were comparable between the two AD tg mouse groups (Fig. 5.9, B). However, in samples of 14-month-old APP/PS1 mice, the numbers of plaques increased significantly compared to age-matched APP/PS1$*$CB2$^{-/-}$ mice ($p < 0.0001$).

In hippocampal brain regions of thioflavin T-stained brain slices, significant age ($F_{1,70} = 91.32$, $p < 0.0001$) and genotype effects ($F_{1,70} = 32.94$, $p < 0.0001$) were detected (Fig. 5.9, C). In brain slices of 9-month-old mice, the number of Aβ plaques was significantly reduced in samples of APP/PS1$*$CB2$^{-/-}$ as compared to samples of age-matched APP/PS1 mice ($p = 0.0004$). With increasing age, the plaque load was elevated in samples of both, APP/PS1 ($p < 0.0001$) and APP/PS1$*$CB2$^{-/-}$ ($p < 0.0001$) mice when compared to the number of plaques in each 9-month-old group. Nevertheless, the number of Aβ plaques per mm^2 was significantly reduced in samples of APP/PS1$*$CB2$^{-/-}$ as compared to APP/PS1 mice ($p = 0.0013$, Fig. 5.9, C).

5.3.2 Altered secretion levels of Aβ40 and Aβ42 in 9-month-old APP/PS1$*$CB2$^{-/-}$ mice

Subsequent to analyses of APP plaque formation, secretion of the two major forms of soluble Aβ, Aβ40 and Aβ42, was measured by ELISA and quantified in total brain lysates of 9- and 14-month-old mice (Fig. 5.10, A and B). The Aβ protein load in pg per ml was adjusted to 500 μg of total protein to adjust for unequal brain sizes.

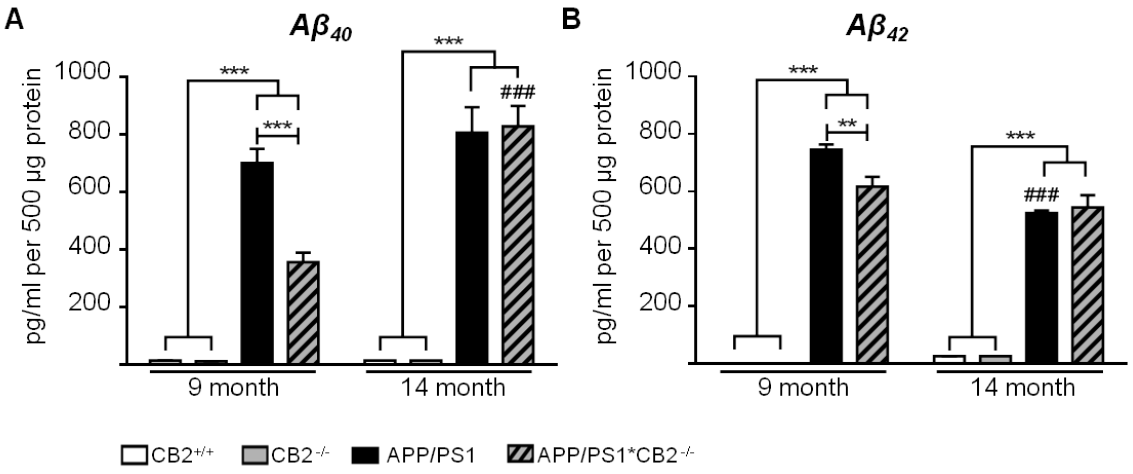

Figure 5.10: Secretion of amyloid species measured by ELISA. Quantification of secreted Aβ40 (A) and Aβ42 (B) in CB2$^{+/+}$ (white bar), CB2$^{-/-}$ (gray bar), APP/PS1$*$CB2$^{+/+}$ (black bar) and APP/PS1$*$CB2$^{-/-}$ (grey striped bar). Secretion of Aβ40 and Aβ42 was decreased in 9-month-old APP/PS1$*$CB2$^{-/-}$ (A and B), whereas secretion levels of both Aβ species was equal in AD mice at the age of 14 months. Secretion of Aβ40 and Aβ42 was not detectable in samples of CB2$^{+/+}$ and CB2$^{-/-}$ mice. n = 5-8; Data were analysed by 2-way ANOVA followed by Tukey's multiple comparisons test, $*p < 0.05$, $**p < 0.01$, $***p < 0.001$; # significance to corresponding 9-month-old group.

Secretion of Aβ40 was reduced by approximately 50% in samples of 9-month-old APP/PS1$*$CB2$^{+/+}$ mice as compared to secretion levels in samples of age-matched APP/PS1 mice ($p < 0.0001$; Fig. 5.10, A). In both control groups, CB2$^{+/+}$ and CB2$^{-/-}$, levels of secreted

Aβ40 were below detection limit. Similarly, secretion levels of Aβ42 were significantly reduced ($p = 0.0068$) in samples of 9-month-old APP/PS1$*$CB2$^{-/-}$ as compared to APP/PS1 mice, while Aβ42 was not detectable in both control groups (Fig. 5.10, B). However, in samples 14-month-old mice, Aβ40 and Aβ42 secretion was comparable between both AD tg mouse groups, APP/PS1 and APP/PS1$*$CB2$^{-/-}$ (Fig. 5.10, A and B).

5.3.3 Comparable expression of full length app in APP/PS1 and APP/PS1$*$CB2$^{-/-}$ mice

Differences in Aβ plaque load and soluble Aβ species could result from differences in the expression level of full-length APP. To examine whether lack of CB2 signalling affected APP gene expression levels, real-time gene expression analysis of *App* mRNA was conducted using hippocampal tissue samples from 9- and 14-month-old mice. As expected, APP/PS1 and APP/PS1$*$CB2$^{-/-}$ mice displayed significantly increased *App* gene expression levels as compared to CB2$^{+/+}$ and CB2$^{-/-}$ mice in both age groups (genotype effect $F_{3,53} = 37.34$, $p < 0.0001$; Fig. 5.11).

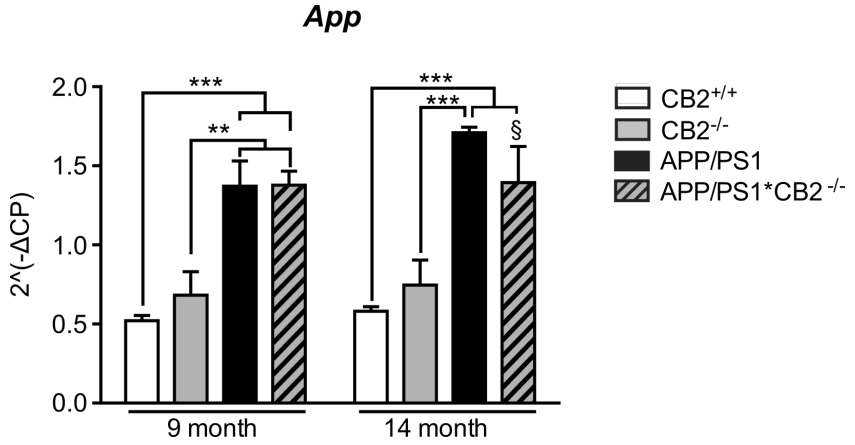

Figure 5.11: Gene expression levels of amyloid precursor protein. *App* gene expression was normalised to expression levels of the corresponding reference gene GAPDH. Expression of *App* was increased in both, 9- and 14-month-old APP/PS1 (black bar) and APP/PS1$*$CB2$^{-/-}$ (grey striped bar) compared to CB2$^{+/+}$ (white bar), CB2$^{-/-}$ (gray bar). n = 5-8; Data were analysed by 2-way ANOVA followed by Tukey's multiple comparisons test, $*p < 0.05$, $**p < 0.01$, $***p < 0.001$; § significance to 14-month-old CB2$^{-/-}$.

In detail, *App* gene expression was significantly increased in 9-month-old AD tg mice as compared to CB2$^{+/+}$ ($p < 0.0001$) and CB2$^{-/-}$ ($p = 0.0015$ and $p = 0.0021$, respectively) mice. A similar gene expression profile was detected in 14-month-old mice. *App* gene expression levels were significantly increased in APP/PS1 and APP/PS1$*$CB2$^{-/-}$ mice when compared to both, CB2$^{+/+}$ ($p < 0.0001$ and $p = 0.0007$, respectively) and CB2$^{-/-}$ mice ($p < 0.0001$ and $p = 0.0202$, respectively). However, gene expression levels of *App* were comparable between APP/PS1 and APP/PS1$*$CB2$^{-/-}$ mice in both age groups, 9- and 14-month-old mice (Fig. 5.11). Therefore, we could exclude that differences seen in Aβ plaque load were due to an altered expression of full-length APP.

5.3.4 Increased mRNA expression of α-secretases in APP/PS1$*$CB2$^{-/-}$ mice

Differences in Aβ plaque load could also be due to differences in proteolytic cleavage of APP by α, β- and γ-secretases. Thus, gene expression analyses using specific TaqMan® probes were conducted. Aβ is generated through cleavage of APP by β-secretases, followed by cleavage through a γ-secretase. Therefore, gene expression analyses of the most prominent β-secretase, *Bace1*, and the main γ-secretases component, *Nicastrin*, were conducted using qRT-PCR. Additionally, expression levels of two α-secretases, *Adam10* and *Adam17*, were analysed. *Adam10* expression showed significant interaction ($F_{3,53} = 2.828$, $p = 0.0472$) and age ($F_{1,53} = 17.20$, $p = 0.0001$) effects (Fig. 5.12, A).

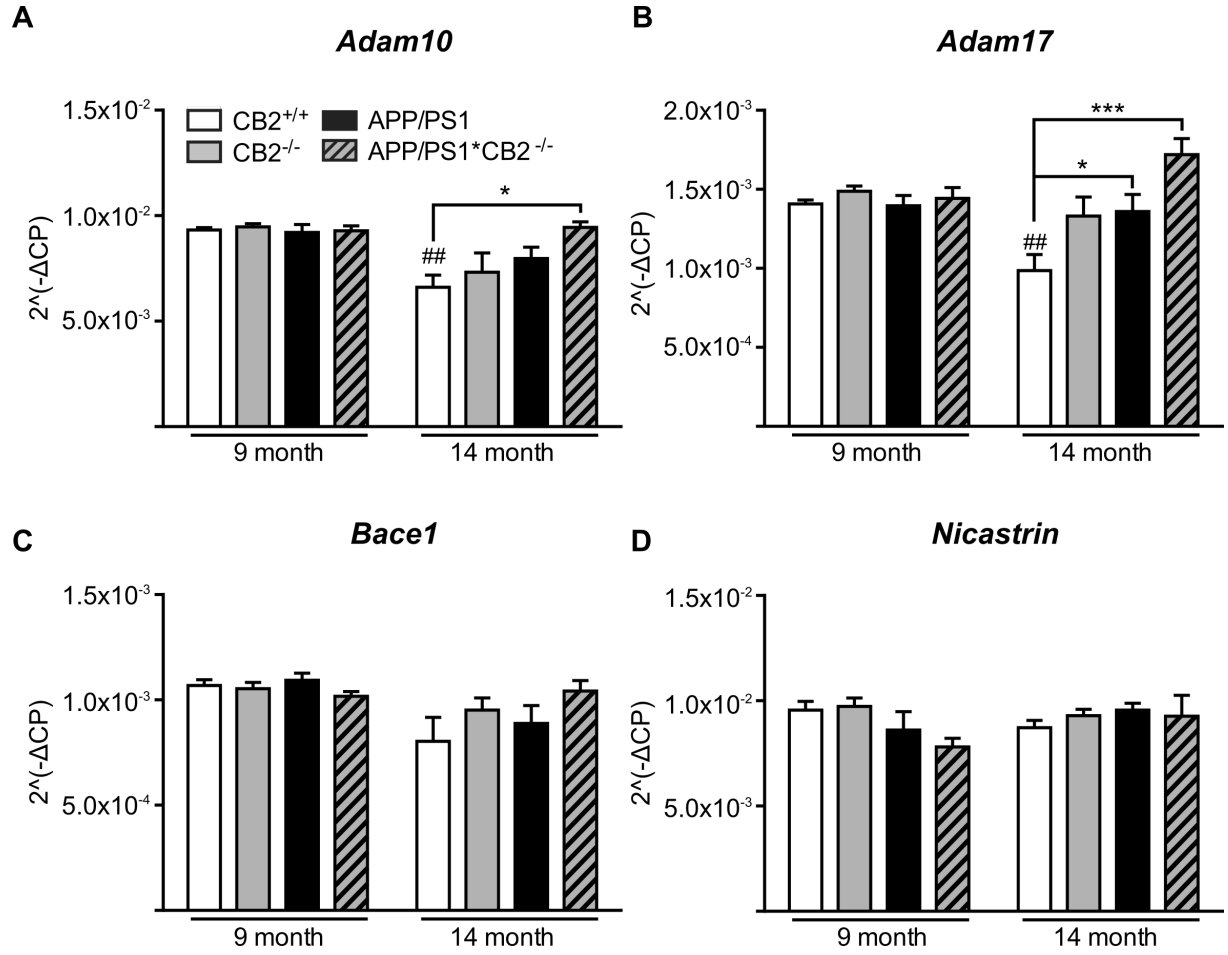

Figure 5.12: Gene expression levels of APP secretases. Gene expression of APP cleavage enzymes were normalised to the corresponding reference gene GAPDH. Expression of the α-secretases, *Adam10* (A) and *Adam17* (B), β-secretase *Bace1* (C) and the main γ-secretases component, *Nicastrin* (D), was analysed and compared within 9-month-old and 14-month-old CB2$^{+/+}$ (white bar), CB2$^{-/-}$ (gray bar), APP/PS1$*$CB2$^{+/+}$ (black bar) and APP/PS1$*$CB2$^{-/-}$ (grey striped bar) mice. n = 5-8; Data were analysed by 2-way ANOVA followed by Tukey's multiple comparisons test, $*p < 0.05$, $**p < 0.01$, $***p < 0.001$; # significance to corresponding 9-month-old group.

In hippocampal tissue of 9-month-old mice, *Adam10* expression levels were comparable between the groups (Fig. 5.12, A). However, in 14-month-old mice, a significant down-regulation of *Adam10* was detected in CB2$^{+/+}$ mice when compared to 9-month-old CB2$^{+/+}$ ($p = 0.0039$) mice as well as in comparison to age-matched APP/PS1$*$CB2$^{-/-}$ mice ($p = 0.0111$; Fig. 5.12, A).

Analysis of *Adam17* gene expression, showed significant interaction ($F_{3,52} = 5.553$, $p = 0.0022$) and genotype ($F_{3,52} = 6.667$, $p = 0.0007$) effects (Fig. 5.12, B). Within all genotypes, *Adam17* expression levels were comparable between tissue samples of 9-month-old mice. In 14-month-old mice, expression levels of *Adam17* decreased significantly in $CB2^{+/+}$ mice in comparison to 9-month-old $CB2^{+/+}$ ($p = 0.0087$) and age-matched APP/PS1 ($p = 0.0306$) mice. In contrast, APP/PS1$*CB2^{-/-}$ showed increased expression levels of *Adam17* as compared to age-matched $CB2^{+/+}$ mice ($p < 0.0001$; Fig. 5.12, B). Expression analysis of *Bace1* showed a significant age effect ($F_{1,52} = 8.316$, $p = 0.0057$; Fig. 5.12, C). However, genotype differences within each age group were not detected. Expression of the γ-secretases component, *Nicastrin*, remained stable within the four genotypes and both age groups (Fig. 5.12, D). Thus, significant differences were not detected. In general, expression levels of *Bace1* and *Nicastrin* remained comparable with increasing age and were not altered due to expression of transgenes or in knockout mice. However, samples of 14-month-old APP/PS1$*CB2^{-/-}$ mice showed increased expression levels of both α-secretases, *Adam10* and *Adam17*.

5.3.5 Altered mRNA expression pattern of Aβ receptors

To evaluate whether CB2 signalling in AD mice influenced the uptake and degradation of Aβ, we further analysed expression levels of the following Aβ specific receptors: advanced glycation end products receptor (*Ager*, also known as *Rage*), macrophage receptor with collagenous structure (*Marco*) and the toll-like receptor 4 (*Tlr4*).

Gene expression of *Ager* was age-dependently increased (age effect $F_{1,54} = 55.41$, $p < 0.0001$; Fig. 5.13, A). Using Tukey multiple comparison test, a significant upregulation of *Ager* was observed in samples of APP/PS1 and APP/PS1$*CB2^{+/+}$ mice when compared to expression levels of each 9-month-old group ($p < 0.0001$ and $p = 0.0135$, respectively). Furthermore, expression of *Ager* in samples of 14-month-old APP/PS1 mice was also significantly increased in comparison to age-matched $CB2^{-/-}$ ($p = 0.0118$) and $CB2^{-/-}$ mice ($p = 0.0008$; Fig. 5.13, A).

Gene expression of *Marco* was age-dependently upregulated in all groups (age effect $F_{1,54} = 87.21$, $p < 0.0001$), however, genotype-dependant differences within both age-groups were not detected (Fig. 5.13, B).

Analysis of *Tlr4* expression revealed significant age ($F_{1,54} = 23.03$, $p < 0.0001$), genotype ($F_{3,54} = 3.105$, $p = 0.0340$) and interaction ($F_{3,54} = 5.116$, $p = 0.0035$) effects (Fig. 5.13, C). Similar to the gene expression profile of *Ager*, a specific upregulation of *Tlr4* expression was detected in samples aged APP/PS1 mice as compared to 9-month-old APP/PS1 mice ($p < 0.0001$) and compared to age-matched $CB2^{+/+}$ ($p = 0.0009$) and $CB2^{-/-}$ mice ($p = 0.0202$; Fig. 5.13, C).

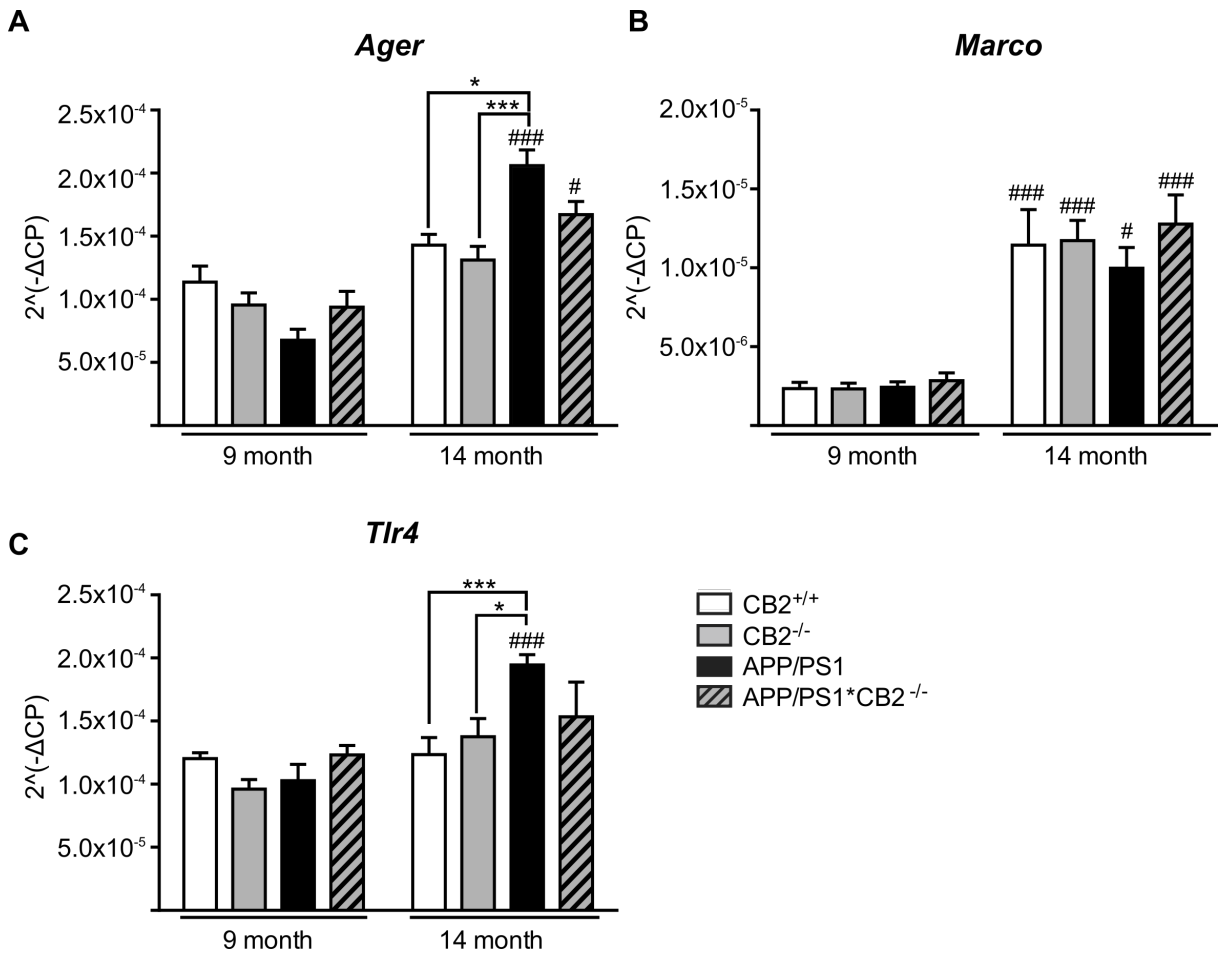

Figure 5.13: Gene expression levels of amyloid receptors. Gene expression of Aβ receptors were normalised to expression of the corresponding reference gene GAPDH. Expression of *Ager* (A), *Marco* (B) and *Tlr4* (C) was analysed and compared within both age groups in hippocampal tissue of $CB2^{+/+}$ (white bar), $CB2^{-/-}$ (gray bar), APP/PS1 (black bar) and APP/PS1$*CB2^{-/-}$ (grey striped bar) mice. n = 5-8; Data were analysed by 2-way ANOVA followed by Tukey's multiple comparisons test, $*p < 0.05$, $**p < 0.01$, $***p < 0.001$; # significance to corresponding 9-month-old group.

5.3.6 Altered mRNA expression pattern of Aβ degrading enzymes

Adjacent to the analyses of Aβ receptors, gene expression levels of Aβ specific degrading enzymes insulin-degrading enzyme (*Ide*), neprilysin (*Nep*) and matrix-metalloproteinase-9 (*Mmp9*), were evaluated in hippocampal tissue samples of 9- and 14-month-old mice.

In 9-month-old mice, expression levels of *Ide* were significantly lower in $CB2^{-/-}$ mice ($p = 0.0137$) as compared to age-matched $CB2^{+/+}$ littermates (Fig. 5.14, A). In contrast, *Ide* expression levels of 14-month-old $CB2^{+/+}$ and $CB2^{-/-}$ mice were comparable. However, *Ide* expression levels were significantly upregulated in 14-month-old APP/PS1$*CB2^{-/-}$ when compared to 9-month-old APP/PS1$*CB2^{-/-}$ mice ($p < 0.0001$) as well as in comparison to age-matched $CB2^{+/+}$ mice and $CB2^{-/-}$ mice ($p < 0.0001$). 2-Way ANOVA revealed significant age- ($F_{1,54} = 12.21$, $p = 0.0010$), genotype ($F_{3,54} = 6.430$, $p = 0.0008$)and interaction effects ($F_{3,54} = 10.50$, $p < 0.0001$).

Expression levels of *Nep* were age-dependently down-regulated in all groups (age effect $F_{1,53} = 259.2$, $p < 0.0001$; Fig. 5.14, B). Within 9-month-old mice, *Nep* expression levels were comparable between

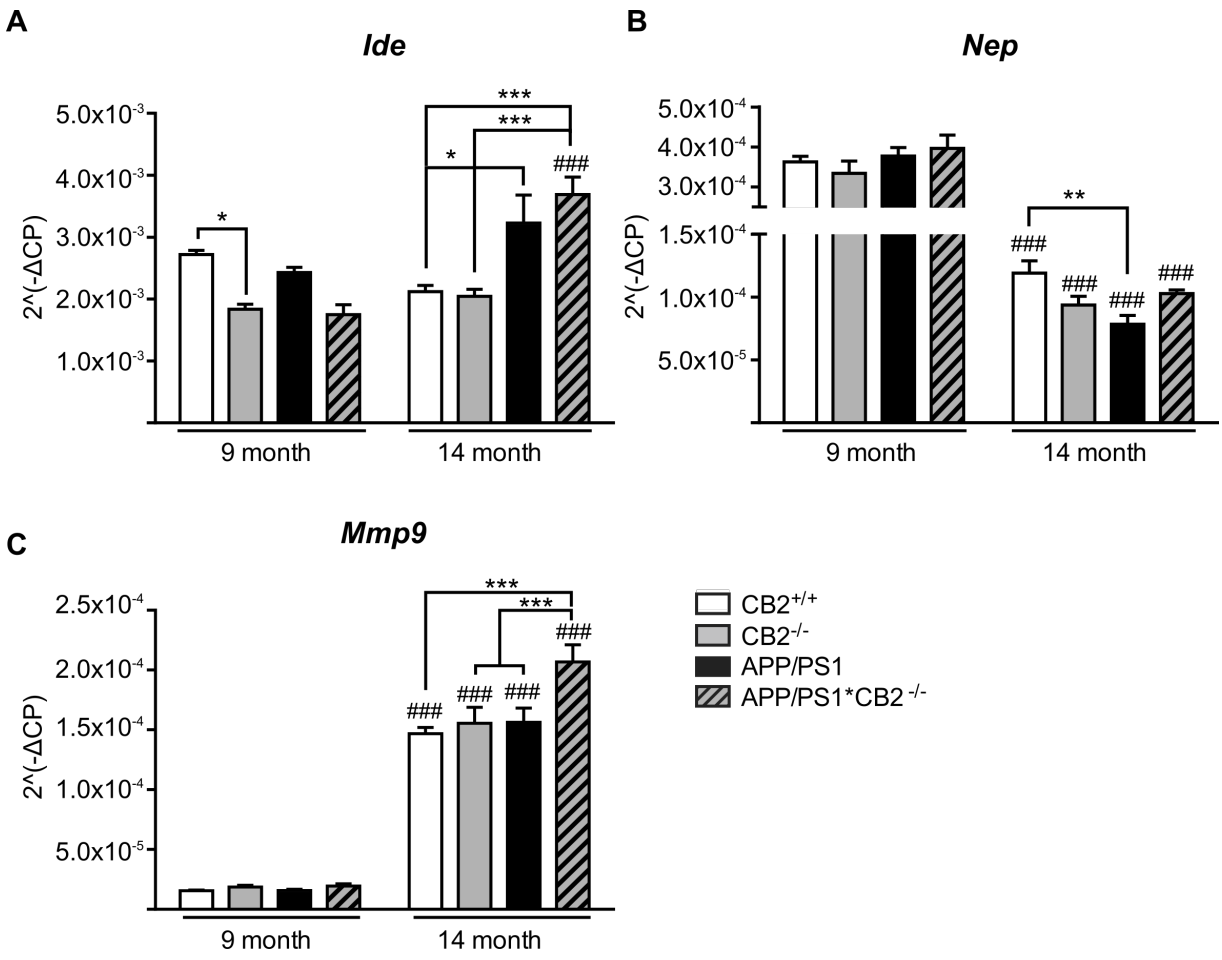

Figure 5.14: Gene expression levels of amyloid degrading enzymes. Gene expression levels of Aβ specific degrading enzymes were normalised to expression levels of the corresponding reference gene GAPDH. Expression of *Ide* (A), *Nep* (B) and *Mmp9* (C) was analysed within hippocampal tissue samples of 9- and 14-month-old $CB2^{+/+}$ (white bar), $CB2^{-/-}$ (gray bar), APP/PS1 (black bar) and APP/PS1$*CB2^{-/-}$ (grey striped bar) mice. n = 5-8; Data were analysed by one-way or 2-way ANOVA, respectively, followed by Tukey's multiple comparisons test, $*p < 0.05$, $**p < 0.01$, $***p < 0.001$; # significance to corresponding 9-month-old group

all genotypes. However, by analysing gene expression levels in tissue samples of 14-month-old mice separately, a significant decrease in *Nep* gene expression levels was observed in APP/PS1 mice as compared to $CB2^{+/+}$ littermates (one-way ANOVA followed by Tukey's multiple comparisons test, $p = 0.0020$), while gene expression levels were comparable between samples of $CB2^{+/+}$ and $CB2^{-/-}$ ($p = 0.0757$) or APP/PS1$*CB2^{-/-}$ mice ($p = 0.3815$, Fig. 5.14, B).

Additionally, gene expression levels of *Mmp9* were analysed. While *Mmp9* expression remained constant within tissue samples of 9-month-old mice, *Mmp9* expression was strongly increased with increasing age in all groups (age-effect, $F_{1,54} = 493.4$, $p < 0.0001$, Fig. 5.14, C). Furthermore, significant interaction ($F_{3,54} = 3.504$, $p = 0.0214$) and genotype ($F_{3,54} = 4.305$, $p = 0.0085$) effects were observed. 14-month-old APP/PS1$*CB2^{-/-}$ mice displayed the strongest increase in *Mmp9* gene expression levels when compared to $CB2^{+/+}$ and $CB2^{-/-}$ ($p = 0.0003$ and $p = 0.0018$, respectively) as well as in comparison to APP/PS1 mice ($p = 0.0022$).

In summary, gene expression levels of Aβ degrading enzymes were almost comparable within

tissue samples of 9-month-old mice. While *Ide* and *Mmp9* expression increased with age, expression levels of *Nep* were age-dependently reduced, especially in tissue samples of APP/PS1 mice. Furthermore, we observed the strongest upregulation of *Ide* and *Mmp9* expression levels in hippocampal tissue samples of APP/PS1$*$CB2$^{-/-}$, while expression in APP/PS1 mice was slightly altered or comparable to expression levels of CB2$^{+/+}$ and CB2$^{-/-}$ littermates.

5.4 Role of CB2 signalling in microgliosis

5.4.1 Equal Iba1 immunoreactivity in samples of 9-month-old mice

As microglia represent an important cellular component in AD-associated neuroinflammation and neurodegeneration, we investigated whether the total number of CNS resident microglia cells, also referred to as microgliosis, was altered in APP/PS1∗CB2$^{-/-}$ mice as compared to control mice and normal AD tg mice. Therefore, sagittal brains slices of 9- and 14-month-old mice were stained with anti-Iba1 and counter stained with DAPI (Fig. 5.15).

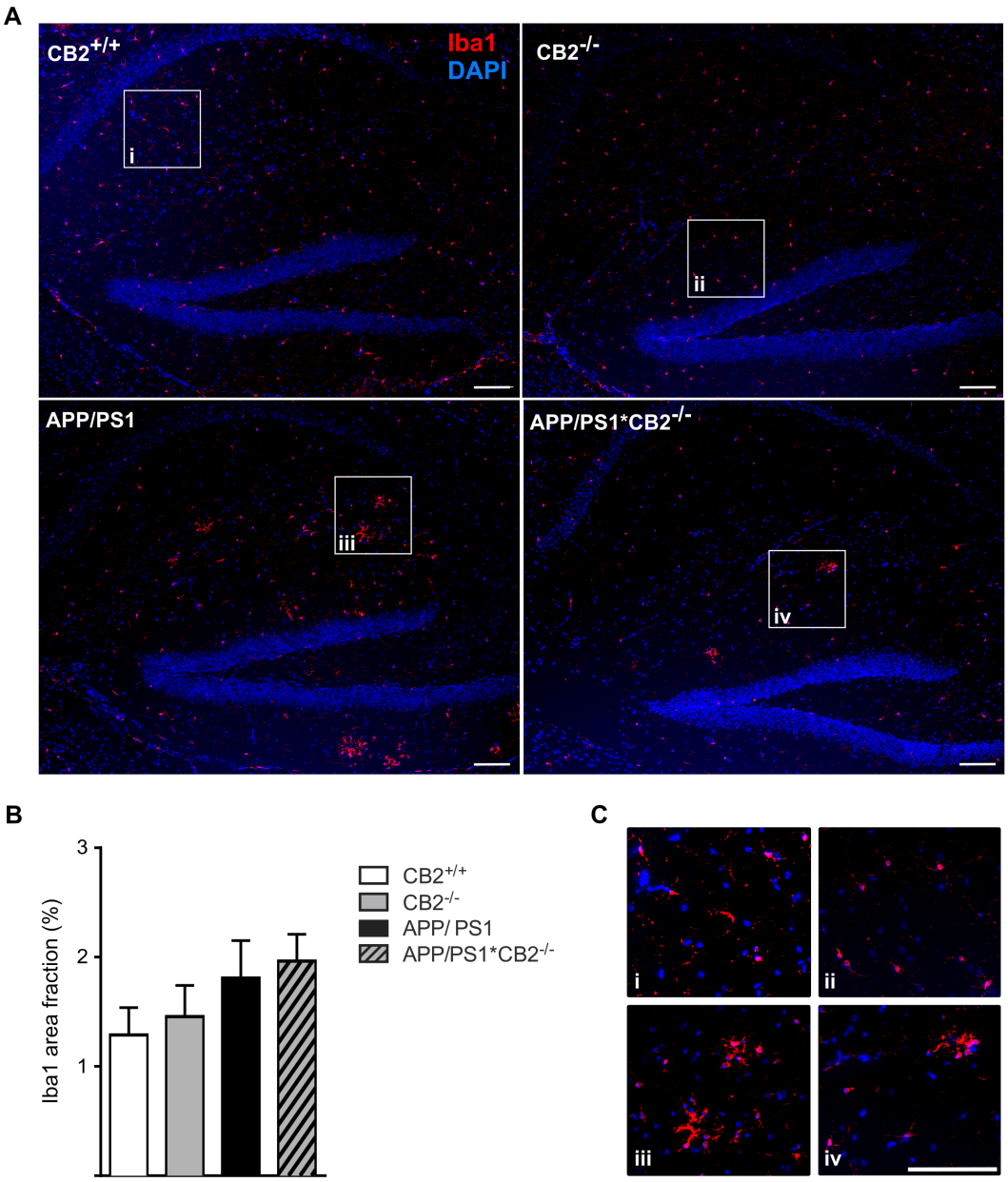

Figure 5.15: Comparable levels of microgliosis in 9-month-old mice. Shown are representative brain tissue sections stained for Iba1 (red) and counter stained with DAPI (blue) in CB2$^{+/+}$ (upper left), CB2$^{-/-}$ (upper right), APP/PS1 (lower left) and APP/PS1∗CB2$^{-/-}$ (lower right) mice (scale bar = 100 μm; A). Quantification of Iba1 stained area fraction showed comparable levels of microgliosis in 9-month-old mice (B). Representative images of enlarged sections (white quadrants in A; scale bar = 100 μm; C). n = 5-8; Data were analysed by 2-way ANOVA followed by Tukey's multiple comparisons test.

In representative images of stained hippocampal tissue sections, Iba1 immunoreactivity was clearly detectable in all groups (Fig. 5.15, A and C). The quantification of Iba1 immunoreactivity revealed comparable levels of microgliosis between the four groups (one-way ANOVA followed by Tukey's multiple comparisons test, $p = 0.0366$; Fig. 5.15, B). Microglia in brain tissue sections of $CB2^{+/+}$ and $CB2^{-/-}$ mice showed smaller cell bodies as compared to microglia in samples of APP/PS1 and APP/PS1$*$$CB2^{-/-}$ mice (Fig. 5.15, A and C). Furthermore, Iba1 stained cells in brain tissue sections of APP/PS1 mice were unevenly distributed and clustered in comparison to microglia of control mice (Fig. 5.15, A and C, iii).

5.4.2 Reduced microgliosis in aged APP/PS1∗CB2$^{-/-}$ mice

As microgliosis is known to increase with age and the number of Aβ plaques, Iba1 staining was subsequently analysed in 14-month-old mice, where plaque load is significantly enhanced. Similar to Iba1 immunoreactivity in 9-month-old mice, CB2$^{+/+}$ mice displayed an even distribution of Iba1 stained microglia throughout the whole hippocampus (Fig. 5.16, A).

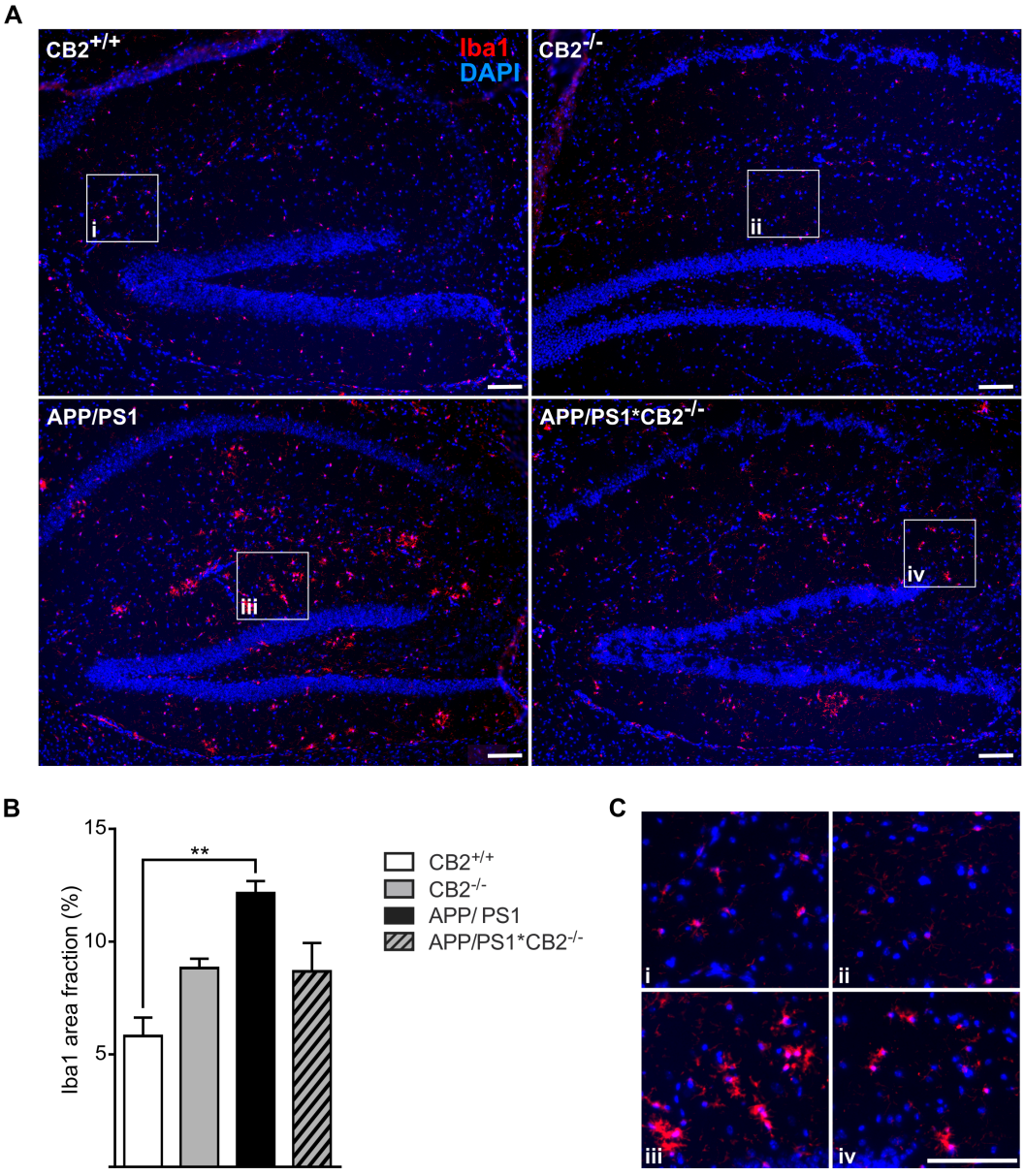

Figure 5.16: Enhanced microgliosis in 14-month-old APP/PS1 mice. Shown are representative brain tissue sections stained for Iba1 (red) and counter stained with DAPI (blue) for the detection of microgliosis in CB2$^{+/+}$ (upper left), CB2$^{-/-}$ (upper right), APP/PS1 (lower left) and APP/PS1∗CB2$^{-/-}$ (lower right) mice (scale bar = 100 μm; A). Quantification of Iba1 stained area fraction showed significantly enhanced microgliosis in samples of 14-month-old APP/PS1 mice (B). Representative images of enlarged sections (white quadrants in A; scale bar = 100 μm; C). n = 5-8; Data were analysed by two-way ANOVA followed by Tukey's multiple comparisons test, $*p < 0.05$, $**p < 0.01$, $***p < 0.001$.

A similar distribution was observed in CB2$^{-/-}$ mice (Fig. 5.16, A, upper right panel). In contrast, in APP/PS1 mice, Iba1 immunoreactivity was significantly enhanced compared to CB2$^{+/+}$ and CB2$^{-/-}$ mice (Fig. 5.16, A-C). Furthermore, microglia clustering was observed; predominantly in

the stratum lacunosum-moleculare of the hippocampal CA1 region and in the molecular layer of the DG. In APP/PS1$*$CB2$^{-/-}$ mice, Iba1 immunoreactivity was reduced and clusters of microglia were less abundant when compared to samples of APP/PS1 mice (Fig. 5.16, A, lower right panel). The quantification of microgliosis revealed a significantly increased Iba1 area fraction in samples of APP/PS1 mice compared to samples of CB2$^{+/+}$ littermates (Fig. 5.16, B; one-way ANOVA, followed by Tukey's multiple comparisons test, $p = 0.0046$). In contrast, Iba1 immunoreactivity was comparable between CB2$^{+/+}$ and CB2$^{-/-}$ ($p = 0.1703$) or APP/PS1$*$CB2$^{-/-}$ ($p = 0.1694$), respectively.

5.4.3 Comparable amounts of intracerebral leucocytes in 9-month-old mice

To evaluate whether increased microgliosis seen in 14-month-old AD mice was due to an increased proliferation of microglia or an increased recruitment of peripheral monocyte-derived macrophages, flow cytometric analyses of ICLs using antibodies against CD11b and the leukocyte common antigen CD45 were performed. For the analysis of the cellular distribution, a primary gate was set on all living cells, namely lifegate. Using dot-plot analyses, the relative distribution of lymphocytes, macrophages and microglia in samples of $CB2^{+/+}$ (upper left panel), $CB2^{-/-}$ (upper right panel), APP/PS1 (lower left panel) and APP/PS1$*$$CB2^{-/-}$ (lower right panel) mice was analysed according to the expression of CD11b (x-axis) and CD45 (y-axis) (representative dotplots in Fig. 5.17).

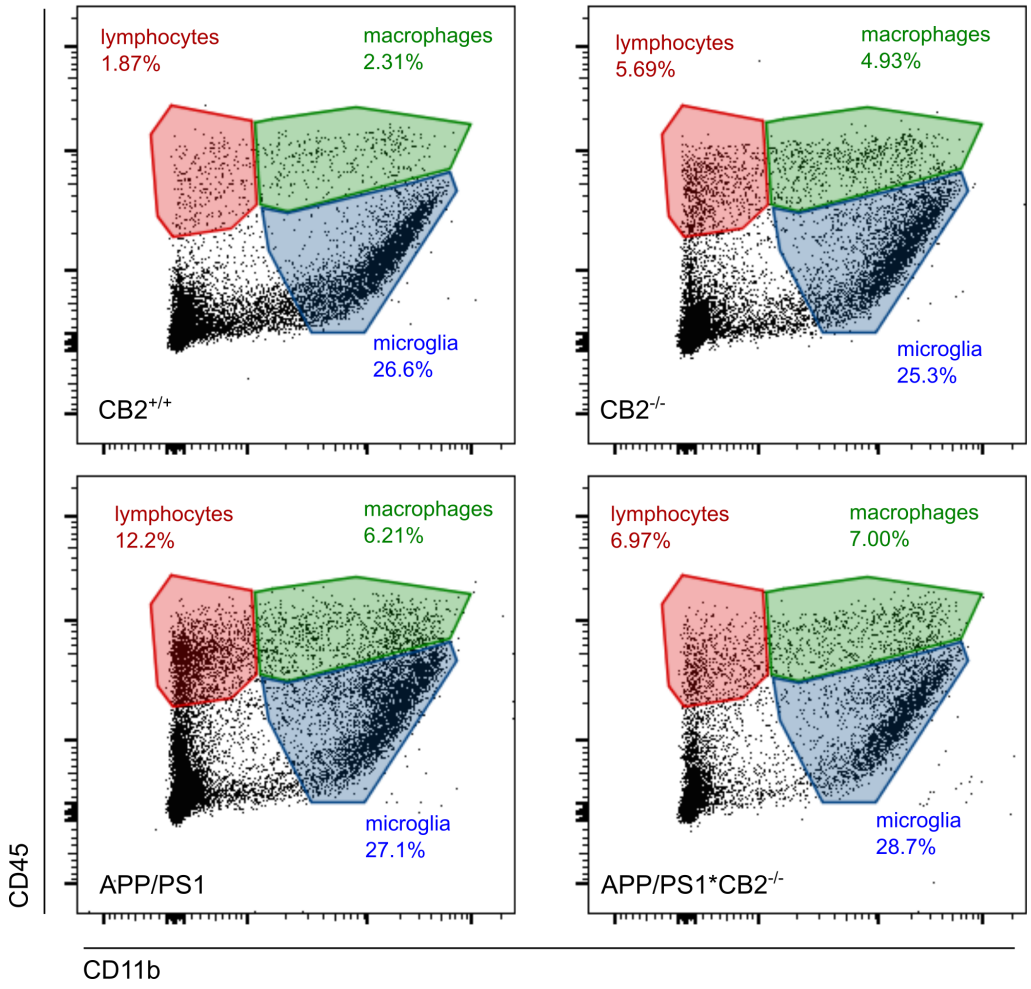

Figure 5.17: Flow cytometric analysis of ICLs in 9-month-old mice. Representative dotplot images show the distribution of lymphocytes, macrophages and microglia in samples of $CB2^{+/+}$ (upper left), $CB2^{-/-}$ (upper right), APP/PS1 (lower left) and APP/PS1$*$$CB2^{-/-}$ (lower right) mice using the markers CD45 (y-axis) and CD11b (x-axis). Lymphocytes ($CD45^{+}CD11b^{-}$) are depicted in red, macrophages ($CD45^{high}CD11b^{+}$) are depicted in green and microglia ($CD45^{low}CD11b^{+}$) are depicted in blue. Analyses were conducted by using FlowJo X software.

Lymphocytes (depicted in red) are known to express high levels of CD45, but expression of CD11b is absent in these cells. Both, microglia and macrophages are known to express high levels of the monocytic marker CD11b. However, while macrophages (depicted in green) also express high

levels of CD45, microglia (depicted in blue) only present a dim expression of CD45 (Fig. 5.17). Fig. 5.18 shows the quantitative analysis of ICLs percentages in samples of 9-month-old $CB2^{+/+}$, $CB2^{-/-}$, APP/PS1 and APP/PS1∗$CB2^{-/-}$ mice.

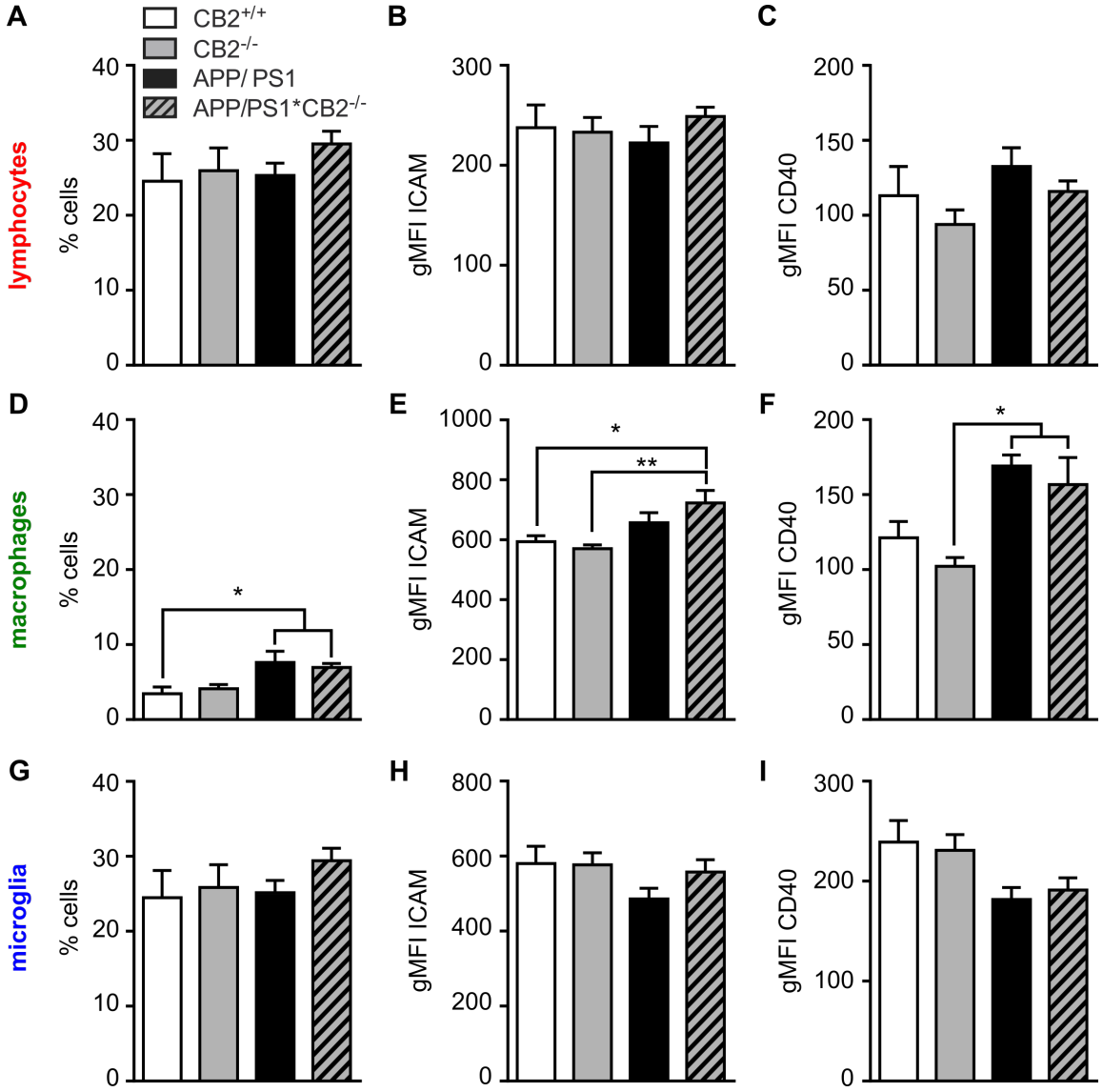

Figure 5.18: Quantification of ICLs in samples of 9-month-old mice. Shown are quantitative analyses of ICLs in $CB2^{+/+}$, $CB2^{-/-}$, APP/PS1 and APP/PS1∗$CB2^{-/-}$ mice using the markers CD45 and CD11b. Percentages of lymphocytes ($CD45^{+}CD11b^{-}$; A) were unaltered within the groups. Lymphocytic expression levels of ICAM (B) and CD40 (C) were comparable. Percentages of macrophages ($CD45^{high}CD11b^{+}$; B) were increased in APP/PS1 and APP/PS1∗$CB2^{-/-}$ compared to $CB2^{+/+}$ mice. Macrophages of APP/PS1∗$CB2^{-/-}$ showed increased expression of ICAM (E) and CD40 (F). Percentages of microglia ($CD45^{low}CD11b^{+}$; G) as well as expression levels of ICAM (H) and CD40 (I) were comparable within the groups. n = 4-6; Data were analysed by one-way ANOVA, followed by Tukey's multiple comparisons test, $*p < 0.05$, $**p < 0.01$, $***p < 0.001$.

In the four groups, percentages of lymphocytes ($CD45^{high}$ and $CD11b^{-}$) were equivalent (mean $26\% \pm 6{,}477$; Fig. 5.18, A). To evaluate the activation profile of each cellular subset, expression levels of ICAM (also known as CD54) and the co-stimulatory molecule CD40, which is commonly found on antigen presenting cells, were analysed. Expression of both molecules was evaluated as geometric mean fluorescence intensity (gMFI) to account for logarithmically increasing fluorescence

intensity. Lymphocytic expression of ICAM was comparable between all groups (Fig. 5.18, B). Similarly, expression levels of CD40 were unaltered within the four groups (Fig. 5.18, C). In comparison to $CB2^{+/+}$ littermates, percentages of macrophages were increased in samples of APP/PS1 ($p = 0.0176$) and APP/PS1$*CB2^{-/-}$ ($p = 0.0269$) mice (one-way ANOVA $F_{3,18} = 5.966$, $p = 0.0052$; Fig. 5.18, D). Furthermore, expression of ICAM was significantly upregulated in in macrophages of APP/PS1$*CB2^{-/-}$ mice as compared to $CB2^{+/+}$ ($p = 0.0182$) and $CB2^{-/-}$ ($p = 0.0050$) mice (one-way ANOVA $F_{3,18} = 6.142$, $p = 0.0046$; Fig. 5.18, E). Similarly, gMFI of the co-stimulatory molecule CD40 was significantly increased in samples of APP/PS1 (169 gMFI; $p = 0.0106$) and APP/PS1$*CB2^{-/-}$ (138 gMFI; $p = 0.0206$) mice as compared to $CB2^{-/-}$ mice (one-way ANOVA $F_{3,18} = 5.981$, $p = 0.0051$; Fig. 5.18, F). Finally, microglia percentages as well as their expression levels of pro-inflammatory markers were analysed in brain samples of 9-month-old mice. Here, percentages of microglia were comparable between the four groups (Fig. 5.18, G). Mean fluorescence intensity of ICAM (gMFI 550 ± 87.9) was equal within the four groups (Fig. 5.18, H). Also, gMFI of CD40 was not significantly altered within the groups (gMFI 213 ± 43.9; Fig. 5.18, I). These results reflect immunohistochemical data (Fig. 5.15), which demonstrated comparable Iba1 immunoreactivity in brain slices of 9-month-old mice. However, as microgliosis was increased with age, we subsequently analysed ICL subsets in brain samples of 14-month-old mice.

5.4.4 Decreased percentages of microglia and BMdM in aged APP/PS1∗CB2$^{-/-}$ mice

Equivalent to ICL analyses described above, brain samples of 14-month-old mice were analysed regarding their relative distribution of lymphocytes, macrophages and microglia (representatively shown in Fig. 5.19). The quantification of the three cellular subsets and their expression levels of the pro-inflammatory molecules ICAM and CD40 is presented in Fig. 5.20.

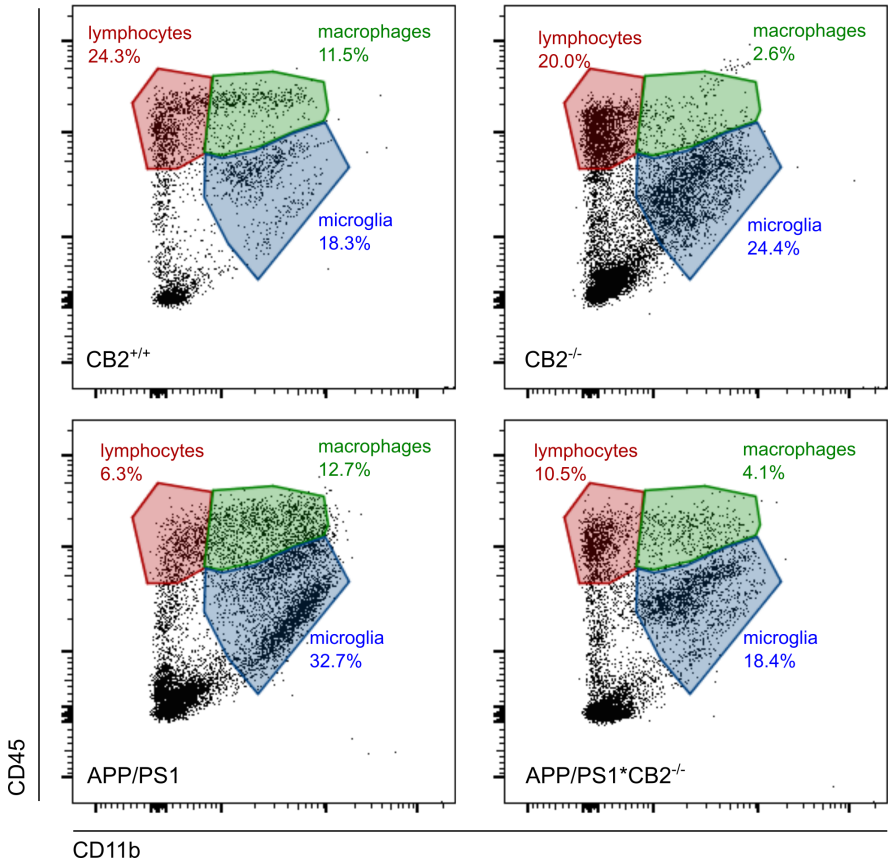

Figure 5.19: Flow cytometric analysis of ICLs in samples of 14-month-old mice. Representative dotplot images show the distribution of lymphocytes, macrophages and microglia in CB2$^{+/+}$ (upper left), CB2$^{-/-}$ (upper right), APP/PS1 (lower left) and APP/PS1∗CB2$^{-/-}$ (lower right) mice using the markers CD45 (y-axis) and CD11b (x-axis). Lymphocytes (CD45^{+}CD11b^{-}) are depicted in red, macrophages (CD45^{high}CD11b^{+}) are depicted in green and microglia (CD45^{low}CD11b^{+}) depicted in blue. Analyses were conducted by using FlowJo X software.

Percentages of lymphocytes (Fig. 5.20, A) as well as expression levels of ICAM (Fig. 5.20, B) and CD40 (Fig. 5.20, C) were comparable between the four groups. Interestingly, the percentage of macrophages was significantly diminished in samples of CB2$^{-/-}$ and APP/PS1∗CB2$^{-/-}$ mice when compared to APP/PS1 mice ($p = 0.0267$ and $p = 0.0128$, respectively; Fig. 5.20, D). This is suggestive for a reduced infiltration of blood-derived monocytes. Expression levels of ICAM and CD40 were comparable between the groups (Fig. 5.20, E and F). Percentages of microglia were significantly increased in samples of APP/PS1 mice when compared to APP/PS1∗CB2$^{-/-}$ (one-way ANOVA $F_{3,20} = 3.592$, $p = 0.0317$; Tukey's multiple comparison test $p = 0.0399$; Fig. 5.20, G). Furthermore, expression levels of the pro-inflammatory cell surface molecule ICAM were significantly

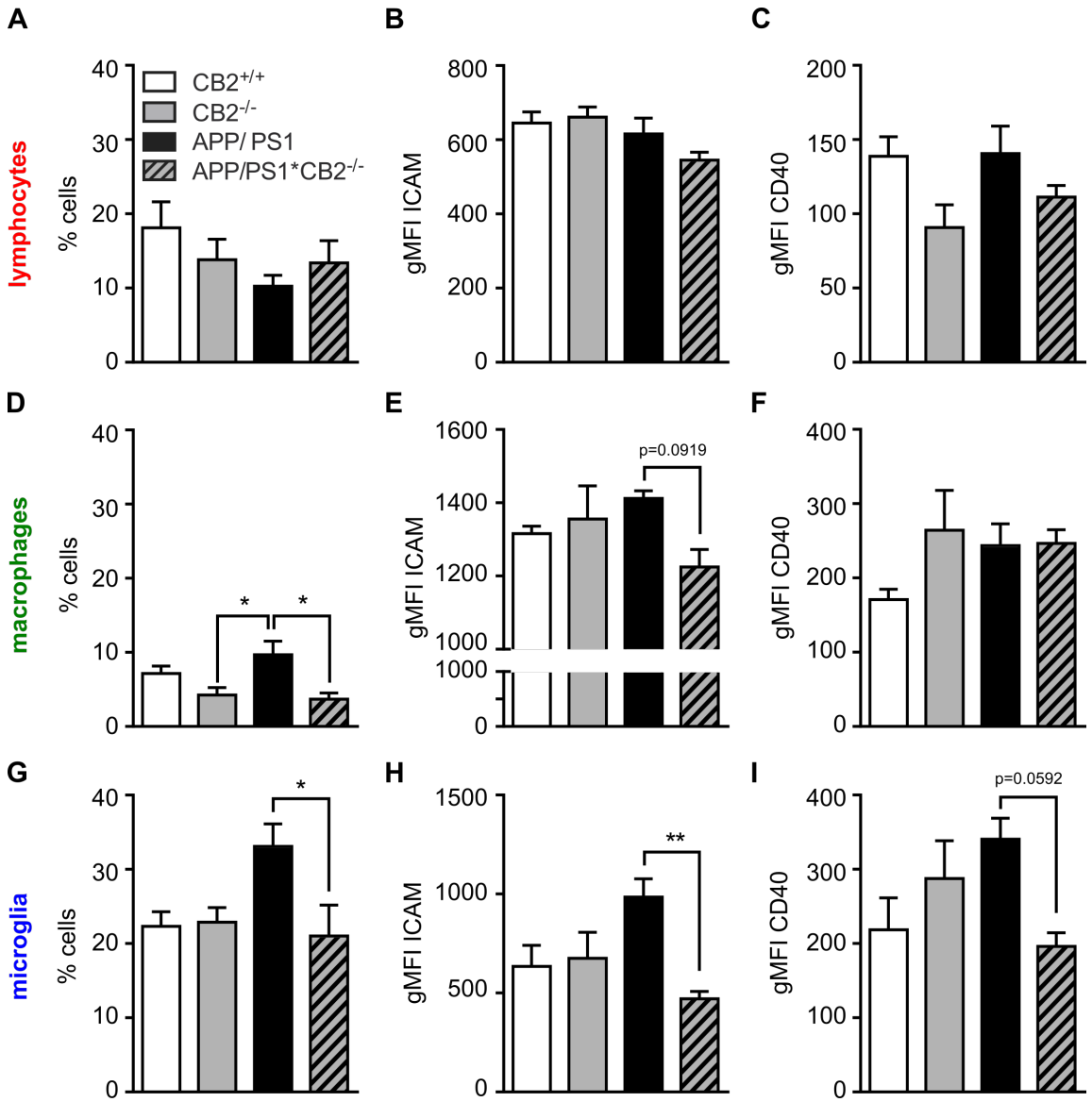

Figure 5.20: Quantification of ICLs in samples of 14-month-old mice. Shown are quantitative analyses of ICL subsets in $CB2^{+/+}$, $CB2^{-/-}$, APP/PS1 and APP/PS1$*CB2^{-/-}$ mice using the marker CD45 and CD11b. Percentages of lymphocytes ($CD45^{+}CD11b^{-}$; A) were comparable within the groups. Expression of ICAM (B) and CD40 (C) were unaltered. Percentages of macrophages ($CD45^{high}CD11b^{+}$; B) were increased in APP/PS1 compared to $CB2^{+/+}$ and APP/PS1$*CB2^{-/-}$ mice. Expression levels of ICAM (E) and CD40 (F) were unchanged. Percentages of microglia ($CD45^{low}CD11b^{+}$; G), as well as expression levels of ICAM (H) and CD40 (I) were increased in APP/PS1 mice as compared to APP/PS1$*CB2^{-/-}$ littermates. n = 4-6; Data were analysed by one-way ANOVA, followed by Tukey's multiple comparisons test, $*p < 0.05$, $**p < 0.01$, $***p < 0.001$.

increased in samples of APP/PS1 mice when compared to age-matched APP/PS1$*CB2^{-/-}$ mice (one-way ANOVA $F_{3,20} = 4.733$, $p = 0.0118$; Tukey's multiple comparison test $p = 0.0074$; Fig. 5.20, H). Additionally, expression levels of CD40 were reduced in samples of APP/PS1$*CB2^{-/-}$ versus samples of APP/PS1 mice, although one-way ANOVA just failed to reach statistical significance ($F_{3,20} = 3.077$, $p = 0.0510$; Tukey's multiple comparisons test $p = 0.0592$; Fig. 5.20, I).

5.5 Role of CB2 signalling in neuroinflammation

5.5.1 Decreased expression of Tnfα and Inos in aged APP/PS1$*$CB2$^{-/-}$ mice

Based on the observation of a reduced microgliosis as well as diminished percentages of microglia and infiltrated macrophages in aged APP/PS1$*$CB2$^{-/-}$ mice, gene expression levels of AD-associated inflammatory markers were analysed. Therefore, TaqMan® gene expression analyses were conducted using specific assays for the pro-inflammatory molecules TNFα, IL-1β, iNOS and IL-6.

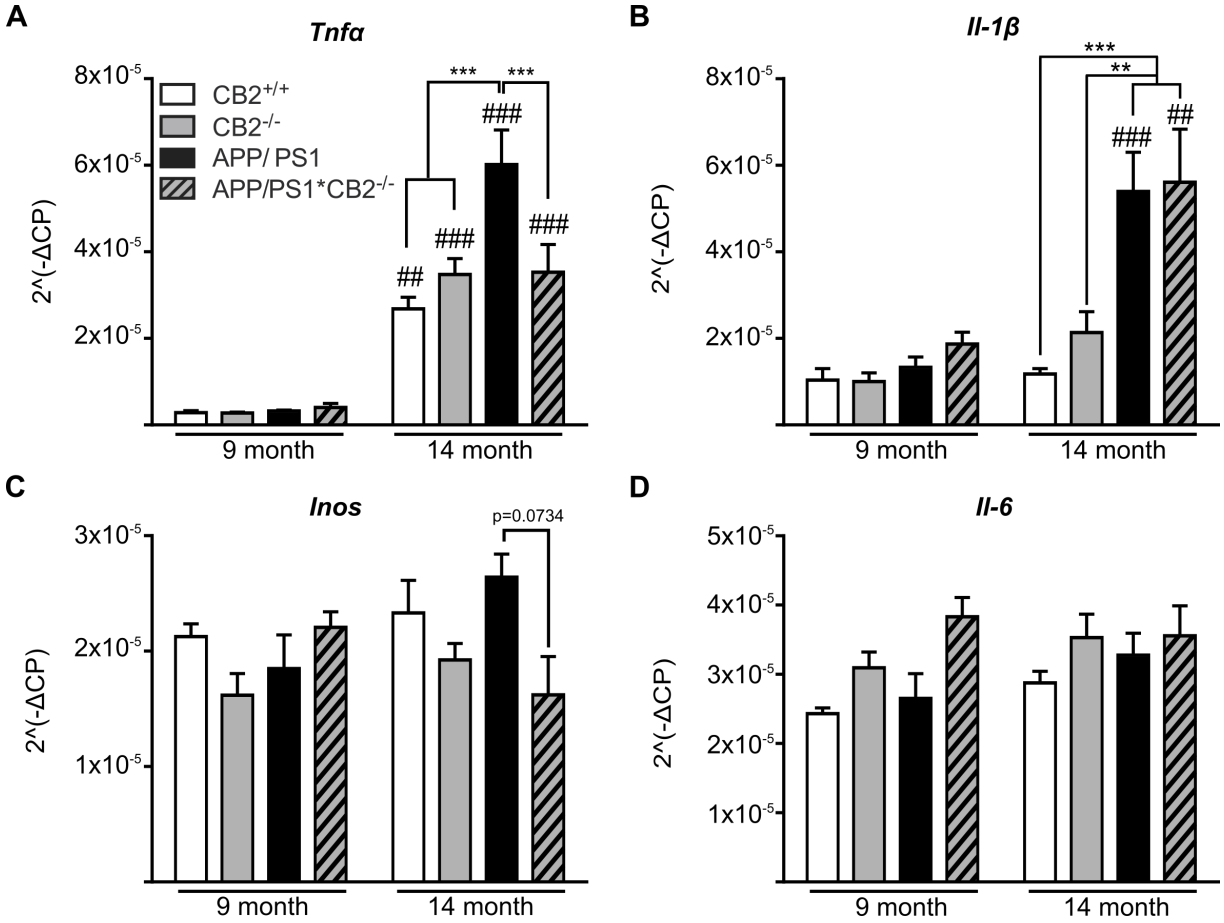

Figure 5.21: Gene expression analyses of inflammatory cytokines. Gene expression levels of pro-inflammatory cytokines were analysed in hippocampal tissue samples of 9- and 14-month-old CB2$^{+/+}$ (white), CB2$^{-/-}$ (gray), APP/PS1 (black) and APP/PS1$*$CB2$^{-/-}$ (black striped) mice. Expression levels of *Tnfα* (A), *Il-1β* (B), *Inos* (C) and *Il-6* (D) were normalised to expression levels of the corresponding reference gene GAPDH. n = 3-13; Data were analysed by 2-way ANOVA followed by Tukey's multiple comparisons test; $*p < 0.05$, $**p < 0.01$, $***p < 0.001$; # significance to corresponding 9-month-old group.

Regarding gene expression levels of *Tnfα*, significant interaction ($F_{3,51} = 4.132$; $p = 0.0107$), age ($F_{1,51} = 129.4$; $p < 0.0001$) and genotype ($F_{3,51} = 4.294$; $p = 0.0089$) effects were found in hippocampal tissue of 9- and 14-month-old mice (Fig. 5.21, A). In samples of 9-month-old mice, a very low expression of *Tnfα* mRNA was detected, while expression levels significantly increased with increasing age in all groups (Tukey's multiple comparison test, CB2$^{+/+}$: $p = 0.0033$, CB2$^{-/-}$: $p < 0.0001$, APP/PS1: $p < 0.0001$ and APP/PS1$*$CB2$^{-/-}$: $p = 0.0004$). Furthermore, *Tnfα* gene expression was highly upregulated in 14-month-old APP/PS1 mice when compared to age-matched

$CB2^{+/+}$ ($p < 0.0001$) and $CB2^{-/-}$ ($p = 0.0009$) mice as well as in comparison to APP/PS1$*CB2^{-/-}$ ($p = 0.0020$) mice. Interestingly, an upregulation of *Tnfα* gene expression was not detected in aged APP/PS1$*CB2^{-/-}$ mice, as *Tnfα* expression levels remained comparable to those of $CB2^{+/+}$ and $CB2^{-/-}$ mice.

In 14-month-old mice, expression levels of *Il-1β* were upregulated in samples of AD tg mice. Statistical analyses detected significant interaction ($F_{3,53} = 6.883$; $p = 0.0005$), age ($F_{1,53} = 35.84$; $p < 0.0001$) and genotype ($F_{3,53} = 11.79$; $p < 0.0001$) effects (Fig. 5.21, B). In detail, hippocampal tissue expression of *Il-1β* was significantly upregulated in aged APP/PS1 (appox. 4.6x) and APP/PS1$*CB2^{-/-}$ (approx. 4.7x) mice when compared to age-matched $CB2^{+/+}$ littermates ($p < 0.0001$). Similarly, *Il-1β*-levels of APP/PS1 and APP/PS1$*CB2^{-/-}$ mice were significantly increased as compared to $CB2^{-/-}$ mice ($p = 0.0012$ and $p = 0.0038$, respectively). However, *Il-1β* gene expression levels remained equivalent in samples of aged APP/PS1 and APP/PS1$*CB2^{-/-}$ mice (Fig. 5.21, B).

Gene expression of *Inos* remained comparable, independently of age and genotype. Solely a significant interaction effect was detected ($F_{3,54} = 2.945$, $p = 0.0410$; Fig. 5.21, C). Expression of *Inos* was not altered between 14-old APP/PS1 and APP/PS1$*CB2^{-/-}$ mice ($p = 0.0734$).

Statistical analysis of gene expression levels of the ambivalent cytokine *Il-6* revealed a significant genotype effect ($F_{3,51} = 4.177$, $p = 0.0102$; Fig.5.21, D). However, Tukey's multiple comparisons test failed to detect significant differences between the single groups. Thus, mRNA expression levels of *Inos* and *Il-6* were neither age- nor genotype-dependently regulated.

5.5.2 Altered mRNA expression pattern of Ccl2 and Ccr2

The monocyte chemoattractant protein 1 (MCP1), which is also referred to as chemokine (c-c motif) ligand 2 (CCL2), is a small inducible cytokine responsible for the recruitment of monocytes, memory t-cells and dendritic cells to sites of inflammation. An involvement of CCL2 in various neurodegenerative diseases, including epilepsy, experimental autoimmune encephalomyelitis (EAE), traumatic brain injury and AD has been demonstrated in various studies [128, 126]. Therefore, the effect of CB2 signalling on *Ccl2* expression levels was analysed in samples of AD and control mice. Using a specific assay targeting *Ccl2*, a strong increase of *Ccl2* gene expression was detected in hippocampal tissue of 14-month-old mice as compared to expression levels in tissue samples of 9-month-old mice ($F_{1,51} = 126.3$, $p < 0.0001$; Fig. 5.22, A). A detailed analysis of the 14-month-old group individually revealed a significant CB2-dependent decrease of *Ccl2* ($p = 0.0152$). This finding is in line with our in vitro data, showing a significantly diminished CCL2 secretion in microglia derived from CB2-deficient mice (see Fig. 5.2, C). In tissue samples of 9-month-old mice, *Ccl2* expression levels remained comparable between the four genotype groups.

Expression of the corresponding receptor *Ccr2* was genotype-dependently altered ($F_{3,51} = 6.766$,

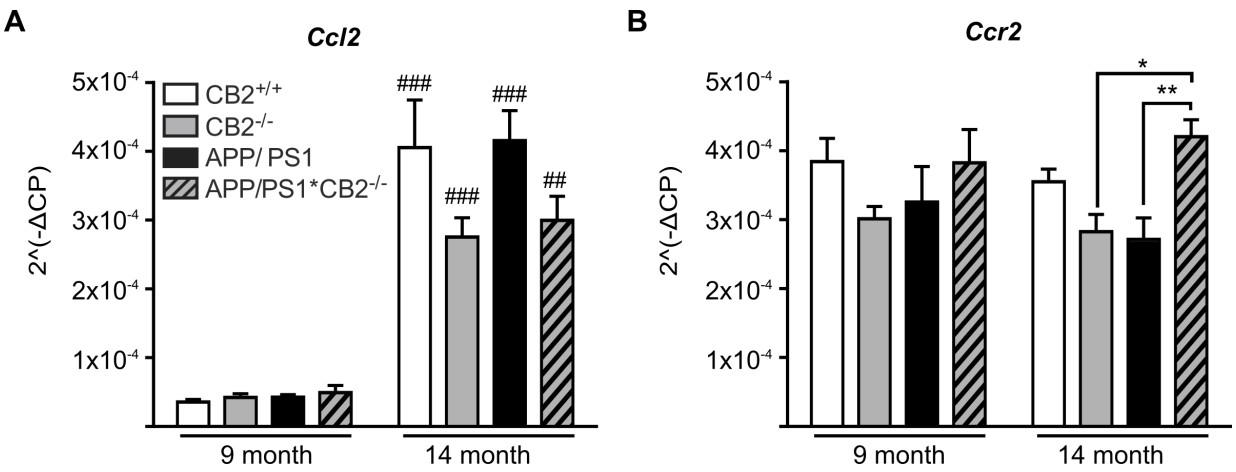

Figure 5.22: Gene expression analysis of the monocytic chemokine CCL2 and its receptor CCR2. Gene expression levels of *Ccl2* and *Ccr2* were analysed in hippocampal tissue of 9- and 14-month-old $CB2^{+/+}$ (white), $CB2^{-/-}$ (gray), APP/PS1 (black) and APP/PS1$*$$CB2^{-/-}$ mice (black striped). Expression levels of *Ccl2* (A)and *Ccr2* (B) were normalised to expression levels of the corresponding reference gene GAPDH. n = 3-13; Data were analysed by 2-way ANOVA followed by Tukey's multiple comparisons test, $*p < 0.05$, $**p < 0.01$, $***p < 0.001$; # significance to corresponding 9-month-old group

p = 0.0006; Fig. 5.22, B). Furthermore, Tukey's multiple comparisons test revealed a significantly increased *Ccr2* expression in samples of aged APP/PS1$*$$CB2^{-/-}$ mice as compared to to samples of age-matched $CB2^{-/-}$ (p = 0.0203) and APP/PS1 (p = 0.0090) mice.

5.6 Rescue of neurodegeneration in aged APP/PS1∗CB2$^{-/-}$ mice

AD-associated neuroinflammation is generally associated with a chronic and progressive loss of neuronal structure and function, resulting in functional and mental impairments [223]. As we already demonstrated a decreased microgliosis and a diminished expression of inflammatory markers in brain samples of 14-month-old APP/PS1∗CB2$^{-/-}$, we subsequently analysed whether AD associated neuronal loss is altered in those mice. Therefore, immunohistochemical analyses of the neuronal marker NeuN were conducted in the hippocampal CA1/2 layer and the thickness of the stratum pyramidale (SP) was measured and subsequently compared between the four groups (Fig. 5.23, A). Representative images of NeuN immunoreactivity in hippocampal CA1/2 regions are shown in Fig. 5.23, B.

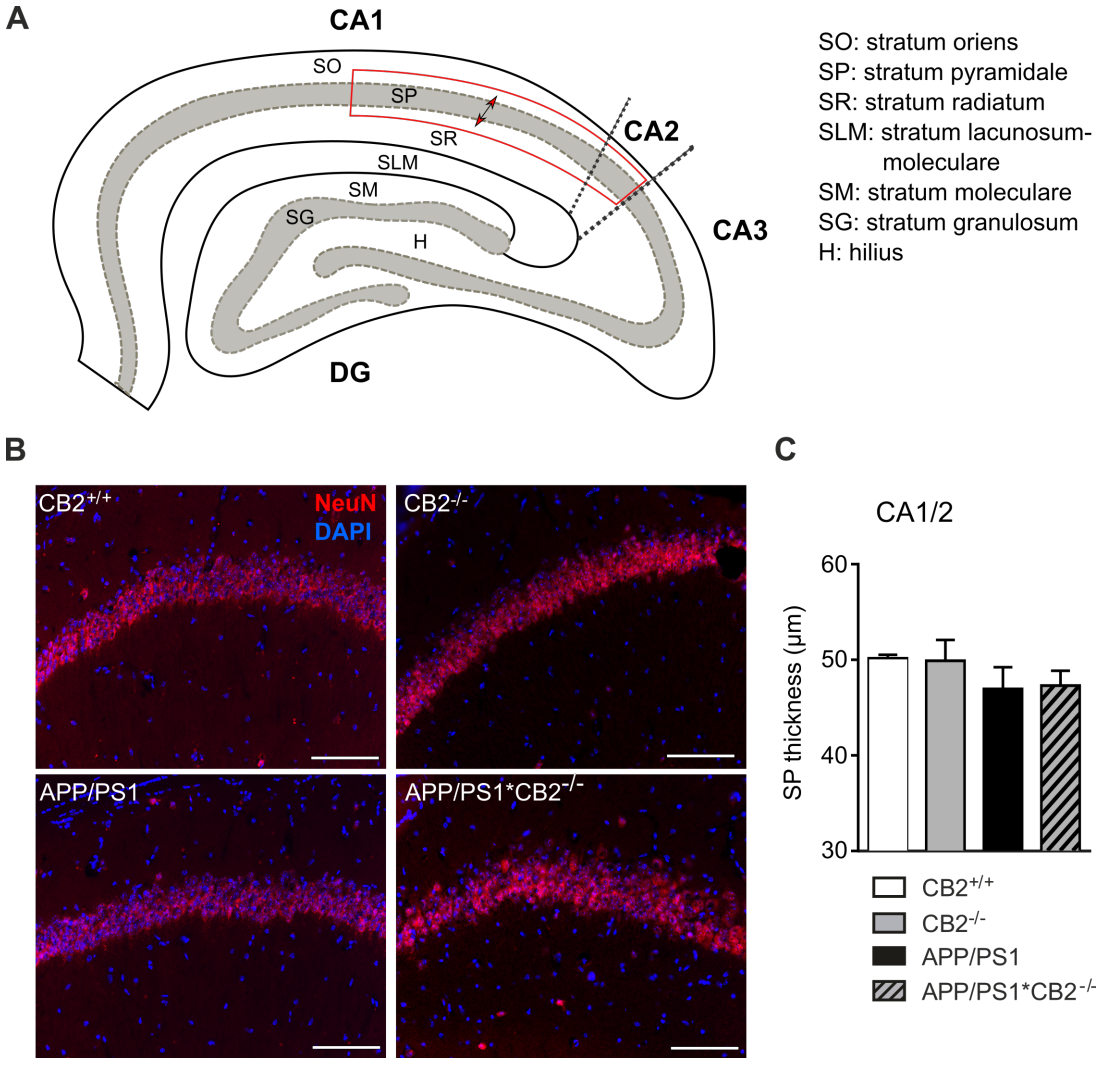

Figure 5.23: Evaluation of hippocampal neurodegeneration in 9-month-old mice. Neuronal loss was evaluated in the stratum pyramidale (SP) of the hippocampal CA1/2 region (A). Representative images of NeuN immunoreactivity in the CA1/2 region in samples of CB2$^{+/+}$ (upper left), CB2$^{-/-}$ (upper right), APP/PS1 (lower left) and APP/PS1∗CB2$^{-/-}$ (lower right) mice show the neuronal distribution (B, scale bar = 100μm). The thickness of the SP layer in μm revealed an equal cellular distribution within the groups (C). N = 3, 6 images per animal; Data were analysed by one-way ANOVA, followed by Tukey's multiple comparisons test. Data and analysis adopted from Gregor Toporowski.

The quantification revealed comparable neuronal densities in samples of 9-month-old $CB2^{+/+}$ (mean 50.10 ± 0.374), $CB2^{-/-}$ (mean 49.86 ± 2.17), APP/PS1 (mean 46.91 ± 2.28) and APP/PS1$*$ $CB2^{-/-}$ (mean 47.26 ± 1.56) mice (one-way ANOVA, $F_{3,8} = 0.9018$, $p = 0.4816$; Fig. 5.23, B and C). Subsequently, the neuronal distribution in cortical areas was analysed as NeuN-positive cells per mm^2 in different cortical regions (Fig. 5.24, A). Representative images of the NeuN immunoreactivity are schown in Fig 5.24, B. Similar to the results described above, a comparable NeuN immunoreactivity was detected in tissue samples of all four 9-month-old groups (one-way ANOVA, $F_{3,8} = 2.549$, $p = 0.1290$; Fig. 5.24, B).

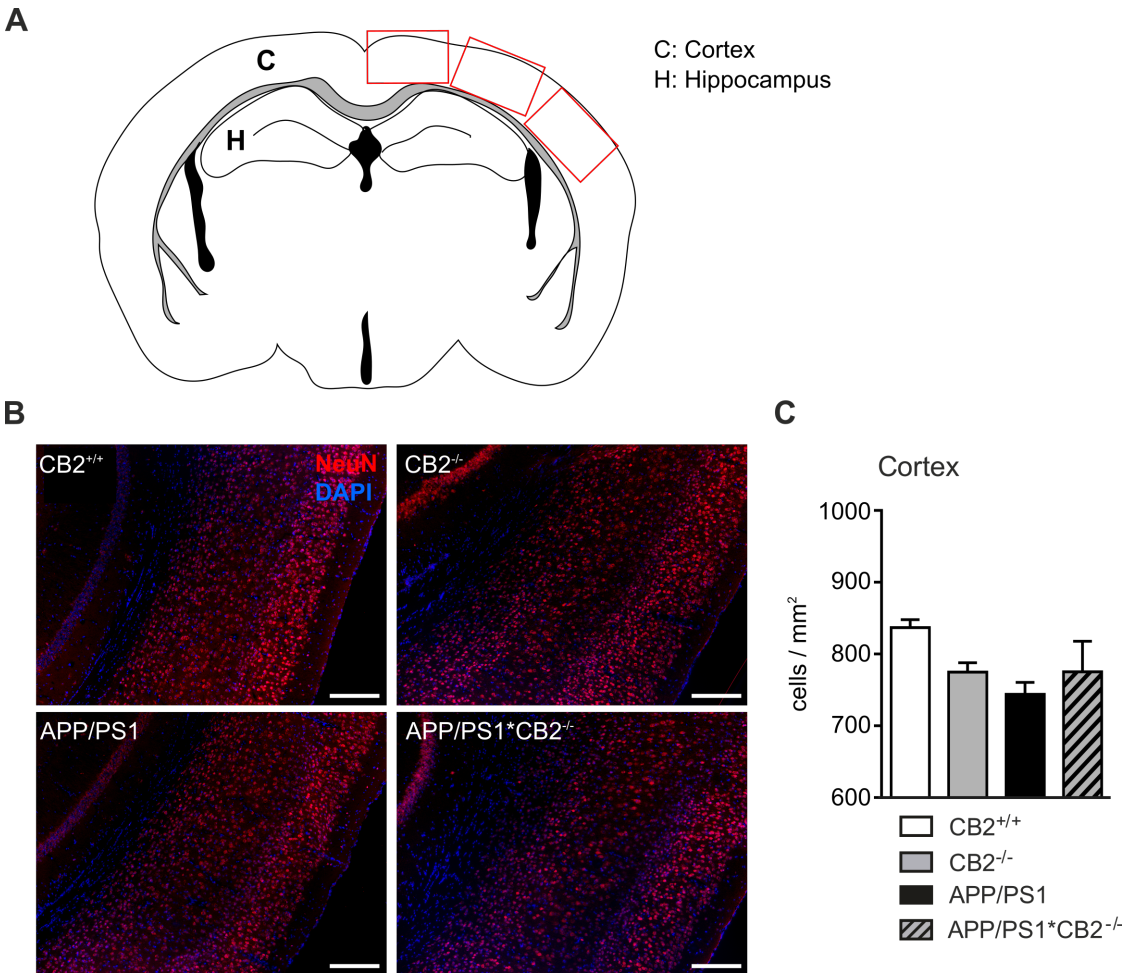

Figure 5.24: Evaluation of cortical neurodegeneration in 9-month-old mice. Neuronal loss was evaluated in cortical areas (red boxes) of coronally sliced brain sections (A). Representative images of NeuN immunoreactivity in $CB2^{+/+}$ (upper left), $CB2^{-/-}$ (upper right), APP/PS1 (lower left) and APP/PS1$*$$CB2^{-/-}$ (lower right) mice show the neuronal distribution in cortical regions (B; scale bar = 100 μm). Quantification of the neuronal bound revealed an equal cellular distribution within the groups (C). N = 3 with 6 images per animal; Data were analysed by one-way ANOVA, followed by Tukey's multiple comparisons test. Data and analysis adopted from Gregor Toporowski.

In contrast to 9-month-old mice, the thickness of the hippocampal CA1/2 pyramidal cell layer was markedly reduced in samples of 14-month-old APP/PS1 mice (Fig. 5.25, A). This finding was confirmed by a quantitative analysis, showing a significantly reduced SP thickness in samples of APP/PS1 mice when compared to age-matched $CB2^{+/+}$ littermates (Fig. 5.25, B; one-way

ANOVA, $F_{3,8} = 4.739$, $p = 0.0349$, followed by Tukey's multiple comparisons test $p = 0.0249$). Interestingly, this effect was rescued in samples of aged APP/PS1∗CB2$^{-/-}$ mice, which showed a comparable SP thickness to samples of age-matched CB2$^{+/+}$ mice (Fig. 5.25, B).

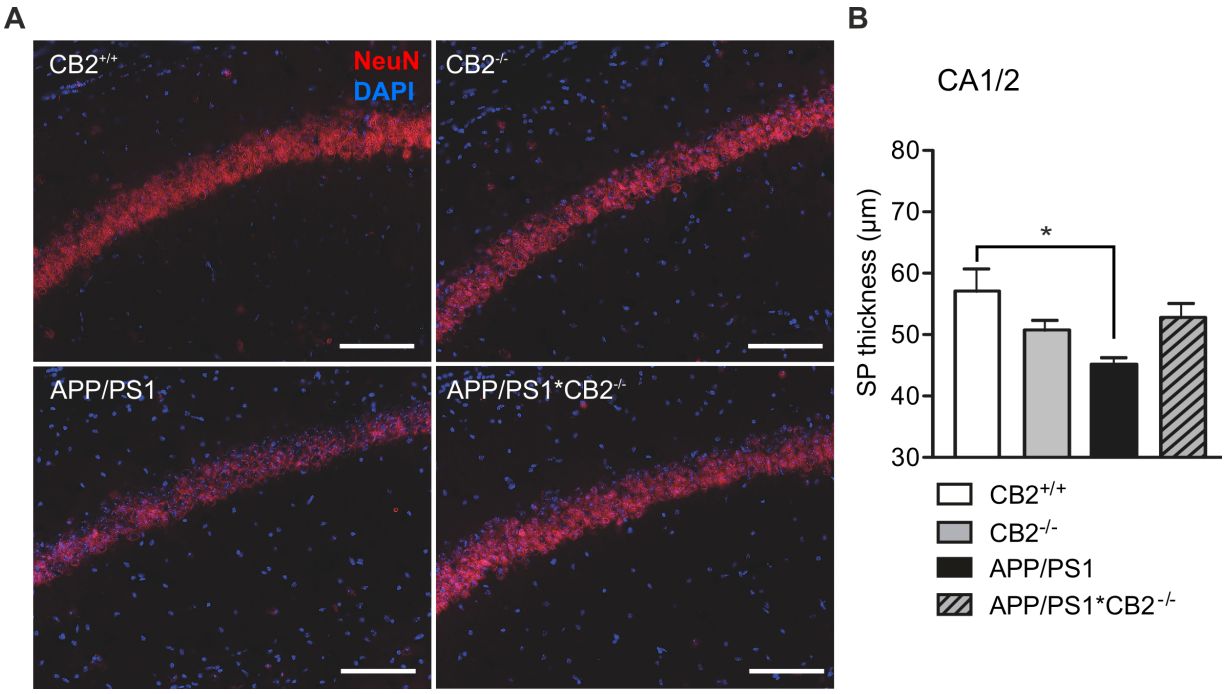

Figure 5.25: Evaluation of hippocampal neurodegeneration in 14-month-old mice. Representative images of NeuN immunoreactivity in the stratum pyramidale (SP) of the CA1/2 region in samples of CB2$^{+/+}$ (upper left), CB2$^{-/-}$ (upper right), APP/PS1 (lower left) and APP/PS1∗CB2$^{-/-}$ (lower right) mice show the neuronal distribution (A, scale bar = 100μm). The thickness of the neuronal CA1/2 pyramidal cell layer in μm revealed a decreased NeuN immunoreactivity in APP/PS1 mice (B). N = 3 with, 6 images per animal; Data were analysed by one-way ANOVA, followed by Tukey's multiple comparisons test, $*p < 0.05$, $**p < 0.01$, $***p < 0.001$. Data and analysis adopted from Gregor Toporowski.

Similarly, the neuronal density in cortical areas was severely diminished in samples of aged APP/PS1 mice; an effect that was not present in samples of CB2$^{-/-}$ and APP/PS1∗CB2$^{-/-}$ mice (Fig. 5.26, A and B). The average number of NeuN-positive cells was significantly reduced in samples of APP/PS1 mice (547 cells / mm^2) as compared to CB2$^{+/+}$ (796 cells / mm^2; $p = 0.0009$), CB2$^{-/-}$ (750 cells / mm^2; $p = 0.0034$) and APP/PS1∗CB2$^{-/-}$ (720 cells / mm^2; $p = 0.0091$) mice (Fig. 5.26, B; one-way ANOVA, followed by Tukey's multiple comparisons test).

In mouse models of AD, a loss of neurons, in particular interneurons, had been demonstrated in various previous studies [140, 203, 257, 271]. Therefore, immunohistochemical analysis using a specific antibody detecting parvalbuminergic interneurons was conducted in tissue samples of 14-month-old mice to further characterise the subpopulation of declining neurons. In line with the findings of overall neuronal loss through NeuN-staining, a significant loss of parvalbuminergic interneurons (parv-positive) was detected in cortical areas aged APP/PS1 mice (Fig. 5.27; A-B). Representative immunohistochemical images display the cellular distribution of parvalbuminergic cells in the four groups (Fig. 5.27, A). The quantification revealed a significant reduction of parv-

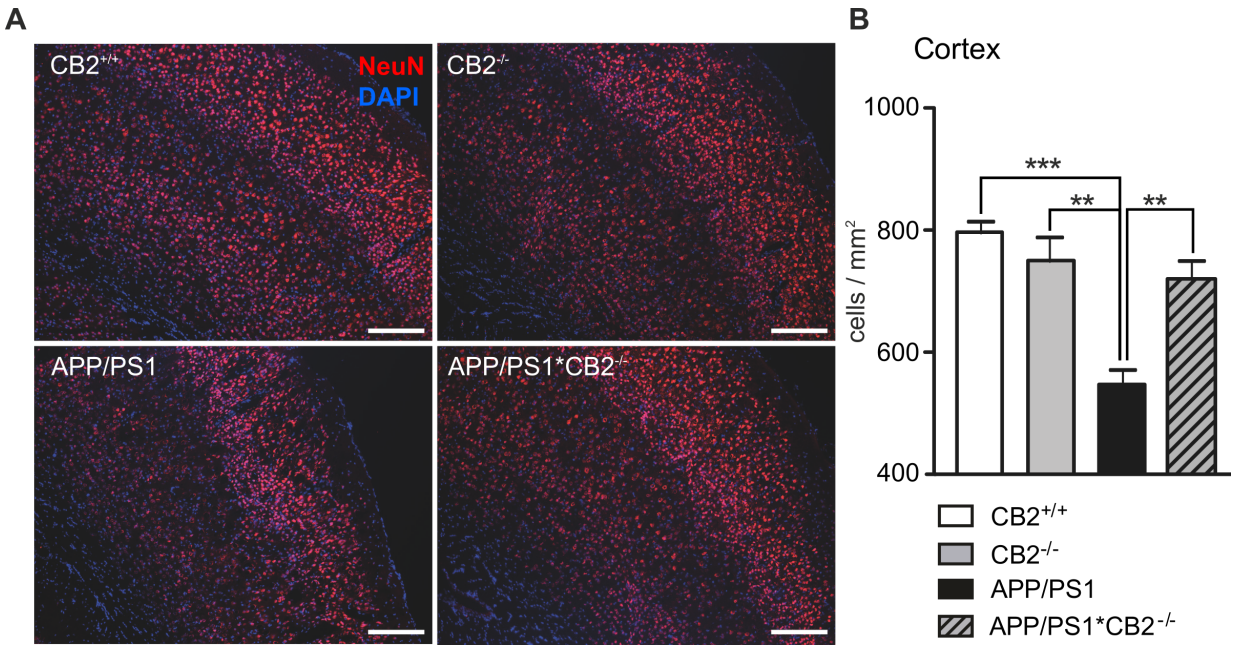

Figure 5.26: Evaluation of cortical neurodegeneration in 14-month-old mice. Representative images of NeuN immunoreactivity in $CB2^{+/+}$ (upper left), $CB2^{-/-}$ (upper right), APP/PS1 (lower left) and APP/PS1$*$$CB2^{-/-}$ (lower right) mice show the neuronal distribution in cortical regions (A; scale bar = 100μm). Quantification of the neuronal density as the number of NeuN positive cells per mm^2 revealed a decreased NeuN immunoreactivity in APP/PS1 mice (B). N = 3 with 6 images per animal; Data were analysed by one-way ANOVA, followed by Tukey's multiple comparisons test, $*p < 0.05$, $**p < 0.01$, $***p < 0.001$. Data and analysis adopted from Gregor Toporowski.

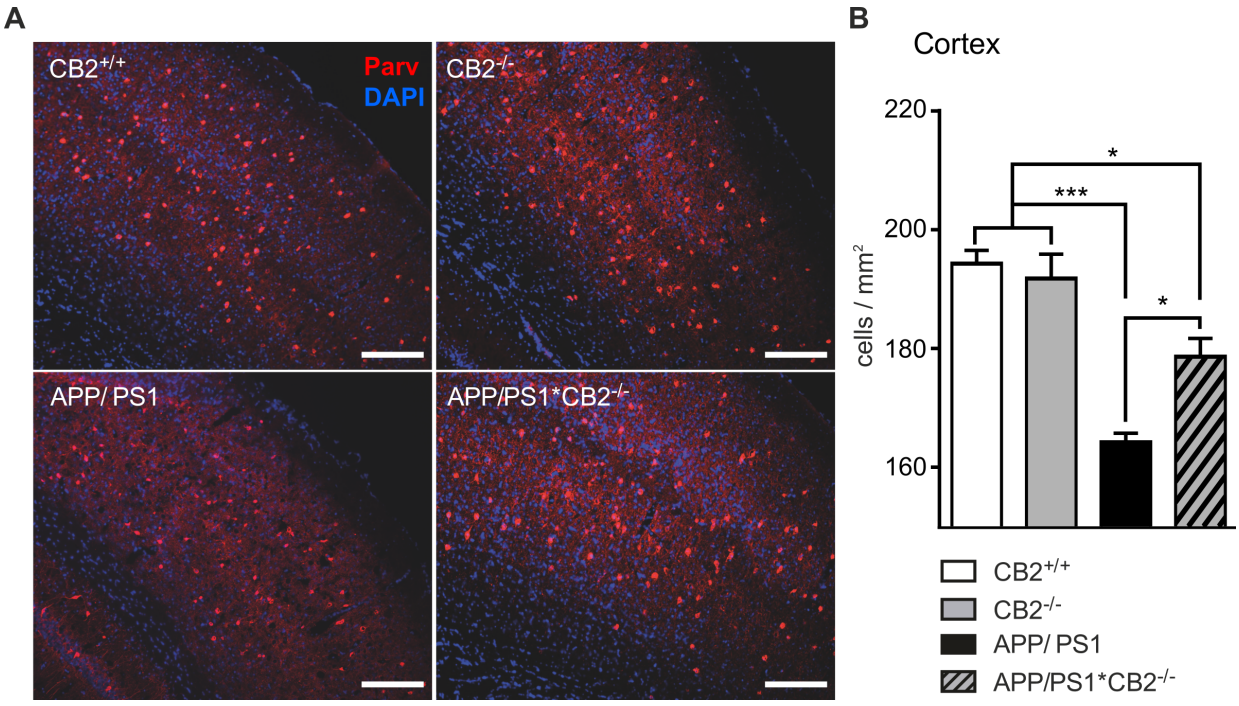

Figure 5.27: Distribution of parvalbuminergic interneurons in 14-month-old mice. Representative images of Parv immunoreactivity in $CB2^{+/+}$ (upper left), $CB2^{-/-}$ (upper right), APP/PS1 (lower left) and APP/PS1$*$$CB2^{-/-}$ (lower right) mice in the cortex (A) (scale bar = 100 μm). The quantification of parv-positive cells per mm^2 (B) revealed a decreased immunoreactivity in APP/PS1 mice. N = 3 with 6 images per animal; Data were analysed by one-way ANOVA, followed by Tukey's multiple comparisons test, $*p < 0.05$, $**p < 0.01$, $***p < 0.001$. Data and analysis adopted from Gregor Toporowski.

positive interneurons in samples of APP/PS1 mice when compared to samples of age-matched $CB2^{+/+}$ ($p = 0.0004$), $CB2^{-/-}$ ($p = 0.0007$) and APP/PS1$*$$CB2^{-/-}$ ($p = 0.0319$) mice (Fig. 5.27, B). However, the cellular density of parvalbuminergic interneurons was also slightly decreased in samples of APP/PS1$*$$CB2^{-/-}$ mice when compared to samples of $CB2^{+/+}$ ($p = 0.0206$) and $CB2^{-/-}$ ($p = 0.0483$) mice, respectively.

5.7 Rescue of cognitive deficits in aged APP/PS1∗CB2$^{-/-}$ mice

Finally, the impact of CB2 signalling on cognitive performance and spatial learning was analysed by using the Morris water maze paradigm. Therefore, 9- and 14-month-old mice were trained to find a hidden platform in a milky water bath. In the 5-day-training period with four training trials per day, 9-month-old CB2$^{+/+}$ and CB2$^{-/-}$ mice showed equal learning curves, represented by comparable escape latencies (Fig. 5.28, A). Within both groups, statistical analyses revealed a highly significant trial effect (2-way ANOVA followed by Sidak's multiple comparisons test, $F_{4,100} = 26.67$, $p < 0.0001$), while a genotype effect was absent ($F_{1,25} = 0.1778$, $p = 0.6769$). Similarly, escape latencies were decreasing over the training period in 9-month-old APP/PS1 and APP/PS1∗CB2$^{-/-}$ (2-way ANOVA followed by Sidak's multiple comparisons test, $F_{4,88} = 22.61$, $p < 0.0001$; Fig. 5.28, B). Again, a significant genotype effect was absent ($F_{4,22} = 2.181$, $p = 0.1539$).

To evaluate potential differences in short-term memory, mean escape latencies of the four individual trials of the first acquisition day were analysed (Fig. 5.28, C, D). In both control groups, CB2$^{+/+}$ and CB2$^{-/-}$, a significant trial effect was detected ($F_{3,84} = 13.93$, $p < 0.0001$), while a general genotype effect was absent ($p = 0.3305$; Fig. 5.28, C). However, statistical analysis using Sidak's multiple comparisons test showed a significant genotype effect between both groups on trial four ($p = 0.0084$), as CB2$^{+/+}$ needed less time to find the platform compared to CB2$^{-/-}$. In APP/PS1 and APP/PS1∗CB2$^{+/+}$ mice a significant difference between the four trials or both genotypes was absent.

Finally, analysis of the mean swim speed over the whole training period showed neither an alteration within CB2$^{+/+}$ and CB2$^{-/-}$ (genotype effect $p = 0.1652$; Fig. 5.28, E), nor within APP/PS1 and APP/PS1∗CB2$^{+/+}$ (genotype effect $p = 0.8540$; Fig. 5.28, F) mice. However, mean swim speed decreased significantly with increasing number of trials in both, the control group - CB2$^{+/+}$ and CB2$^{-/-}$ (trial effect: $F_{4,112} = 68.84$, $p < 0.0001$; Fig. 5.28, E) - as well as in the AD tg group - APP/PS1 and APP/PS1∗CB2$^{+/+}$ (trial effect: $F_{4,92} = 40.43$, $p < 0.0001$; Fig. 5.28, F).

In 14-month-old mice, mean escape latency was comparable between CB2$^{+/+}$ and CB2$^{-/-}$ mice (Fig. 5.29, A). In both groups, the time needed to find the hidden platform decreased significantly with increasing number of trials (time effect: $F_{4,64} = 23.37$, $p > 0.0001$), while a difference between both genotypes was absent ($p = 0.8414$). More interestingly, a highly significant genotype effect ($F_{1,11} = 13.01$, $p = 0.0041$) regarding the mean time spent to find the hidden platform was detected between aged APP/PS1 and APP/PS1∗CB2$^{-/-}$ mice (Fig. 5.29, B). Similar to control groups, performance of both AD tg groups improved significantly during the acquisition phase, which is reflected by a significant trial effect ($F_{4,44} = 21.81$, $p < 0.0001$). Moreover, Sidak's multiple comparisons test showed a significant improvement in the escape latency of APP/PS1∗CB2$^{-/-}$ versus APP/PS1 mice on trial three ($p = 0.0267$) and trial five ($p = 0.0311$). Equivalent to 9-month-old

mice, short-term memory was evaluated as the decrease in mean escape latency over the four trials of the first day of acquisition. With 1 h intertrial time, $CB2^{+/+}$ as well as $CB2^{-/-}$ mice learned equally fast to find the hidden platform (trial effect: $F_{3,48} = 6.550$, $p = 0.0008$), thus, no significant difference was detected in short-term memory (genotype effect $p = 0.2266$; Fig. 5.29, C).

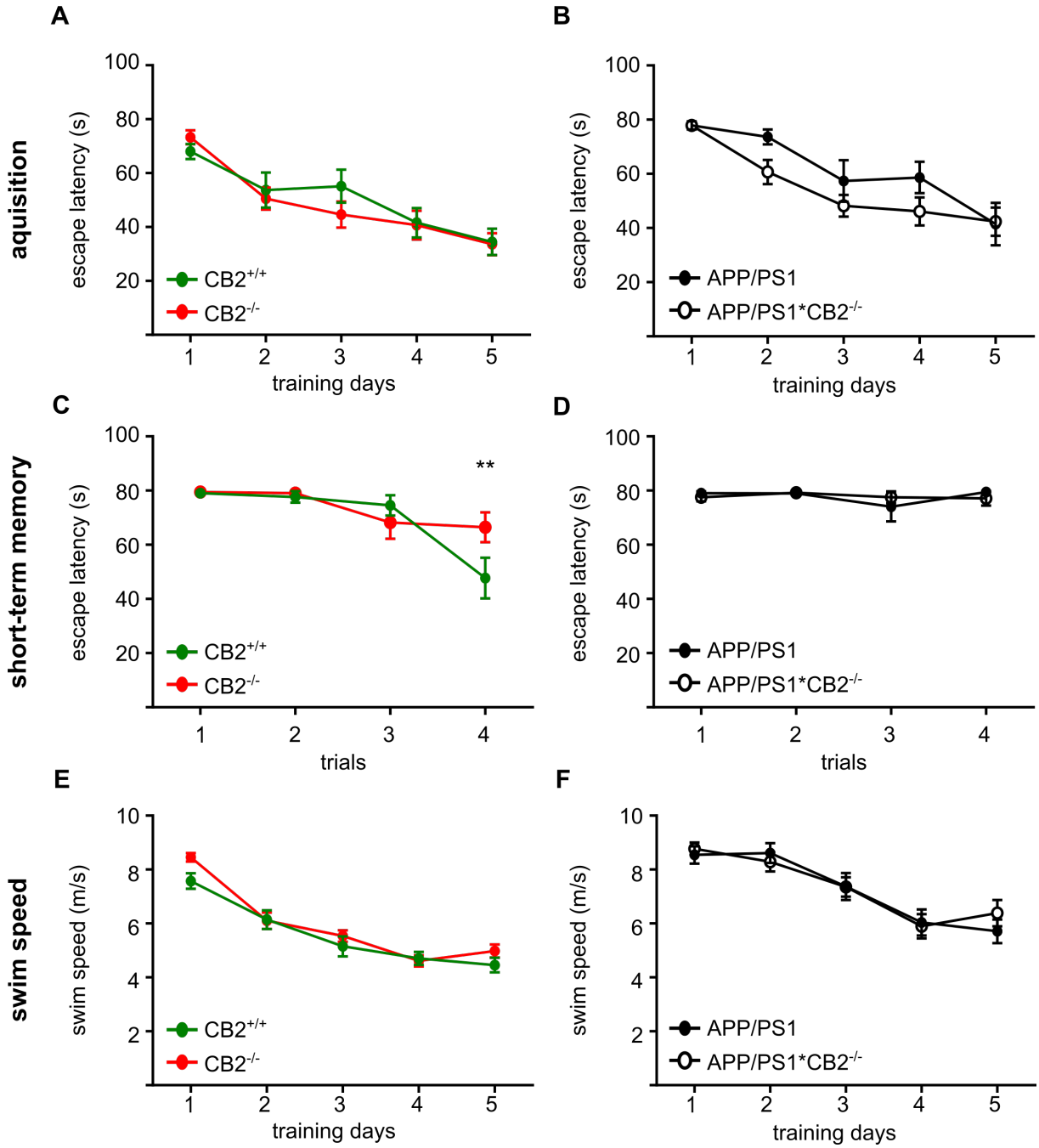

Figure 5.28: Cognitive performance of 9-month-old mice in the Morris water maze paradigm. Leaning curves show mean escape latency (A, B), short-term memory (C, D) and swim speed (D, E) of 9-month-old mice. Statistical comparison was conducted between $CB2^{+/+}$ (green) and $CB2^{-/-}$ (red; A, C and E), as well as between APP/PS1 (black filled) and APP/PS1$*$$CB2^{-/-}$ (white filled; B, D and F). N = 8-16; data were analysed by two-way ANOVA, followed by Sidaks multiple comparison test for repeated measures, $*p < 0.05$, $**p < 0.01$, $***p < 0.001$

In contrast, APP/PS1$*$$CB2^{-/-}$ performed significantly better in the test paradigm, which was already visible on the first training day (genotype effect: $F_{1,11} = 14.87$, $p = 0.0027$; Fig. 5.29, D).

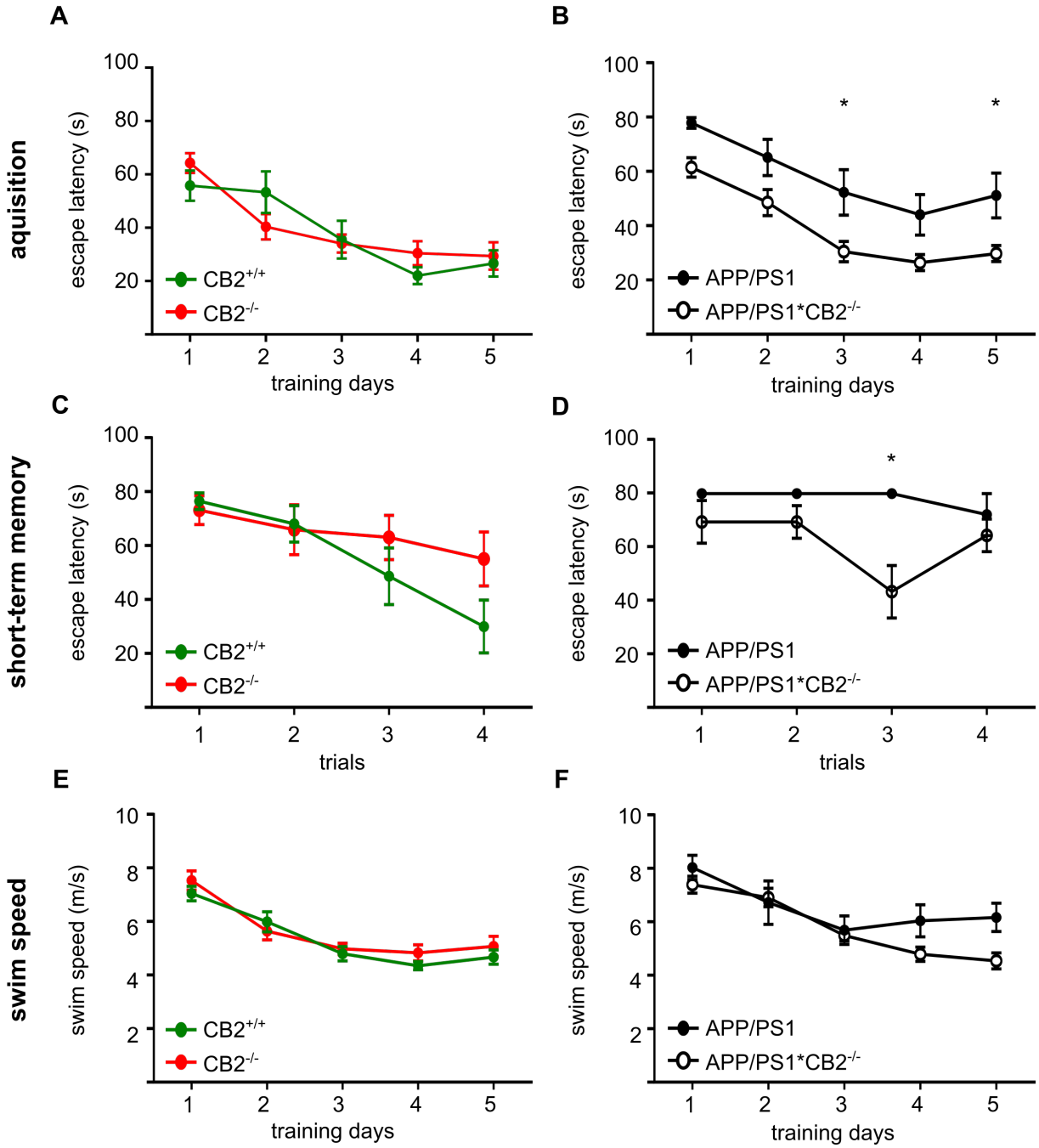

Figure 5.29: Cognitive performance of 14-month-old mice in the Morris water maze paradigm. Leaning curves show mean escape latency (A, B), short-term memory (C, D) and swim speed (D, E) of 14-month-old mice. Statistical comparison was conducted between $CB2^{+/+}$ (green) and $CB2^{-/-}$ (red; A, C and E), as well as between APP/PS1 (black filled) and APP/PS1$*CB2^{-/-}$ (white filled; B, D and F). N = 8-16; data were analysed by two-way ANOVA, followed by Sidaks multiple comparison test for repeated measures, $*p < 0.05$, $**p < 0.01$, $***p < 0.001$

Particularly, escape latencies of the third trial dropped significantly in APP/PS1$*CB2^{-/-}$ when compared to age-matched APP/PS1 mice ($p = 0.0008$). However, this difference was abolished at trial four ($p = 0.8659$).

To assess whether genotype-dependent differences seen in APP/PS1 and APP/PS1$*CB2^{-/-}$ mice were due to physiological reasons, the mean swim speed was analysed over the whole training period. In both control groups, $CB2^{+/+}$ and $CB2^{-/-}$ mice, the mean swim speed was sta-

tistically equivalent (genotype effect: $p = 0.4306$; Fig. 5.29, E). However, a significant decrease of the mean swim speed over time was detected (time effect: $F_{4,64} = 43.03$, $p < 0.0001$). Similarly, APP/PS1 and APP/PS1$*$CB2$^{-/-}$ mice swam slower with increasing training days (time effect: $F_{4,44} = 24.75$, $p < 0.0001$), but genotype-dependent differences were absent (genotype effect: $F_{1,11} = 1.90132$, $p = 0.1954$; Fig. 5.29, F).

6 Discussion

The present study was designed to investigate the effects of CB2 signalling in AD associated neuroinflammation. Therefore, a CB2 deficient ($CB2^{-/-}$) murine model reflecting the main pathomechanism of AD (APP/PS1$*$$CB2^{-/-}$) was analysed and compared to $CB2^{+/+}$, $CB2^{-/-}$ and APP/PS1 littermates. In comparison to age-matched APP/PS1 mice, 14-month-old APP/PS1$*$$CB2^{-/-}$ mice showed reduced levels of Aβ plaque load in the cerebral cortex and hippocampus and increased mRNA expression levels of the Aβ degrading enzymes *Ide* and *Mmp9*, while soluble Aβ40 and Aβ42 as well as mRNA expression of full length *App* was comparable. Furthermore, we detected a significantly enhanced Iba1 immunoreactivity in aged APP/PS1 mice, while the amount of Iba1-positive cells in samples of APP/PS1$*$$CB2^{-/-}$ mice was comparable to levels detected in $CB2^{+/+}$ mice. This finding was in line with flow cytometric analyses of intracerebral leucocytes, showing reduced percentages of resident microglia as well as invading macrophages. Interestingly, AD-associated neuroinflammatory marker, such as ICAM, CD40, TNF-α or iNOS, were reduced in brain samples of 14-month-old APP/PS1$*$$CB2^{-/-}$ mice, but not in APP/PS1 mice. These findings were accompanied by a reduced neuronal loss, evaluated by NeuN and parvalbumin immunoreactivity. Consecutively, the observed differences in plaque load, inflammatory molecules and neurodegeneration resulted in a rescue of cognitive deficits in aged APP/PS1$*$$CB2^{-/-}$ mice.

6.1 Analysis of CB2 signalling in neonatal microglia

To assess the functional role of CB2 in the inflammatory response of microglia, neonatal microglia were challenged with pro-inflammatory stimuli. The presence of functional CB2 receptors on microglia cells had already been demonstrated by various studies [36, 57]. Furthermore, it was shown that exposure of neonatal rat microglia to the exogenous cannabinoid THC resulted in a reduction of LPS-induced mRNA expression levels of IL-1α, IL-1β, IL-6 and TNFα [210]. Thus, these data already implicated that CB2 plays an important role in activated immune cells and particularly in an inflammatory milieu.

6.1.1 CB2 deficient microglia are less responsive to pro-inflammatory insults

According to the Th-1/Th-2 nomenclature of T-lymphocytes, microglia cells can also be primed into different activation states [261, 42, 43]. In the current study, the ability of $CB2^{+/+}$ and $CB2^{-/-}$ microglia regarding their response to pro-inflammatory stimuli was evaluated. Thereby, we clearly demonstrated that microglia derived from $CB2^{-/-}$ mice were much less responsive to pro-inflammatory stimulation than cells from control mice, while alternative activation markers are increased in these mice. In contrast, it was demonstrated that the alternative activation (M2) is hampered in microglia from CB2 knockout animals [170]. However, Mecha et al. used the

commercially available CB2 knockout strain generated by Deltagen ($Cnr2^{tm1Dgen}$), which contains a 391 bp deletion at the N terminus. Thus, the different CB2 knockout strategy as well as the different genetic background of these mice could be an explanation for the contradictory results. In comparison to CB2 receptor deletion, the activation of microglial CB2 receptors with synthetic or exogenous cannabinoids was generally shown to suppress microglia activation. A study by Ehrhart et al. showed that selective stimulation of CB2 receptors by the synthetic agonist JWH-015 suppressed microglia activity in terms of a reduced IFNγ-induced expression of CD40, TNFα and iNOS [57]. Thus, the current data suggest a context- and system-dependent role of CB2 regarding microglial activation pattern.

In the current study, we could also demonstrate that the LPS/IFNγ-induced secretion of the monocytic chemotactic cytokine CCL2 was markedly reduced in microglia cells derived from $CB2^{-/-}$ mice, while the pro-inflammatory challenge in $CB2^{+/+}$ cultures dramatically induced the CCL2 secretion. These results are in line with a study by Deveaux et al., demonstrating that genetic or pharmacological inactivation of CB2 receptors reduced CCL2 and TNFα expression in adipose tissue macrophages associated with obesity [52]. In different studies, induction of CCL2 was demonstrated not only at sites of acute inflammation but also in the context of various chronic inflammatory diseases, including atherosclerosis, autoimmune diseases, cancer and chronic infection [50]. In the CNS, CCL2 was shown as the responsible mediator for the recruitment of immune cells in neuroinflammatory conditions such as AD, ischemic and traumatic brain injury, multiple sclerosis, experimental autoimmune encephalomyelitis and viral encephalitis [21, 41, 153, 284, 128, 275]. These results suggests that CB2 deficient microglia are less able to recruit peripheral immune cells to sites of inflammation.

Ever since Stein et al. observed the effect of IL-4 stimulation on the expression of the mannose receptor (MMR), the alternative activation pattern has been an area of interest [250]. Generally, acute pro-inflammatory stimulations leads to a decreased expression of anti-inflammatory marker molecules, such as MMR [195]. Interestingly, $CB2^{-/-}$ microglia already exhibited increased levels of MMR at baseline conditions. After stimulation, a decreased MMR expression was detected in cells derived from $CB2^{+/+}$ mice, while MMR expression in $CB2^{-/-}$ cells remained constant in response to LPS and IFNγ. Furthermore, secretion of the anti-infammatory cytokine IL-10 was induced in both cultures, $CB2^{+/+}$ and $CB2^{-/-}$, upon inflammatory conditions. However, microglia cells from $CB2^{-/-}$ mice displayed a two-fold increase of IL-10 upon LPS and IFNγ challenge as compared to $CB2^{+/+}$ cells. As CB2 receptor activation is generally proposed to be anti-inflammatory [224, 62], a distinct M1 phenotype would be expected in microglia cells lacking CB2 signalling. Thus, the current data suggest a crucial role of CB2 deletion on microglia function independent from pharmacological inhibition.

6.1.2 Phagocytic capacity is unaltered in neonatal microglia and macrophages

To investigate whether the altered inflammatory profile of $CB2^{-/-}$ microglia also affected their ability to phagocytose exogenous material, we further quantified the uptake of fluorescently labelled Aβ-peptides in both, $CB2^{+/+}$ and $CB2^{-/-}$ cultures. The ability of microglia to phagocytose Aβ *in vitro* was already shown in 1991 [279]. In the current study we demonstrated that lack of CB2 signalling did not alter the uptake of fluorescently labelled Aβ by neonatal microglia or BMdM. Quantification via flow cytometry revealed comparable phagocytic capacities of cultures derived from $CB2^{+/+}$ and $CB2^{-/-}$ mice.

It was shown that the cannabinoid agonist JWH-015 triggered the phagocytic capacity of human macrophages incubated with Aβ and induced the removal of native Aβ from human frozen tissue sections [259]. This effect was at least partially CB2 mediated, as the selective CB2 antagonist SR144528 could prevent the JHW-015-induced plaque removal *in situ*. In contrast, in a recent study by Mai et al. it was demonstrated that activation of CB1 (not CB2) increased macrophage phagocytic activity, while pharmacological or genetic ablation of CB1 inhibited the particle uptake. CB2 activation or inhibition, however, had no effect on macrophage phagocytic activity [154]. Thus, the influence of CB2 signalling on microglia phagocytosis seems to be cell-type and context-dependent.

6.2 Endocannabinoid system components in APP/PS1$*$$CB2^{-/-}$ mice

6.2.1 Altered expression of cannabinoid receptors with age and disease

In the current study we could demonstrate that *Cnr1* mRNA expression decreased with increasing age, particularly in mice expressing tg APP. These data are in correspondence with studies by Ramirez and Solas which showed a significant decrease in CB1 receptor levels as well as CB1 protein nitration in areas of microglial activation in AD brains [215, 248]. Additionally, independent findings by Bedse and Kalifa demonstrated a decreased CB1 protein expression mouse models of AD when compared to age-matched control mice [18, 117]. In contrast, in a study by Kärkkäine et al., who used functional autoradiography to assess CB1-receptor-dependent G(i)-protein activation, no significant difference between APP/PS1 tg and control mice in CB1 receptor signalling was found [118]. Furthermore, it was shown that CB1 activity is increased in early AD stages but decreased in advanced stages [156]. The initial hyperactivity of the ECS in brain areas, which lack pathological hallmarks, suggests a compensatory attempt for the early synaptic impairment. However, with progression of the disease this compensatory mechanism might then be excelled. Thus, the direct role of *Cnr1* receptor expression and CB1 receptor activity in tg mouse models of AD still needs to be clarified in future research.

Besides the regulation of CB1 receptors, the role of CB2 signalling is an area of great interest

for recent years, since AD is intensively investigated as an inflammatory condition of the CNS. In the current study *Cnr2* was equally expressed in hippocampal tissues of APP/PS1 mice compared to control littermates. Benito at al. showed a selective overexpression of CB2 in neurotic plaque-associated microglia [20]. These findings were in accordance with studies using AD-associated mouse models, which also revealed CB2 overexpression in Aβ affected brain areas [107, 233]. Likewise, rats and rat astroglioma cells showed an up-regulation of CB2 receptor and an increase in 2-AG concentration after treatment with Aβ [60]. Thus, our current results do not directly reflect previous research results. However, this controversy might be due to different methodological approaches used to detect CB2 expression. Benito and colleagues used western blot and immunohistochemistry to detect and quantify CB2 receptor density in posmortem brains of seven AD patients. For *in vivo* evaluations of CB2 receptor density, Horti et al. described the development of a new potential radioligand ([^{11}C]A836339) for PET imaging studies [107]. Thereby, they were able to prove that CB2 receptor binding can be measured in neuroinflammatory conditions. However, the newly synthesised ligand showed relatively high non-specific binding properties, which were analysed by blocking CB2 receptors with the specific antagonist AM630 [107]. The working group of Savonenko et al. also used the radioligand [^{11}C]A836339 to evaluate CB2 receptor binding density in AD tg mouse models and claimed CB2 as a potential biomarker in Aβ-induced neuroinflammation [233]. Thereby, CB2 receptors were particularly observed in microglial processes forming engulfment synapses with Aβ plaques [233]. Thus, results obtained in our study and by using PET radioligands are not directly comparable as CB2 mRNA levels do not always reflect protein levels.

More interestingly, we found a markedly increased *Cnr2* expression in APP/PS1$*$CB2$^{-/-}$. This finding can be explained by the generation of the used CB2$^{-/-}$ mouse line. Through homologous recombination, the 3' region of the coding exon was replaced with a PGK neomycin sequence. By using this strategy, a part of the intracellular loop, the transmembrane regions 6 and 7 and the carboxy terminus were deleted. However, current available real-time gene expression assays target the remaining 5' untranslated region, therefore, the alignment of TaqMan® probes still reveal *Cnr2* mRNA expression. Furthermore, two different isoforms of the murine *Cnr2* gene (CB2A and CB2B) were detected due to the presence of two separate promoters [147]. Liu and colleagues also described a compensatory effect of *Cnr2* promoter activities, which upregulates the expression of both CB2 isoforms in the currently used CB2 knockout mouse model by [33]. Therefore, our results obtained in the present study directly reflect the findings by Liu et al. The significantly increased expression of *Cnr2* in APP/PS1$*$CB2$^{-/-}$ mice suggests an additional intrinsic compensatory mechanism to counterbalance the insufficient endocannabinoid signalling. However, these speculative explanations and their possible consequences need to be analysed in future studies.

Additionally to *Cnr1* and *Cnr2* gene expression analyses, we found an APP-dependent increase

in mRNA levels of the orphan G-protein coupled receptor *Gpr18* in aged AD tg mice. After the first reports describing GPR18 in 1997 [75], various research groups aimed to identify GRP18 expressing tissue and binding partner [267, 130, 288]. A potential link between GPR18 and microglia was provided by Hugh and colleagues in 2010 [168]. In their study, GPR18 was proposed as an unidentified abnormal-cannabinoid receptor expressed by BV-2 immortalised microglia cell line as well as in primary microglia cells. Furthermore, GPR18 has been demonstrated to regulate cellular migration through binding with its ligand N-arachidonoyl glycine (NAGly) [168]. Additionally, a subsequent study by the same working group provided evidence for a NAGly-GPR18-mediated microglia activation and cytokine production in the BV-2 microglia model system [169]. Our results suggests that GPR18 is not only involved in microglia cell cultures systems but is particularly involved in neuroinflammatory conditions *in vivo*, where it might act in neuronal-microglial communication. However, future studies need to elucidate the role of GPR18-mediated signalling events in microglia-involved neuroinflammatory conditions.

6.2.2 Altered expression of ECS synthesizing and hydrolysing enzymes

The role of the ECS in AD-associated neuroinflammation was also intensively investigated in recent years. Bisogno and Di Marzo reviewed the dual role of endocannabinoids in AD [28]. While an increased tone of endocannabinoids might exert beneficial functions by reducing pro-inflammatory microglial priming in a CB2-dependent manner [215], modulation of CB1 receptors can gate Aβ neurotoxicity and protect against Aβ-induced amnesia in hippocampal learning tasks [164]. Expression of endocannabinoid system components have been demonstrated to change with age [202] as well as in neuroinflammatory conditions, such as AD [180]. Therefore, we investigated gene expression levels of the main endocannabinoid synthesising enzymes *Dagl*α and *Nape-pld* as well as their hydrolysing enzymes *Magl* and *Faah*.

In 9-month-old mice, mRNA expression levels of *Dagl*α were comparable between the genotypes. However, in 14-month-old mice, *Dagl*α was specifically and significantly upregulated in APP/PS1$*$CB2$^{-/-}$ mice as compared to CB2$^{+/+}$, CB2$^{-/-}$ and APP/PS1 mice. The role of 2-AG metabolism has been directly connected with AD progression by studies showing that *Magl* inhibition reduces Aβ formation, neuroinflammation and neurodegeneration, while long-term potentiation and spatial memory were increased in AD tg mice [40, 201]. These results suggest that an increased 2-AG tone could also ameliorate disease pathology in AD tg mice. However, as 2-AG has been demonstrated to exert its beneficial effects through CB2 receptor binding, therefore, our results would suggest that a different cannabinoid receptor would be involved.

Gene expression of the 2-AG hydrolysing enzyme *Magl* did not show any genotype specific alterations in the current study. However, with increasing age, *Magl* mRNA was age-dependently increased. An increased MAGL activity with increasing age in mouse hippocampi was also shown

by [202], suggesting a general age-dependent down-regulation of 2-AG tone in hippocampal areas. However, in the current context, APP expression did not alter the physiological upregulation of *Magl*.

Expression of the main enzyme responsible for synthesising AEA, *Nape-Pld*, was age-dependently down-regulated in a CB2- and APP-dependent manner, while mRNA expression was not altered in samples of aged $CB2^{+/+}$ mice. This finding suggests that AEA expression is context-dependently altered in samples of aged mice, however, expression of the main hydrolysing enzyme *Faah* was similarly regulated with age and genotype. These findings are in line with results obtained by Piyanova et al., showing an altered expression of 2-AG but a stable expression of AEA with age [202].

6.2.3 Levels of endocannabinoids

The importance of endocannabinoid signalling in neurodegenerative diseases was described in various reviews, for instance see [161].

According to gene expression analyses of the main endocannabinoid synthesizing and hydrolysing enzymes, endocannabinoids levels were analysed in hippocampal and cortical brain tissue samples of 9- and 14-month-old. In the current study, we detected an age and APP-dependent downregulation of AEA protein levels in hippocampal tissue, while expression in cortical tissue remained constant. Similarly, Maroof et al. showed stable AEA levels in the frontal cortex of four-, six- and 8-month-old AD tg mice, when compared to age-matched control mice [157]. However, in contrast to the study by Maroof and colleagues, we detected an age-related decrease in cortical 2-AG levels in AD tg mice and an overall decline of hippocampal 2-AG levels in all genotypes aged 14 months. These alternations could be due to the age groups used for analyses. As Maroof and colleagues used mice in the age of four, six and eight month, we evaluated mice in the age of nine and 14 month due to the presence of plaque development and inflammation at later stages of disease progression. In line with our analyses, Maroof et al. did not detect alterations in hippocampal or cortical PEA levels with age or genotype [157]. Increased expression levels of *Daglα* detected in 14-month-old $APP/PS1{*}CB2^{-/-}$ mice were not reflected by increased 2-AG levels in the same mouse group. These results clearly demonstrate that mRNA expression levels are not always correspondent with protein levels and conclusions from gene expression analyses should be drawn with caution.

In general, lack of CB2 signalling did not influence the levels of principal endocannabinoids and related derivatives in an age- and disease-dependent matter. Thus, secretion of endocanabinoids seem to be age-dependently regulated in both, physiological brain ageing and in neuroinflammatory or neurodegenerative conditions.

6.3 Decreased Aβ deposition in aged APP/PS1$*$CB2$^{-/-}$ mice

6.3.1 Lack of CB2 signalling decreases Aβ species and plaque load

Using thioflavin staining, we detected a decreased Aβ plaque load in cortical tissue of 14-month-old mice as well as in hippocampal tissue of 9- and 14-month-old APP/PS1$*$CB2$^{-/-}$ compared to age-matched APP/PS1 mice. These results suggest a CB2-dependent mechanism involved in APP expression, processing or degradation.

In contrast, Koppel et al. showed that deficiency of CB2 receptors in an AD mouse model resulted in increased amyloid pathology [132]. While the same CB2 knockout mouse model was used in Koppel's study and our set up, namely the CB2$^{-/-}$ (by [33]), Koppel and colleagues used the J20 tg amyloid mouse model (by [179]). These mice develop plaques between the age of 7 and 10 months and plaque load was analysed after one year using the human specific antibody 6E10 on immunohistochemical brain slices. In the current study, the APP/PS1 mouse model by [31], which develops plaques already by the age of 6 months, while plaque load was measured in samples of 9- and 14-month-old mice by using thioflavin staining of cryosectioned brain tissue slices. The difference in AD mouse models and plaque staining techniques within both studies could be responsible for the conflicting results. Thus we hypothesize that the influence of CB2 signalling on APP processing is strongly context dependent and should be further examined in future studies.

Besides a direct association between CB2 signalling and plaque development, an indirect correlation via the modulation of microglial activity was speculated. Yamamoto et al. and colleagues demonstrated that a Swedish APP tg mouse model lacking the IFNγ receptor type 1 resulted in reduced gliosis and amyloid plaque load by the age of 14 month, suggesting a direct relationship between pro-inflammatory cytokines and AD pathogenesis [285]. Another study showed that pharmacological or genetic inhibition of MAGL, the main hydrolysing enzyme of 2-AG, reduces Aβ plaque formation as well as neuroinflammation and neurodegeneration, while long-term-potentiation and spatial memory were improved in APP tg animals [40, 201]. Therefore, we hypothesized that blockade of CB2 signalling in APP/PS1 mice affects amyloidosis by modulating the inflammatory milieu through a diverse glia activation, which in turn affected Aβ plaque load. However, the exact mechanism of CB2 signalling on neuroinflammatory modulation still needs to be elucidated in further studies.

6.3.2 Expression of APP and APP-cleavage enzymes remains stable

To investigate whether APP gene expression *per se* was influenced by CB2 signalling, we evaluated *App* mRNA expression levels in both age- and all four mouse-groups. As expected, AD tg mice showed increased *App* mRNA levels as compared to CB2$^{+/+}$ and CB2$^{-/-}$ mice. However, within AD tg mice, lack of CB2 signalling did not influence *App* expression levels, as *App* mRNA levels

were comparable between APP/PS1 and APP/PS1∗CB2$^{-/-}$ mice. Thus, we can exclude that CB2 signalling directly influences Aβ levels by an up-regulation of *App* mRNA levels.

Up to date, other studies did not directly investigate the role of CB2 deficiency on APP expression. However, the role of CB2 receptor signalling in the context of AD, both in cell culture models as well as in diverse AD tg mouse models, was of increasing interest in various research groups over the last decade [57, 215, 59, 62, 159, 11, 281, 15, 39, 12]. Most studies used pharmacological stimulation of CB2 receptors in Aβ triggered myeloid cells or tg mouse models. Direct CB2 receptor activation using specific ligands reduced Aβ plaque load and diminished the amount of soluble Aβ species [259, 159, 11, 281, 39, 35]. As these effects were mostly in accordance with anti-inflammatory activation of microglia cells, an indirect mechanism of CB2 signalling on APP plaque load via microglia polarisation can be hypothesised.

Consecutively, we investigated expression levels of different APP cleavage enzymes, namely α- and β-secretases. As already mentioned in the introduction, APP cleavage is regulated differently in the CNS of healthy and AD subjects. In the current study, hippocampal mRNA expression levels of the β-secretase *Bace1* did not differ between the groups. Therefore, we can exclude that differences seen in Aβ plaque load and soluble Aβ levels are due to differentially expressed cleavage enzymes which could result in an unbalanced APP processing. Nevertheless, it should be kept in mind that mRNA expression levels do not always correspond to protein levels or even enzyme activity. Further studies should therefore examine the enzyme activity of APP proteases to clarify this aspect.

6.3.3 Expression levels of Aβ receptors and degrading enzymes

The role of microglial Aβ uptake and degradation was analysed by evaluating mRNA expression levels of the most abundant receptors and degrading enzymes, which have been shown to interact with different Aβ species. While we were able to detect an age-dependent increase in mRNA levels of *Ager*, *Marco* and *Tlr4*, CB2 deficiency did not influence expression levels in comparison to age-matched APP/PS1 mice. Therefore, our results do not provide evidence for an increased Aβ-uptake in APP/PS1∗CB2$^{-/-}$ mice due to differentially expressed receptors.

According to Aβ degrading enzymes, aged APP/PS1∗CB2$^{-/-}$ mice displayed increased levels of *Ide* and *Mmp9* compared to age-matched control groups. These data suggest an increased ability of amyloid degradation and thus a possible mechanism for the observed effects of reduced Aβ plaque load in APP/PS1∗CB2$^{-/-}$ in comparison to APP/PS1 mice. In accordance with results by [274], showing increased levels of *Ide* and decreased levels of *Nep* mRNA in AD patients, we also detected increased levels of *Ide* mRNA in aged AD tg mice, while gene expression levels of *Nep* were decreased with age. The ≈110 kDa thiol zink-metalloendopeptidase IDE is located in the cytosol, peroxisomes, endosomes and on the cell surface [83, 240, 56, 268]. IDE was shown to cleave small proteins

which mostly share a β-pleated sheet-rich structure, such as amyloid fibrils [136, 111] and was therefore initially identified as a major protease that degrades Aβ [213]. Furthermore, increasing evidence suggested a crucial link between IDE and AD, showing that IDE is also associated with neuroinflammation. Previous studies showed an up-regulation of IDE due to increased levels of Aβ40 and Aβ42 in APP/PS1 tg mice [269]. In contrast to our study, Hickmann et al. detected decreased levels of *Ide*, *Nep* and *Mmp9* at the age of 1.5, 3, 8 and 14 month in CD11b$^+$ cells from the AD tg mouse model APP/PS1 compared to cells from CB2$^{+/+}$ littermates [102]. Conflicting results could be due to the analysed tissue samples. While [102] evaluated expression levels exclusively in sorted cells, we analysed expression levels in hippocampal brain lysates of 9- and 14-month-old mice. This could lead to a washout effect and should therefore be evaluated in specific cell culture experiments.

6.4 Decreased microgliosis in APP/PS1$*$CB2$^{-/-}$ mice

The role of CB2 receptor signalling on microglial activation has been studied intensively in the past decade. Already in 2005, Ehrhart and colleagues demonstrated that the specific CB2 receptor activation by JWH-015 was able to suppress IFNγ-induced activation of mouse primary microglial cells [57]. Furthermore, Aβ- and CD40L-induced expression of TNFα or NO was opposed by CB2 receptor stimulation by interfering with the JAK/STAT pathway [57]. In line with this, a study by Ramirez et al. showed reduced microglial reactivity to Aβ-insults in primary rat microglial cultures when stimulated with cannabinoid ligands (HU-210, WIN55,212-2 and JWH-133; [215]). Similar to these *in vitro* studies, JWH-133 and WIN55,212-2 stimulation in the AD mouse model TgAPP-2576 reduced microglial responses to Aβ [159]. Similarly, a study by Aso et al. demonstrated reduced microglial activity in the APP/PS1 tg mouse model after JWH-133 administration [11]. In general, these studies provide evidence for anti-inflammatory effects of CB2 receptor stimulation in the context of amyloidosis and neuroinflammation.

Therefore, we expected an enhanced neuroinflammatory response and increased microgliosis in the current AD mouse model lacking CB2 receptor signalling when compared to age-matched control AD mice. However, lack of CB2 signalling resulted in a diminished microgliosis. While the amount of Iba1$^+$ positive cells was comparable between samples of 9-month-old mice, an increased Iba1 immunoreactivity was observed in APP/PS1 mice with increasing age and AD-associated neuroinflammation. Interestingly, this effect was reversed in APP/PS1$*$CB2$^{-/-}$ mice. These data suggests that lack of CB2 signalling in an aged and inflamed AD brain has a dramatic influence on microgliosis.

In contrast to our findings, Koppel et al. reported an up-regulation of plaque-associated microglia [132]. However, as already discussed above, Koppel and colleagues used a different AD tg mouse model, the J20 AD tg mice. Furthermore, Iba1 overexpression was restricted to sites of Aβ plaques,

while an overall up-regulation of Iba1 immunoreactivity was not detected in the study by [132]. In our current study, Iba1 immunoreactivity was generally decreased in APP/PS1$*$CB2$^{-/-}$ mice.

As described before, these contradictory findings could be due to usage of two different AD tg mouse models. J20 tg mice, used by [132] express the human amyloid protein with the Swedish mutation (Lys670Asn and Met671Leu) together with the Indiana mutation (Val717Phe; [179]). However, data on neuroinflammatory changes are rare in this model model. In contrast, we used the double tg APP/PS1 mouse model, which overexpresses human APP with the Swedish mutation additionally to expression of the mutant presenilin-1 gene. This leads to pronounced amyloidogenic processing of APP, resulting in elevated Aβ levels [137, 214].

As the neuroinflammatory milieu is known to regulate microglia activation states, proliferation and the recruitment of peripheral cells, these data suggest that a different inflammatory microenvironment might be reasonable for the contradictory results described above. Therefore, future studies are needed to analyse the influence of diverse AD tg mouse models and their mediated neuroinflammatory profile on microglial phenotypes.

Consecutively, we further analysed if the observed up-regulation of Iba1 immunoreactivity resulted from an increased microglia proliferation or from an enhanced recruitment of peripheral myeloid cells to sites of Aβ-induced inflammation. A distinct and non-redundant role of microglia and circulating monocytes was already described by Ginhoux et al., demonstrating that microglia arise from yolk sac-primitive macrophages [78]. Additionally, studies from [5] and [174] showed that circulating monocytes do not contribute to the microglia pool under normal physiological conditions and that local expansion of microglia is solely dependent on microglial self-renewal. Due to functional differences of these cell types, an experimental distinction was demonstrated through different expression levels of CD45 and CD11b (reviewed by [209]).

As expected, we did not observe alterations in the percentage of microglia cells (CD11b^{+}, CD45^{low}) or recruited bone-marrow derived macrophages (CD11b^{+}, CD45^{high}) in the CNS of 9-month-old mice in the current study. However, flow cytometric analyses of 14-month-old mice revealed enhanced percentages of both, resident microglia and bone-marrow derived macrophages, in APP/PS1 mice as compared to age-matched APP/PS1$*$CB2$^{-/-}$. This finding indicates that microglia proliferation on the one hand, as well as recruitment of myeloid cells on the other hand, is altered in APP/PS1$*$CB2$^{-/-}$ mice, and suggests a strong influence on the inflammatory milieu in the CNS of these mice. These finding are further endorsed by the observation of markedly reduced ICAM and CD40 expression levels in microglia and bone-marrow derived macrophages of APP/PS1$*$CB2$^{-/-}$ mice. These data are in line with the exceedingly reduced capability of primary CB2$^{-/-}$ microglia regarding their capability to express pro-inflammatory molecules in response to activating stimuli

In summary, our results suggests an important role of CB2 receptor signalling in microglia acti-

vation, however only in an age- and disease-associated context, as CB2$^{-/-}$ mice were comparable to age-matched CB2$^{+/+}$ littermates.

6.5 Altered neuroinflammatory profile in APP/PS1∗CB2$^{-/-}$ mice

Over the past two decades, the dogma of an immunologically privileged brain has been completely overturned. Until the early 1990s, it was believed that the BBB impedes the passages of immune cells or humeral factors into the CNS. Epidemiological studies by McGeer and colleagues first demonstrated that patients suffering from arthritis, who chronically medicated their condition with NSAIDs, had approximately half the risk for developing AD than did the broader population [165, 167]. Nowadays, neuroinflammation, as characterised by gliosis and an elevated presence of inflammatory mediators, is a widely studied feature of physiological ageing and neurodegenerative diseases. Experimental as well as clinical evidence has demonstrated an increased synthesis of pro-inflammatory cytokines, e.g. TNFα, IFNγ, IL-1β, IL-6, IL-18, and the up-regulation of their cognate receptors [22, 1, 229, 192].

In the current study, gene expression levels of *Tnfα* increased dramatically in 14-month-old mice; this was especially prominent in aged APP/PS1 mice. In line with this, Babcock and colleagues found significantly upregulated levels of *Tnfα* mRNA in neocortical tissue samples of aged APP/PS1 mice when compared to aged-matched CB2$^{+/+}$ littermates [14]. In contrast, Tnfα gene expression levels were equal in APP/PS1∗CB2$^{-/-}$ mice and CB2$^{+/+}$ and CB2$^{-/-}$ littermates. This finding, together with our *in vitro* data of CB2$^{-/-}$ microglia, suggests that deficiency of CB2 receptor signalling impedes microglial ability to respond to inflammatory stimuli via the up-regulation of pro-inflammatory cytokines. A recent review, summarizing the important role of TNFα signalling in AD pathogenesis, points out the potential role of TNFα-inhibitors as a clinical treatment option to slow down disease progression and cognitive decline [48]. Hence, we hypothesize that a decreased expression of TNFα in APP/PS1∗CB2$^{-/-}$ mice beneficially modulates AD-associated neuroinflammation.

IL-1β has long been implicated in the initiation and propagation of neuroinflammatory changes associated with AD pathogenesis [178], due to the initial finding of increased IL-1β expression in reactive microglia surrounding amyloid plaques [89]. Since then, elevated IL-1β levels were detected in AD mouse models and plaque associated microglia [22, 146]. These studies are in accordance with data of the current study, showing an APP- and age-dependent elevation of *Il-1β* mRNA expression levels. The interaction of cannabinoids and IL-1β was first discovered while studying the effects of cannabis on consumers susceptibility to infections [68]. Later on, Esposito and colleagues demonstrated that treatment of mice with cannabidiol was able to impair iNOS and IL-1β protein expression [60]. Therefore, an antagonistic interplay between cannabinoids and IL-1β is hypothesised, in which proliferation and formation of new neurons is initiated by cannabinoids

but blocked through IL-1β expression [77]. This finding is of great importance in the context of ageing and neurodegerative diseases. In the current study, we could contribute to these findings by demonstrating that genetic deletion of CB2 receptor signalling did not influence IL-1β expression, neither in an age-dependent context, nor in AD-associated environment.

However, the detrimental role of IL-1β is currently under debate, as recent studies also supported a beneficial role of neuroinflammatory changes in AD pathogenesis (reviewed by [282]). In a murine model of AD, which chronically over-expresses IL-1β, a reduction of both plaque pathology and insoluble amyloid peptide was observed without evidence of effects on Aβ processing or APP expression [242, 162]. Conclusively, the picture of IL-1β-mediated neuroinflammation in ageing and AD pathogenesis might be much more complex and thus, further research is crucial to unravel the molecular interplay of IL-1β in neurodegenerative diseases.

A significant up-regulation of iNOS expression in the context of APP expression was demonstrated by various research groups in the past. In cortical neurons insulted with Aβ and in fore-brain tissue of APP/PS1 mice at the age of 6 months, an up-regulation of *Inos* mRNA was demonstrated [273]. In line with these results, Shi and colleagues recently showed an 8-fold increase in mRNA expression levels of *Inos* in APP-tg mice versus CB2$^{+/+}$ littermates [244]. However, in the current study, we were not able to detect APP-dependent differences in *Inos* mRNA expression levels in comparison to age-matched control mice. As both working groups used the same AD mouse model, the age of the mice might be a possible explanation for the different findings. Wan et al. and Shi et al. analysed mice already at the age of 6 and 7 months, respectively, while *Inos* mRNA levels were not measured in older mouse groups. Furthermore, it is known that increasing age *per se* already results in elevated expression levels of iNOS [270, 64]. Thus, an APP-dependent up-regulation of iNOS might already be overlaid by the age of 9 or 14 months. Consecutively, further studies are needed to unravel the role of an impaired CB2 signalling regarding *Inos* expression levels in AD tg mice.

The important role of CCL2-CCR2 signalling in AD was widely analysed in recent years. Many studies have linked elevated levels of CCL2 in the cerebrospinal fluid with a transition from mild cognitive impairment to AD [72]. Furthermore, *in vitro* studies demonstrated that Aβ - used as a stimulatory trigger - was able to induce CCL2 expression by astrocytes and oligodendrocytes [115]. In an *in vivo* study with a triple-tg mouse model of AD, increased CCL2 levels were found in the entorhinal cortex but not in the hippocampus of 3- to 6-month-old animals [113]. In the current study, elevated levels of CCL2 were detected in aged CB2$^{+/+}$ and APP/PS1 mice. El Khoury et al. demonstrated that CCR2 deficiency in an AD mouse model resulted in an accumulation of Aβ due to impaired microglia accumulation, resulting in accelerated ageing and disease progression [58]. Similar results were obtained by the working group of Naert and Rivest, showing that memory impairment was accelerated in AD mice lacking CCR2 expression, while soluble Aβ levels increased

significantly [183]. Gene expression levels of the chemokine *Ccl2* were reduced in aged mice lacking CB2 signalling. Diminished *Ccl2* gene expression levels in $CB2^{-/-}$ and APP/PS1$*$$CB2^{-/-}$ mice could be one possible explanation for the reduced percentages of monocyte-derived macrophages detected in the CNS of aged APP/PS1$*$$CB2^{-/-}$ mice. This leads to the hypothesis that the recruitment of peripheral myeloid cells to sites of inflammation is hampered in the absence of CB2 signalling. However, the dramatic decrease of CCL2 secretion seen in neonatal microglia derived from $CB2^{-/-}$ mice was not present in aged mice. One the one hand, this finding might be explained by a washout effect. In contrast to microglia-enriched cell culture experiments, gene expression analyses were conducted using whole hippocampal tissue samples of aged mice, which contained various cell types. On the other hand, CCL2 secretion in neonatal microglia was quantified by using ELISA, thus protein concentrations were compared between different genotype groups. In aged mice, protein quantification was not feasible due to a fast degradation of chemokines and cytokines within the process of tissue harvesting. Therefore, the measurement of cytokine or chemokine expression was only possible by using real-time gene expression analyses. Nevertheless, also aged mice showed decreased levels of *Ccl2* mRNA when CB2 signalling was lacking. These results suggest an impact of CB2 signalling on CCL2 expression, which could be direct or indirect. However, the exact mechanism needs to be evaluated in further studies. Experiments using tissue samples of cell-type specific CB2 knockout mice could elucidate the role of CB2 signalling on CCL2 expression in future studies.

6.6 Decreased neurodegeneration in APP/PS1$*$$CB2^{-/-}$ mice

Neurodegeneration, initially characterised by progressive loss of synaptic structure up to neuronal loss, is one of the most prevalent histological hallmarks of AD [82]. At initial stages of the disease, basal forebrain cholinergic neurons and adrenergic neurons in the locus coeruleus are affected from neuronal loss, followed by a massive loss of hippocampal and cortical neurons at later stages of the disease [27]. In the presently used murine model of AD, some neuronal subpopulation were previously shown to alter with increasing age and disease progression. Aged female tg APP/PS1 mice were shown to develop a selective degeneration of catecholaminergic neurons in the locus coeruleus [194]. Furthermore, decreasing levels of calcium-binding proteins, especially calbindin, calretinin and parvalbumin, were detected in the dentate gyrus of APP/PS1 mice, suggesting the involvement of calcium-dependent pathways in the pathogenesis of AD [203]. This finding was further substantiated by Takahashi et al., showing a 40-50% loss of parvalbuminergic and a 37-52% loss of calretinergic interneurons in the hippocampus of APP/PS1 mice [257]. In line with these recent findings, we detected a decreased density of the pyramidal cell layer in the CA1/2 region in samples of 14-month-old APP/PS1 mice when compared to age-matched $CB2^{+/+}$ mice. Furthermore, the general number of NeuN-positive cells per mm^2 was significantly decreased in

APP/PS1 mice. However, this finding was rescued inAPP/PS1∗CB2$^{-/-}$ mice, which showed a comparable neuronal density than age-matched CB2$^{+/+}$ and CB2$^{-/-}$ mice. In accordance with Takahashi et al., numbers of parvalbumigergic interneurons in cortical brain tissue sections were significantly decreased in APP/PS1 mice [257].

These results indicate that lack of CB2 signalling positively influenced the age-dependent AD associated neurodegenerative process.

6.7 Rescue of cognitive impairments in APP/PS1∗CB2$^{-/-}$ mice

Neurodegenerative processes as well as chronic expression of neuroinflammatory mediators and increasing Aβ accumulation have been linked to deficits in spatial learning and memory in APP/PS1 mice [211, 97, 152, 73], and cognitive impairments in correlation with Aβ levels in APP/PS1 mice have been described by diverse research groups [232, 291, 140, 109]. Recently, Kim and colleagues reported that oral co-administration of 4-(2-hydroxyethyl)-1-piperazinepropane-sulphonic acid (EPPS), an amyloid-clearing chemical, and donepezil, an acetylcholinesterase inhibitor, improved cognitive impairments in 50 weeks old APP/PS1 mice, measured by Y-maze test [123].

In the current study, the impact of CB2 signalling on AD associated cognitive impairments was evaluated by using an exacerbated MWM paradigm. In a previous study, we were not able to detect cognitive differences between aged (14-month-old) APP/PS1 and APP/PS1∗CB2$^{-/-}$ mice by using the MWM with an intertrail time of five minutes [235]. Therefore, we elevated the task difficulty in the current study by using an intertrial time of 1 h. This allowed the detection of minor learning differences between the groups. In line with our previous findings, escape latencies in 14-month-old APP/PS1 mice were significantly increased in comparison to age-matched control mice. However and more interestingly, cognitive deficits in 14-month-old APP/PS1∗CB2$^{-/-}$ mice were rescued, as escape latencies were comparable to CB2$^{+/+}$ and CB2$^{-/-}$ mice. These results suggest that differences seen in neuroinflammatory markers as well as in Aβ load and neuronal loss positively influenced cognitive abilities in aged APP/PS1∗CB2$^{-/-}$ mice. In a previous study, CB2 receptor deletion was already shown to enhance spatial working memory in animals at the age of 2.5-4 months, while long-term memory was impaired in these mice [144]. Furthermore, the authors demonstrated that acute blockade of CB2 receptors by administration of the antagonist AM630 had no effect on working memory [144].

Therefore, we conclude that the genetic deletion of CB2 receptors cannot be directly compared to the pharmacological inactivation of the same receptors and that brains regions and the surrounding microenvironment plays a crucial role in CB2 receptor signalling. Thus, further studies are highly needed to address the aspect of CB2 signalling in more detail using time- and cell-type-specific CB2 knockout mouse models.

7 Conclusion

The current data clearly demonstrate a crucial role of CB2 signalling in the development of AD-like phenotypes in the APP/PS1 mouse model. A fundamental effect of CB2 receptor deletion was already observed in microglia cultures derived from neonatal mice, showing that microglia derived from $CB2^{-/-}$ mice were significantly less responsive to pro-inflammatory stimuli regarding their upregulation of inflammatory cell surface marker ICAM and CD40 as well as the secretion of the cytokines TNF-α, IL-6 or CCL2. However, $CB2^{-/-}$ microglia responded with an upregulation of the 'M2'-like maker molecules MMR and IL-10 to inflammatory stimuli. These findings suggest that constitutive CB2 knockout mice already show an alternative maturation of microglia cells in early embryonic development, which might play an important role on microglia polarisation in an inflammatory environment. We therefore hypothesise that lack of functional CB2 receptor signalling influences the development of microglia in early developmental stages, which in turn are less proned against pro-inflammatory stimuli.

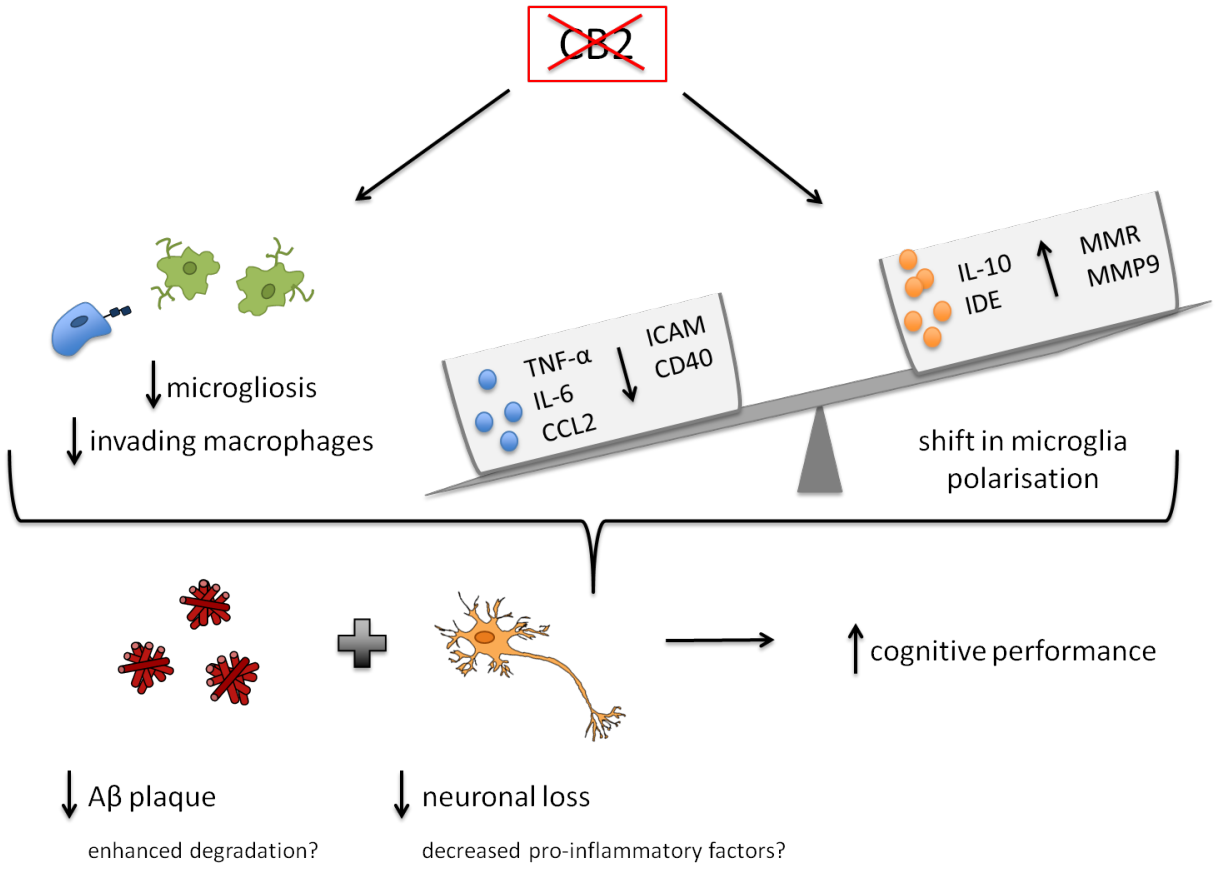

Figure 7.1: CB2 deficiency in APP/PS1 mice. Lack of CB2 signalling reduced number of microglia and macrophages as well as the expression of pro-inflammatory factors, while expression of anti-inflammatory mediators was enhanced in neonatal microglia and aged mice. In turn, Aβ clearance might be increased due to increased expression of degrading enzymes, resulting in reduced neuronal loss and consecutively ameliorated cognitive performance.

These findings are in line with many other studies showing that modulation of microglial function in AD models can restore or improve memory function [127, 198, 70, 286].

Thus, our current findings demonstrate that an altered microglia polarisation contributes dramatically to memory deficits associated with AD progression due to their production of modulatory substances and their ability to interact with the local brain environment. However, despite the widely reported immunomodulatory effects of cannabinoids in central and peripheral immune cells, the exact mechanism, by which lack of CB2 signalling affects the development and polarisation of microglia in the current AD mouse model, needs further investigations. Due to recent findings demonstrating CB2 receptor expression in hippocampal principal neurons, the involvement of other cell types influencing the AD-associated progression cannot be ruled out [252]. Thus, usage of conditional murine models with a cell type-specific CB2 receptor deletion or a time-specific CB2 receptor deletion could be a helpful model system to unravel to the role of CB2 signalling in a neuroinflammatory and neurodegenrative context.

8 Acknowledgement

Mit der vorliegenden Arbeit danke ich zunächst ganz herzlich Professor Dr. Andreas Zimmer für die Möglichkeit, meine Dissertation im Institut für molekulare Psychiatrie an der Universität Bonn anfertigen zu können. Es war für mich eine tolle und lehrreiche Zeit, die mir sehr viel Spaß und Freude bereitet hat. Die konstruktiven Ratschläge, die Expertise - nicht nur auf dem Gebiet des Endocannabinoidsystems - und das stets offene Ohr haben mich dabei ständig begleitet. Vielen Dank!

Des Weiteren möchte ich mich hiermit auch ganz herzlich bei Professor Dr. Waldemar Kolanus für die Übernahme der Zweitkorrektur bedanken.

All meinen Kolleginnen und Kollegen aus dem Institut danke ich für die tolle Arbeitsatmosphäre im Labor und außerhalb. Zahlreiche Lab Retreats, Sommerfeste, Weihnachts- und Karnevalparties haben ihr übriges dazu beigetragen, vielen Dank dafür an Anne und Andreas Zimmer.

Anne Schmöle danke ich für die tolle Zusammenarbeit in diesem spannenden Projekt, für die technische und fachliche Unterstützung, für lange Abende am FACS und bei der Präparation der neonatalen Microglia. Für die immunhistologische Unterstützung im Rahmen seiner medizinischen Doktorarbeit bedanke ich mich bei Gregor Toporowski.

Mein ganz besonderer Dank gilt Kerstin Michel (nun Nicolai), Hanna Schrage, Imke Jenniches und Eva Beins für die zahlreichen Diskussionsrunden bei einer Tasse Kaffee und euren Beistand auch in kritischen Phasen. Ohne euch wäre die Zeit nicht halb so schön gewesen!!!

Meiner Familie, meinen Freunden und ganz besonders meinem Mann Andreas danke ich für den Zuspruch, die Geduld und das Verständnis in der vergangen Zeit, auch wenn ich dabei manchmal etwas launisch werden konnte. Ihr seid die Besten!

9 Appendix

List of Tables

List of Figures

References

[1] N. Abbas, I. Bednar, E. Mix, S. Marie, D. Paterson, A. Ljungberg, C. Morris, B. Winblad, A. Nordberg, and J. Zhu. Up-regulation of the inflammatory cytokines IFN-gamma and IL-12 and down-regulation of IL-4 in cerebral cortex regions of APP(SWE) transgenic mice. *J. Neuroimmunol.*, 126(1-2):50–7, may 2002.

[2] A. Aguzzi, B. A. Barres, and M. L. Bennett. Microglia: Scapegoat, Saboteur, or Something Else? *Science (80-.).*, 339(6116):156–161, jan 2013.

[3] A. Aguzzi and T. O'Connor. Protein aggregation diseases: pathogenicity and therapeutic perspectives. *Nat. Rev. Drug Discov.*, 9(3):237–248, 2010.

[4] H. J. Aizenstein, R. D. Nebes, J. a. Saxton, J. C. Price, C. a. Mathis, N. D. Tsopelas, S. K. Ziolko, J. a. James, B. E. Snitz, P. R. Houck, W. Bi, A. D. Cohen, B. J. Lopresti, S. T. DeKosky, E. M. Halligan, and W. E. Klunk. Frequent amyloid deposition without significant cognitive impairment among the elderly. *Arch. Neurol.*, 65(11):1509–1517, 2008.

[5] B. Ajami, J. L. Bennett, C. Krieger, W. Tetzlaff, and F. M. V. Rossi. Local self-renewal can sustain CNS microglia maintenance and function throughout adult life. *Nat. Neurosci.*, 10(12):1538–1543, dec 2007.

[6] M. A. Ajmone-Cat, M. Mancini, R. De Simone, P. Cilli, and L. Minghetti. Microglial polarization and plasticity: evidence from organotypic hippocampal slice cultures. *Glia*, 61(10):1698–711, oct 2013.

[7] H. Akiyama, T. Arai, H. Kondo, E. Tanno, C. Haga, and K. Ikeda. Cell mediators of inflammation in the Alzheimer disease brain. *Alzheimer Dis. Assoc. Disord.*, 14 Suppl 1:S47–53, 2000.

[8] M. Y. Aksenov, M. V. Aksenova, D. a. Butterfield, J. W. Geddes, and W. R. Markesbery. Protein oxidation in the brain in Alzheimer's disease. *Neuroscience*, 103(2):373–383, 2001.

[9] W. Araki, N. Kitaguchi, Y. Tokushima, K. Ishii, H. Aratake, S. Shimohama, S. Nakamura, and J. Kimura. Trophic effect of beta-amyloid precursor protein on cerebral cortical neurons in culture. *Biochem Biophys Res Commun*, 181(1):265–271, 1991.

[10] M. Aslan and T. Ozben. Reactive oxygen and nitrogen species in Alzheimer's disease. *Curr. Alzheimer Res.*, 1(2):111–9, may 2004.

[11] E. Aso, S. Juvés, R. Maldonado, and I. Ferrer. CB2 cannabinoid receptor agonist ameliorates Alzheimer-like phenotype in AβPP/PS1 mice. *J. Alzheimers. Dis.*, 35(4):847–58, jan 2013.

[12] E. Aso, A. Sanchez-Plac, E. Vegas-Lozano, R. Maldonado, and I. Ferrer. Cannabis-Based Medicine Reduces Multiple Pathological Processes in A beta PP/PS1 Mice. *J. Alzheimers Dis.*, 43(3):977–991, 2015.

[13] B. K. Atwood and K. Mackie. CB2: a cannabinoid receptor with an identity crisis. *Br. J. Pharmacol.*, 160(3):467–79, jun 2010.

[14] A. a. Babcock, L. Ilkjær, B. H. Clausen, B. Villadsen, L. Dissing-Olesen, A. T. Bendixen, L. Lyck, K. L. Lambertsen, and B. Finsen. Cytokine-producing microglia have an altered beta-amyloid load in aged APP/PS1 Tg mice. *Brain. Behav. Immun.*, 2015.

[15] C. Bachmeier, D. Beaulieu-Abdelahad, M. Mullan, and D. Paris. Role of the cannabinoid system in the transit of beta-amyloid across the blood-brain barrier. *Mol. Cell. Neurosci.*, 56:255–262, 2013.

[16] S. O. Bachurin, E. V. Bovina, and A. A. Ustyugov. Drugs in Clinical Trials for Alzheimer's Disease: The Major Trends. *Med. Res. Rev.*, 37(5):1186–1225, sep 2017.

[17] J. Bauer, S. Strauss, U. Schreiter-Gasser, U. Ganter, P. Schlegel, I. Witt, B. Yolk, and M. Berger. Interleukin-6 and alpha-2-macroglobulin indicate an acute-phase state in Alzheimer's disease cortices. *FEBS Lett.*, 285(1):111–114, 1991.

[18] G. Bedse, A. Romano, S. Cianci, A. M. Lavecchia, P. Lorenzo, M. R. Elphick, F. M. Laferla, G. Vendemiale, C. Grillo, F. Altieri, T. Cassano, and S. Gaetani. Altered expression of the CB1 cannabinoid receptor in the triple transgenic mouse model of Alzheimer's disease. *J. Alzheimers. Dis.*, 40(3):701–12, jan 2014.

[19] R. D. Bell and B. V. Zlokovic. Neurovascular mechanisms and blood–brain barrier disorder in Alzheimer's disease. *Acta Neuropathol.*, 118(1):103–113, jul 2009.

[20] C. Benito, R. M. Tolo, E. J. Carrier, A. Ra, and C. J. Hillard. Cannabinoid CB 2 Receptors and Fatty Acid Amide Hydrolase Are Selectively Overexpressed in Neuritic Plaque-Associated Glia in Alzheimer ' s Disease Brains. *Neurology*, 23(35):11136–11141, 2003.

[21] J. Bennett, A. Elhofy, M. Canto, and M. Tani. CCL2 Transgene Expression in the Central Nervous System Directs Diffuse Infiltration of CD45highCD11b+ Monocytes and Enhanced Theiler's Murine. *J.*, 2003.

[22] W. C. Benzing, J. R. Wujek, E. K. Ward, D. Shaffer, K. H. Ashe, S. G. Younkin, and K. R. Brunden. Evidence for glial-mediated inflammation in aged APP(SW) transgenic mice. *Neurobiol. Aging*, 20(6):581–9, 1999.

[23] L. Bertram, M. B. McQueen, K. Mullin, D. Blacker, and R. E. Tanzi. Systematic meta-analyses of Alzheimer disease genetic association studies: the AlzGene database. *Nat. Genet.*, 39(1):17–23, 2007.

[24] L. Bertram and R. E. Tanzi. Thirty years of Alzheimer's disease genetics: the implications of systematic meta-analyses. *Nat. Rev. Neurosci.*, 9(10):768–778, 2008.

[25] I. Bezprozvanny and M. P. Mattson. Neuronal calcium mishandling and the pathogenesis of Alzheimer's disease. *Trends Neurosci.*, 31(9):454–463, 2008.

[26] K. Biber, H. Neumann, K. Inoue, and H. W. G. M. Boddeke. Neuronal 'On' and 'Off' signals control microglia. *Trends Neurosci.*, 30(11):596–602, nov 2007.

[27] A. Bilkei-Gorzo. Genetic mouse models of brain ageing and Alzheimer's disease. *Pharmacol. Ther.*, 142(2):244–257, 2014.

[28] T. Bisogno and V. Di Marzo. The role of the endocannabinoid system in Alzheimer's disease: facts and hypotheses. *Curr. Pharm. Des.*, 14(23):2299–3305, 2008.

[29] S. K. Biswas and A. Mantovani. Macrophage plasticity and interaction with lymphocyte subsets: cancer as a paradigm. *Nat. Immunol.*, 11(10):889–896, 2010.

[30] D. R. Borchelt, T. Ratovitski, J. Van Lare, M. K. Lee, V. Gonzales, N. a. Jenkins, N. G. Copeland, D. L. Price, and S. S. Sisodia. Accelerated amyloid deposition in the brains of transgenic mice coexpressing mutant presenilin 1 and amyloid precursor proteins. *Neuron*, 19(4):939–945, 1997.

[31] D. R. Borchelt, G. Thinakaran, C. B. Eckman, M. K. Lee, F. Davenport, T. Ratovitsky, C. M. Prada, G. Kim, S. Seekins, D. Yager, H. H. Slunt, R. Wang, M. Seeger, a. I. Levey, S. E. Gandy, N. G. Copeland, N. a. Jenkins, D. L. Price, S. G. Younkin, and S. S. Sisodia. Familial Alzheimer's disease-linked presenilin 1 variants elevate Abeta1-42/1-40 ratio in vitro and in vivo. *Neuron*, 17(5):1005–1013, 1996.

[32] H. Braak, E. Braak, and M. Strothjohann. Abnormally phosphorylated tau protein related to the formation of neurofibrillary tangles and neuropil threads in the cerebral cortex of sheep and goat. *Neurosci. Lett.*, 171(1-2):1–4, apr 1994.

[33] N. E. Buckley, K. L. McCoy, E. Mezey, T. Bonner, a. Zimmer, C. C. Felder, and M. Glass. Immunomodulation by cannabinoids is absent in mice deficient for the cannabinoid CB(2) receptor. *Eur. J. Pharmacol.*, 396(2-3):141–9, may 2000.

[34] G. a. Cabral, E. S. Raborn, L. Griffin, J. Dennis, and F. Marciano-Cabral. CB 2 receptors in the brain: role in central immune function. *Br. J. Pharmacol.*, 153(2):240–251, jan 2008.

[35] C. Cao, Y. Li, H. Liu, G. Bai, J. Mayl, X. Lin, K. Sutherland, N. Nabar, and J. Cai. The Potential Therapeutic Effects of THC on Alzheimer's Disease. *J. Alzheimer's Dis. JAD*, 42:973–984, 2014.

[36] S. J. Carlisle, F. Marciano-Cabral, a. Staab, C. Ludwick, and G. a. Cabral. Differential expression of the CB2 cannabinoid receptor by rodent macrophages and macrophage-like cells in relation to cell activation. *Int. Immunopharmacol.*, 2(1):69–82, 2002.

[37] L. Cassetta, E. Cassol, and G. Poli. Macrophage polarization in health and disease. *ScientificWorldJournal.*, 11:2391–402, jan 2011.

[38] B. Chen, K. Bromley-Brits, G. He, F. Cai, X. Zhang, and W. Song. Effect of synthetic cannabinoid HU210 on memory deficits and neuropathology in Alzheimer's disease mouse model. *Curr. Alzheimer Res.*, 7(3):255–261, 2010.

[39] R. Chen, J. Zhang, N. Fan, Z.-Q. Teng, Y. Wu, H. Yang, Y.-P. Tang, H. Sun, Y. Song, and C. Chen. Δ9-THC-caused synaptic and memory impairments are mediated through COX-2 signaling. *Cell*, 155(5):1154–65, nov 2013.

[40] R. Chen, J. Zhang, Y. Wu, D. Wang, G. Feng, Y.-P. Tang, Z. Teng, and C. Chen. Monoacylglycerol lipase is a therapeutic target for Alzheimer's disease. *Cell Rep.*, 2(5):1329–39, nov 2012.

[41] Y. Chen, J. Hallenbeck, C. Ruetzler, and D. Bol. Overexpression of monocyte chemoattractant protein 1 in the brain exacerbates ischemic brain injury and is associated with recruitment of inflammatory cells. *J. Cereb.*, 2003.

[42] C. A. Colton. Heterogeneity of Microglial Activation in the Innate Immune Response in the Brain. *J. Neuroimmune Pharmacol.*, 4(4):399–418, 2009.

[43] C. A. Colton and D. M. Wilcock. Assessing activation states in microglia. *CNS Neurol. Disord. Drug Targets*, 9(2):174–91, apr 2010.

[44] C. K. Combs, D. E. Johnson, J. C. Karlo, S. B. Cannady, and G. E. Landreth. Inflammatory Mechanisms in Alzheimer's Disease: Inhibition of beta -Amyloid-Stimulated Proinflammatory Responses and Neurotoxicity by PPARgamma Agonists. *J. Neurosci.*, 20(2):558–567, 2000.

[45] L. Console-Bram, E. Brailoiu, G. C. Brailoiu, H. Sharir, and M. E. Abood. Activation of GPR18 by cannabinoid compounds: a tale of biased agonism. *Br. J. Pharmacol.*, 171(16):3908–3917, aug 2014.

[46] E. H. Corder, A. M. Saunders, W. J. Strittmatter, D. E. Schmechel, P. C. Gaskell, G. W. Small, A. D. Roses, J. L. Haines, and M. A. Pericak-Vance. Gene dose of apolipoprotein E type 4 allele and the risk of Alzheimer's disease in late onset families. *Science*, 261(5123):921–3, aug 1993.

[47] E. K. de Jong. Vesicle-Mediated Transport and Release of CCL21 in Endangered Neurons: A Possible Explanation for Microglia Activation Remote from a Primary Lesion. *J. Neurosci.*, 25(33):7548–7557, aug 2005.

[48] B. Decourt, D. Lahiri, and M. Sabbagh. Targeting Tumor Necrosis Factor Alpha for Alzheimer's Disease. *Curr. Alzheimer Res.*, 13(999):1–1, sep 2016.

[49] A. Demuro, I. Parker, and G. E. Stutzmann. Calcium signaling and amyloid toxicity in Alzheimer disease. *J. Biol. Chem.*, 285(17):12463–12468, 2010.

[50] S. L. Deshmane, S. Kremlev, S. Amini, and B. E. Sawaya. Monocyte Chemoattractant Protein-1 (MCP-1): An Overview. *J. Interf. Cytokine Res.*, 29(6):313–326, jun 2009.

[51] W. A. Devane, L. Hanus, A. Breuer, R. G. Pertwee, L. A. Stevenson, G. Griffin, D. Gibson, A. Mandelbaum, A. Etinger, and R. Mechoulam. Isolation and structure of a brain constituent that binds to the cannabinoid receptor. *Science*, 258(5090):1946–9, dec 1992.

[52] V. Deveaux, T. Cadoudal, Y. Ichigotani, F. Teixeira-Clerc, A. Louvet, S. Manin, J. T.-V. Nhieu, M. P. Belot, A. Zimmer, P. Even, P. D. Cani, C. Knauf, R. Burcelin, A. Bertola, Y. Le Marchand-Brustel, P. Gual, A. Mallat, and S. Lotersztajn. Cannabinoid CB2 receptor potentiates obesity-associated inflammation, insulin resistance and hepatic steatosis. *PLoS One*, 4(6):e5844, 2009.

[53] A. Dey, J. Allen, and P. a. Hankey-Giblin. Ontogeny and Polarization of Macrophages in Inflammation: Blood Monocytes Versus Tissue Macrophages. *Front. Immunol.*, 5(January):1–15, 2015.

[54] J. C. Dodart, C. Mathis, J. Saura, K. R. Bales, S. M. Paul, and A. Ungerer. Neuroanatomical abnormalities in behaviorally characterized APP(V717F) transgenic mice. *Neurobiol. Dis.*, 7(2):71–85, 2000.

[55] S. Du Yan, H. Zhu, J. Fu, S. F. Yan, A. Roher, W. W. Tourtellotte, T. Rajavashisth, X. Chen, G. C. Godman, D. Stern, and a. M. Schmidt. Amyloid-beta peptide-receptor for advanced glycation endproduct interaction elicits neuronal expression of macrophage-colony stimulating factor: a proinflammatory pathway in Alzheimer disease. *Proc. Natl. Acad. Sci. U. S. A.*, 94(10):5296–301, may 1997.

[56] W. C. Duckworth, R. G. Bennett, and F. G. Hamel. Insulin Degradation: Progress and Potential. *Endocr. Rev.*, 19(5):608–624, oct 1998.

[57] J. Ehrhart, D. Obregon, T. Mori, H. Hou, N. Sun, Y. Bai, T. Klein, F. Fernandez, J. Tan, and R. D. Shytle. Stimulation of cannabinoid receptor 2 (CB2) suppresses microglial activation. *J. Neuroinflammation*, 2:29, jan 2005.

[58] J. El Khoury, M. Toft, S. E. Hickman, T. K. Means, K. Terada, C. Geula, and A. D. Luster. Ccr2 deficiency impairs microglial accumulation and accelerates progression of Alzheimer-like disease. *Nat. Med.*, 13(4):432–8, apr 2007.

[59] G. Esposito, D. De Filippis, L. Steardo, C. Scuderi, C. Savani, V. Cuomo, and T. Iuvone. CB1 receptor selective activation inhibits β-amyloid-induced iNOS protein expression in C6 cells and subsequently blunts tau protein hyperphosphorylation in co-cultured neurons. *Neurosci. Lett.*, 404(3):342–346, sep 2006.

[60] G. Esposito, C. Scuderi, C. Savani, L. Steardo, D. De Filippis, P. Cottone, T. Iuvone, V. Cuomo, and L. Steardo. Cannabidiol in vivo blunts beta-amyloid induced neuroinflammation by suppressing IL-1beta and iNOS expression. *Br. J. Pharmacol.*, 151(8):1272–1279, 2007.

[61] R. A. Ezekowitz and S. Gordon. Alterations of surface properties by macrophage activation: expression of receptors for Fc and mannose-terminal glycoproteins and differentiation antigens. *Contemp. Top. Immunobiol.*, 13:33–56, 1984.

[62] G. Fakhfouri, A. Ahmadiani, R. Rahimian, A. a. Grolla, F. Moradi, and A. Haeri. WIN55212-2 attenuates amyloid-beta-induced neuroinflammation in rats through activation of cannabinoid receptors and PPAR-γ pathway. *Neuropharmacology*, 63(4):653–66, sep 2012.

[63] C. Ferri, M. Prince, C. Brayne, H. Brodaty, L. Fratiglioni, M. Ganguli, K. Hall, K. Hasegawa, H. Hendrie, Y. Huang, and Others. Global prevalence of dementia: a Delphi consensus study. *Lancet*, 366(9503):2112–2117, 2006.

[64] M. Ferrini, C. Wang, R. S. Swerdloff, A. P. Sinha Hikim, J. Rajfer, and N. F. Gonzalez-Cadavid. Aging-related increased expression of inducible nitric oxide synthase and cytotoxicity markers in rat hypothalamic regions associated with male reproductive function. *Neuroendocrinology*, 74(1):1–11, jul 2001.

[65] D. Finelli, S. Rollinson, J. Harris, M. Jones, A. Richardson, A. Gerhard, J. Snowden, D. Mann, and S. Pickering-Brown. TREM2 analysis and increased risk of Alzheimer's disease. *Neurobiol. Aging*, 36(1):546.e9–13, 2015.

[66] R. Francis, G. McGrath, J. Zhang, D. A. Ruddy, M. Sym, J. Apfeld, M. Nicoll, M. Maxwell, B. Hai, M. C. Ellis, A. L. Parks, W. Xu, J. Li, M. Gurney, R. L. Myers, C. S. Himes, R. Hiebsch, C. Ruble, J. S. Nye, and D. Curtis. aph-1 and pen-2 are required for Notch pathway signaling, gamma-secretase cleavage of betaAPP, and presenilin protein accumulation. *Dev. Cell*, 3(1):85–97, jul 2002.

[67] I. P. Fraser, H. Koziel, and R. a. Ezekowitz. The serum mannose-binding protein and the macrophage mannose receptor are pattern recognition molecules that link innate and adaptive immunity. *Semin. Immunol.*, 10(5):363–72, oct 1998.

[68] H. Friedman, T. Klein, S. Specter, S. Pross, C. Newton, D. K. Blanchard, and R. Widen. Drugs of abuse and virus susceptibility. *Adv. Biochem. Psychopharmacol.*, 44:125–37, 1988.

[69] K. Furukawa, B. L. Sopher, R. E. Rydel, J. G. Begley, D. G. Pham, G. M. Martin, M. Fox, and M. P. Mattson. Increased activity-regulating and neuroprotective efficacy of alpha-secretase-derived secreted amyloid precursor protein conferred by a C-terminal heparin-binding domain. *J. Neurochem.*, 67(5):1882–1896, 1996.

[70] S. P. Gabbita, M. K. Srivastava, P. Eslami, M. F. Johnson, N. K. Kobritz, D. Tweedie, N. H. Greig, F. P. Zemlan, S. P. Sharma, and M. E. Harris-White. Early intervention with a small molecule inhibitor for tumor nefosis factor-α prevents cognitive deficits in a triple transgenic mouse model of Alzheimer's disease. *J. Neuroinflammation*, 9(1):578, dec 2012.

[71] S. Galiègue, S. Mary, J. Marchand, D. Dussossoy, D. Carrière, P. Carayon, M. Bouaboula, D. Shire, G. Le Fur, and P. Casellas. Expression of central and peripheral cannabinoid receptors in human immune tissues and leukocyte subpopulations. *Eur. J. Biochem.*, 232(1):54–61, aug 1995.

[72] D. Galimberti, C. Fenoglio, C. Lovati, E. Venturelli, I. Guidi, B. Corrà, D. Scalabrini, F. Clerici, C. Mariani, N. Bresolin, and E. Scarpini. Serum MCP-1 levels are increased in mild cognitive impairment and mild Alzheimer's disease. *Neurobiol. Aging*, 27(12):1763–1768, 2006.

[73] J. J. Gallagher, A. M. Minogue, and M. A. Lynch. Impaired performance of female APP/PS1 mice in the Morris water maze is coupled with increased Aβ accumulation and microglial activation. *Neurodegener. Dis.*, 11(1):33–41, 2013.

[74] D. Games. Alzheimer-type neuropathology in transgenic mice overexpressing V717F ß-amyloid precuros protein. *Nature*, 373(9):523–527, 1995.

[75] I. Gantz, A. Muraoka, Y. K. Yang, L. C. Samuelson, E. M. Zimmerman, H. Cook, and T. Yamada. Cloning and chromosomal localization of a gene (GPR18) encoding a novel seven transmembrane receptor highly expressed in spleen and testis. *Genomics*, 42(3):462–6, jun 1997.

[76] Y. Gaoni and R. Mechoulam. Isolation, Structure, and Partial Synthesis of an Active Constituent of Hashish. *J. Am. Chem. Soc.*, 86(8):1646–1647, apr 1964.

[77] D. García-Ovejero, Á. Arévalo-Martín, B. Navarro-Galve, E. Pinteaux, E. Molina-Holgado, and F. Molina-Holgado. Neuroimmmune interactions of cannabinoids in neurogenesis: focus on interleukin-1β (IL-1β) signalling. *Biochem. Soc. Trans.*, 41(6):1577–82, 2013.

[78] F. Ginhoux, M. Greter, M. Leboeuf, S. Nandi, P. See, S. Gokhan, M. F. Mehler, S. J. Conway, L. G. Ng, E. R. Stanley, I. M. Samokhvalov, and M. Merad. Fate mapping analysis reveals that adult microglia derive from primitive macrophages. *Science*, 330(6005):841–5, nov 2010.

[79] F. Ginhoux, S. Lim, G. Hoeffel, D. Low, and T. Huber. Origin and differentiation of microglia. *Front. Cell. Neurosci.*, 7(April):45, jan 2013.

[80] A. Goate, M. C. Chartier-Harlin, M. Mullan, J. Brown, F. Crawford, L. Fidani, L. Giuffra, A. Haynes, N. Irving, and L. James. Segregation of a missense mutation in the amyloid precursor protein gene with familial Alzheimer's disease. *Nature*, 349(6311):704–706, 1991.

[81] M. Goedert. Tau protein and the neurol brillary pathology of AIzheimer ' s disease. *Trends Neurosci.*, 16(11):460–465, 1993.

[82] M. Goedert and M. G. Spillantini. A Century of Alzheimer ' s Disease. *Science (80-.).*, 314(November):777–781, 2006.

[83] I. D. Goldfine, J. A. Williams, A. C. Bailey, K. Y. Wong, Y. Iwamoto, K. Yokono, S. Baba, and R. A. Roth. Degradation of Insulin by Isolated Mouse Pancreatic Acini: Evidence for Cell Surface Protease Activity. *Diabetes*, 33(1), 1984.

[84] T. Goldmann, P. Wieghofer, M. J. C. Jordão, F. Prutek, N. Hagemeyer, K. Frenzel, L. Amann, O. Staszewski, K. Kierdorf, M. Krueger, G. Locatelli, H. Hochgerner, R. Zeiser, S. Epelman, F. Geissmann, J. Priller, F. M. V. Rossi, I. Bechmann, M. Kerschensteiner, S. Linnarsson, S. Jung, and M. Prinz. Origin, fate and dynamics of macrophages at central nervous system interfaces. *Nat. Immunol.*, 17(7):797–805, jul 2016.

[85] E. Gomez Perdiguero, K. Klapproth, C. Schulz, K. Busch, E. Azzoni, L. Crozet, H. Garner, C. Trouillet, M. F. de Bruijn, F. Geissmann, and H.-R. Rodewald. Tissue-resident macrophages originate from yolk-sac-derived erythro-myeloid progenitors. *Nature*, 518(7540):547–551, dec 2015.

[86] C. Goutte, M. Tsunozaki, V. A. Hale, and J. R. Priess. APH-1 is a multipass membrane protein essential for the Notch signaling pathway in Caenorhabditis elegans embryos. *Proc. Natl. Acad. Sci. U. S. A.*, 99(2):775–9, jan 2002.

[87] M. Greter and M. Merad. Regulation of microglia development and homeostasis. *Glia*, 61(1):121–127, 2013.

[88] A. Griciuc, A. Serrano-Pozo, A. Parrado, A. Lesinski, C. Asselin, K. Mullin, B. Hooli, S. Choi, B. Hyman, and R. Tanzi. Alzheimer's Disease Risk Gene CD33 Inhibits Microglial Uptake of Amyloid Beta. *Neuron*, 78(4):631–643, 2013.

[89] W. S. Griffin, L. C. Stanley, C. Ling, L. White, V. MacLeod, L. J. Perrot, C. L. White, and C. Araoz. Brain interleukin 1 and S-100 immunoreactivity are elevated in Down syndrome and Alzheimer disease. *Proc. Natl. Acad. Sci. U. S. A.*, 86(19):7611–7615, 1989.

[90] R. Guerreiro, A. Wojtas, J. Bras, M. Carrasquillo, E. Rogaeva, E. Majounie, C. Cruchaga, C. Sassi, J. S. K. Kauwe, S. Younkin, L. Hazrati, J. Collinge, J. Pocock, T. Lashley, J. Williams, J.-C. Lambert, P. Amouyel, A. Goate, R. Rademakers, K. Morgan, J. Powell, P. St. George-Hyslop, A. Singleton, J. Hardy, P. St George-Hyslop, A. Singleton, and J. Hardy. TREM2 variants in Alzheimer's disease. *N. Engl. J. Med.*, 368(2):117–127, jan 2013.

[91] C. Haass and D. J. Selkoe. Soluble protein oligomers in neurodegeneration: lessons from the Alzheimer's amyloid beta-peptide. *Nat. Rev. Mol. Cell Biol.*, 8(2):101–12, 2007.

[92] U.-K. Hanisch. Functional diversity of microglia – how heterogeneous are they to begin with? *Front. Cell. Neurosci.*, 7(May):1–18, 2013.

[93] J. Hardy and G. Higgins. Alzheimer's disease: the amyloid cascade hypothesis. *Science (80-.).*, 256(5054):184–185, apr 1992.

[94] C. A. Hawkes and J. McLaurin. Selective targeting of perivascular macrophages for clearance of beta-amyloid in cerebral amyloid angiopathy. *Proc. Natl. Acad. Sci. U. S. A.*, 106(4):1261–6, jan 2009.

[95] S. Hellwig, S. Brioschi, S. Dieni, L. Frings, A. Masuch, T. Blank, and K. Biber. Altered microglia morphology and higher resilience to stress-induced depression-like behavior in CX3CR1-deficient mice. *Brain. Behav. Immun.*, pages 1–12, 2015.

[96] S. Hellwig, A. Heinrich, and K. Biber. The brain's best friend: microglial neurotoxicity revisited. *Front. Cell. Neurosci.*, 7(May):71, 2013.

[97] M. T. Heneka, M. P. Kummer, A. Stutz, A. Delekate, S. Schwartz, A. Vieira-Saecker, A. Griep, D. Axt, A. Remus, T.-C. Tzeng, E. Gelpi, A. Halle, M. Korte, E. Latz, and D. T. Golenbock. NLRP3 is activated in Alzheimer's disease and contributes to pathology in APP/PS1 mice. *Nature*, 493(7434):674–678, dec 2012.

[98] M. T. Heneka, M. K. O'Banion, D. Terwel, and M. P. Kummer. Neuroinflammatory processes in Alzheimer's disease. *J. Neural Transm.*, 117(8):919–947, aug 2010.

[99] K. Hensley. Neuroinflammation in Alzheimer's disease: mechanisms, pathologic consequences, and potential for therapeutic manipulation. *J. Alzheimers. Dis.*, 21(1):1–14, 2010.

[100] K. Herrup. The case for rejecting the amyloid cascade hypothesis. *Nat Neurosci*, 18(6):794–799, 2015.

[101] M. Hesse, M. Modolell, A. C. La Flamme, M. Schito, J. M. Fuentes, A. W. Cheever, E. J. Pearce, and T. A. Wynn. Differential Regulation of Nitric Oxide Synthase-2 and Arginase-1 by Type 1/Type 2 Cytokines In Vivo: Granulomatous Pathology Is Shaped by the Pattern of L-Arginine Metabolism. *J. Immunol.*, 167(11):6533–6544, 2001.

[102] S. E. Hickman, E. K. Allison, and J. El Khoury. Microglial dysfunction and defective beta-amyloid clearance pathways in aging Alzheimer's disease mice. *J. Neurosci.*, 28(33):8354–60, aug 2008.

[103] S. E. Hickman and J. El Khoury. Mechanism of mononuclear phagocyte recruitment in Alzheimer ' s Disease. *CNS Neurol. Disord. Drug Targets*, 9(2):168–173, 2010.

[104] G. Hoeffel, J. Chen, Y. Lavin, D. Low, F. Almeida, P. See, A. Beaudin, J. Lum, I. Low, E. Forsberg, M. Poidinger, F. Zolezzi, A. Larbi, L. Ng, J. Chan, M. Greter, B. Becher, I. Samokhvalov, M. Merad, and F. Ginhoux. C-Myb+ Erythro-Myeloid Progenitor-Derived Fetal Monocytes Give Rise to Adult Tissue-Resident Macrophages. *Immunity*, 42(4):665–678, 2015.

[105] G. Hoeffel and F. Ginhoux. Ontogeny of Tissue-Resident Macrophages. *Front. Immunol.*, 6(September), 2015.

[106] P. Hollingworth, D. Harold, R. Sims, A. Gerrish, J.-C. Lambert, M. M. Carrasquillo, R. Abraham, M. L. Hamshere, J. S. Pahwa, V. Moskvina, K. Dowzell, N. Jones, A. Stretton, C. Thomas, A. Richards, D. Ivanov, C. Widdowson, J. Chapman, S. Lovestone, J. Powell, P. Proitsi, M. K. Lupton, C. Brayne, D. C. Rubinsztein, M. Gill, B. Lawlor, A. Lynch,

K. S. Brown, P. A. Passmore, D. Craig, B. McGuinness, S. Todd, C. Holmes, D. Mann, A. D. Smith, H. Beaumont, D. Warden, G. Wilcock, S. Love, P. G. Kehoe, N. M. Hooper, E. R. L. C. Vardy, J. Hardy, S. Mead, N. C. Fox, M. Rossor, J. Collinge, W. Maier, F. Jessen, E. Rüther, B. Schürmann, R. Heun, H. Kölsch, H. van den Bussche, I. Heuser, J. Kornhuber, J. Wiltfang, M. Dichgans, L. Frölich, H. Hampel, J. Gallacher, M. Hüll, D. Rujescu, I. Giegling, A. M. Goate, J. S. K. Kauwe, C. Cruchaga, P. Nowotny, J. C. Morris, K. Mayo, K. Sleegers, K. Bettens, S. Engelborghs, P. P. De Deyn, C. Van Broeckhoven, G. Livingston, N. J. Bass, H. Gurling, A. McQuillin, R. Gwilliam, P. Deloukas, A. Al-Chalabi, C. E. Shaw, M. Tsolaki, A. B. Singleton, R. Guerreiro, T. W. Mühleisen, M. M. Nöthen, S. Moebus, K.-H. Jöckel, N. Klopp, H.-E. Wichmann, V. S. Pankratz, S. B. Sando, J. O. Aasly, M. Barcikowska, Z. K. Wszolek, D. W. Dickson, N. R. Graff-Radford, R. C. Petersen, C. M. van Duijn, M. M. B. Breteler, M. A. Ikram, A. L. DeStefano, A. L. Fitzpatrick, O. Lopez, L. J. Launer, S. Seshadri, C. Berr, D. Campion, J. Epelbaum, J.-F. Dartigues, C. Tzourio, A. Alpérovitch, M. Lathrop, T. M. Feulner, P. Friedrich, C. Riehle, M. Krawczak, S. Schreiber, M. Mayhaus, S. Nicolhaus, S. Wagenpfeil, S. Steinberg, H. Stefansson, K. Stefansson, J. Snaedal, S. Björnsson, P. V. Jonsson, V. Chouraki, B. Genier-Boley, M. Hiltunen, H. Soininen, O. Combarros, D. Zelenika, M. Delepine, M. J. Bullido, F. Pasquier, I. Mateo, A. Frank-Garcia, E. Porcellini, O. Hanon, E. Coto, V. Alvarez, P. Bosco, G. Siciliano, M. Mancuso, F. Panza, V. Solfrizzi, B. Nacmias, S. Sorbi, P. Bossù, P. Piccardi, B. Arosio, G. Annoni, D. Seripa, A. Pilotto, E. Scarpini, D. Galimberti, A. Brice, D. Hannequin, F. Licastro, L. Jones, P. A. Holmans, T. Jonsson, M. Riemenschneider, K. Morgan, S. G. Younkin, M. J. Owen, M. O'Donovan, P. Amouyel, and J. Williams. Common variants at ABCA7, MS4A6A/MS4A4E, EPHA1, CD33 and CD2AP are associated with Alzheimer's disease. *Nat. Genet.*, 43(5):429–35, 2011.

[107] A. G. Horti, Y. Gao, H. T. Ravert, P. Finley, H. Valentine, D. F. Wong, C. J. Endres, A. V. Savonenko, and R. F. Dannals. Synthesis and biodistribution of [11C]A-836339, a new potential radioligand for PET imaging of cannabinoid type 2 receptors (CB2). *Bioorganic Med. Chem.*, 18(14):5202–5207, 2010.

[108] K. Hsiao, P. Chapman, S. Nilsen, C. Eckman, Y. Harigaya, S. Younkin, F. Yang, and G. Cole. Correlative Memory Deficits, Aß Elevation, and Amyloid Plaques in Transgenic Mice. *Science (80-.).*, 274(October):99–102, 1996.

[109] H. Huang, S. Nie, M. Cao, C. Marshall, J. Gao, N. Xiao, G. Hu, and M. Xiao. Characterization of AD-like phenotype in aged APPSwe/PS1dE9 mice. *Age (Omaha).*, 38(4):303–322, aug 2016.

[110] X. G. Huang, B. K. Yee, S. Nag, S. T. H. Chan, and F. Tang. Behavioral and neurochemical characterization of transgenic mice carrying the human presenilin-1 gene with or without the leucine-to-proline mutation at codon 235. *Exp. Neurol.*, 183(2):673–681, 2003.

[111] E. Hubin, F. Cioffi, J. Rozenski, N. A. J. van Nuland, and K. Broersen. Characterization of insulin-degrading enzyme-mediated cleavage of Aβ in distinct aggregation states. *Biochim. Biophys. Acta*, 1860(6):1281–90, jun 2016.

[112] A. Jacob and A. R. Todd. Cannabis Indica. Part II. Isolation of Cunnabidiol from Egyptian Hashish. Observations on the Structure of Cannabinol. *J. Chem. Soc.*, pages 649–653, 1940.

[113] M. C. Janelsins, M. A. Mastrangelo, S. Oddo, F. M. LaFerla, H. J. Federoff, and W. J. Bowers. Early correlation of microglial activation with enhanced tumor necrosis factor-alpha and monocyte chemoattractant protein-1 expression specifically within the entorhinal cortex of triple transgenic Alzheimer's disease mice. *J. Neuroinflammation*, 2:23, oct 2005.

[114] J. L. Jankowsky, L. H. Younkin, V. Gonzales, D. J. Fadale, H. H. Slunt, H. a. Lester, S. G. Younkin, and D. R. Borchelt. Rodent Aβ modulates the solubility and distribution of amyloid deposits in transgenic mice. *J. Biol. Chem.*, 282(31):22707–22720, 2007.

[115] M. Johnstone, A. J. Gearing, and K. M. Miller. A central role for astrocytes in the inflammatory response to beta-amyloid; chemokines, cytokines and reactive oxygen species are produced. *J. Neuroimmunol.*, 93(1-2):182–93, jan 1999.

[116] T. Jonsson, H. Stefansson, S. Steinberg, I. Jonsdottir, P. V. Jonsson, J. Snaedal, S. Bjornsson, J. Huttenlocher, A. I. Levey, J. J. Lah, D. Rujescu, H. Hampel, I. Giegling, O. A. Andreassen, K. Engedal, I. Ulstein, S. Djurovic, C. Ibrahim-Verbaas, A. Hofman, M. A. Ikram, C. M. van Duijn, U. Thorsteinsdottir, A. Kong, and K. Stefansson. Variant of TREM2 Associated with the Risk of Alzheimer's Disease. *N. Engl. J. Med.*, 368(2):107–116, 2013.

[117] S. Kalifa, E. K. Polston, J. S. Allard, and K. F. Manaye. Distribution patterns of cannabinoid CB1 receptors in the hippocampus of APPswe/PS1ΔE9 double transgenic mice. *Brain Res.*, 1376:94–100, feb 2011.

[118] E. Kärkkäine, H. Tanila, and J. T. Laitinen. Functional autoradiography shows unaltered cannabinoid CB1 receptor signalling in hippocampus and cortex of APP/PS1 transgenic mice. *CNS Neurol. Disord. Drug Targets*, 11(8):1038–44, dec 2012.

[119] Y. Kawamura. The CB1 Cannabinoid Receptor Is the Major Cannabinoid Receptor at Excitatory Presynaptic Sites in the Hippocampus and Cerebellum. *J. Neurosci.*, 26(11):2991–3001, 2006.

[120] H. Kettenmann, U.-K. Hanisch, M. Noda, and A. Verkhratsky. Physiology of Microglia. *Physiol. Rev.*, 91(2):461–553, apr 2011.

[121] K. Kierdorf, D. Erny, T. Goldmann, V. Sander, C. Schulz, E. G. Perdiguero, P. Wieghofer, A. Heinrich, P. Riemke, C. Hölscher, D. N. Müller, B. Luckow, T. Brocker, K. Debowski, G. Fritz, G. Opdenakker, A. Diefenbach, K. Biber, M. Heikenwalder, F. Geissmann, F. Rosenbauer, and M. Prinz. Microglia emerge from erythromyeloid precursors via Pu.1- and Irf8-dependent pathways. *Nat. Neurosci.*, 16(3):273–280, 2013.

[122] K. A. Kigerl, J. C. Gensel, D. P. Ankeny, J. K. Alexander, D. J. Donnelly, and P. G. Popovich. Identification of two distinct macrophage subsets with divergent effects causing either neurotoxicity or regeneration in the injured mouse spinal cord. *J. Neurosci.*, 29(43):13435–13444, 2009.

[123] H. Y. Kim, H. V. Kim, D. K. Lee, S.-H. Yang, Y. Kim, P. N. Tariot, N. H. Trinh, J. Hoblyn, S. Mohanty, K. Yaffe, E. Sinforiani, L. M. Banchieri, C. Zucchella, L. Bernasconi, G. Nappi, S. Salloway, R. S. Doody, C. R. Jack, H. Y. Kim, D. Cao, H. Lu, T. L. Lewis, L. Li, J. Knowles, H. B. Guo, D. Galimberti, E. Scarpini, I. A. Lockhart, S. A. Mitchell, S. Kelly, S. R. Wray, A. Cowan, M. S. Fanselow, T. J. Tighe, R. G. Phillips, J. E. LeDoux, Z. Li, K. Herrmann, F. Pohlenz, and T. Kawarabayashi. Rapid and sustained cognitive recovery in APP/PS1 transgenic mice by co-administration of EPPS and donepezil. *Sci. Rep.*, 6:34165, oct 2016.

[124] J. Kim, J. M. Basak, and D. M. Holtzman. The role of apolipoprotein E in Alzheimer's disease. *Neuron*, 63(3):287–303, aug 2009.

[125] D. L. King and G. W. Arendash. Behavioral characterization of the Tg2576 transgenic model of Alzheimer's disease through 19 months. *Physiol. Behav.*, 75(5):627–642, apr 2002.

[126] T. Kiyota, H. E. Gendelman, R. A. Weir, E. E. Higgins, G. Zhang, and M. Jain. CCL2 affects β-amyloidosis and progressive neurocognitive dysfunction in a mouse model of Alzheimer's disease. *Neurobiol. Aging*, 34(4):1060–8, apr 2013.

[127] T. Kiyota, S. Okuyama, R. J. Swan, M. T. Jacobsen, H. E. Gendelman, and T. Ikezu. CNS expression of anti-inflammatory cytokine interleukin-4 attenuates Alzheimer's disease-like pathogenesis in APP+PS1 bigenic mice. *FASEB J.*, 24(8):3093–102, aug 2010.

[128] T. Kiyota, M. Yamamoto, H. Xiong, M. P. Lambert, W. L. Klein, H. E. Gendelman, R. M. Ransohoff, and T. Ikezu. CCL2 accelerates microglia-mediated Abeta oligomer formation and progression of neurocognitive dysfunction. *PLoS One*, 4(7):e6197, jan 2009.

[129] R. S. Klein, E. Lin, B. Zhang, A. D. Luster, J. Tollett, M. a. Samuel, M. Engle, and M. S. Diamond. Neuronal CXCL10 directs CD8+ T-cell recruitment and control of West Nile virus encephalitis. *J. Virol.*, 79(17):11457–11466, 2005.

[130] M. Kohno, H. Hasegawa, A. Inoue, M. Muraoka, T. Miyazaki, K. Oka, and M. Yasukawa. Identification of N-arachidonylglycine as the endogenous ligand for orphan G-protein-coupled receptor GPR18. *Biochem. Biophys. Res. Commun.*, 347(3):827–832, sep 2006.

[131] S. Koizumi, K. Ohsawa, K. Inoue, and S. Kohsaka. Purinergic receptors in microglia: Functional modal shifts of microglia mediated by P2 and P1 receptors. *Glia*, 61(1):47–54, 2013.

[132] J. Koppel, V. Vingtdeux, P. Marambaud, C. D'Abramo, H. Jimenez, M. Stauber, R. Friedman, and P. Davies. CB2 receptor deficiency increases amyloid pathology and alters tau processing in a transgenic mouse model of Alzheimer's disease. *Mol. Med.*, 20(1):29–36, 2014.

[133] G. Krabbe, A. Halle, V. Matyash, J. L. Rinnenthal, G. D. Eom, U. Bernhardt, K. R. Miller, S. Prokop, H. Kettenmann, and F. L. Heppner. Functional impairment of microglia coincides with Beta-amyloid deposition in mice with Alzheimer-like pathology. *PLoS One*, 8(4):e60921, 2013.

[134] S. J. Krinsky-McHale, D. A. Devenny, H. Gu, E. C. Jenkins, P. Kittler, V. V. Murty, N. Schupf, L. Scotto, B. Tycko, T. K. Urv, L. Ye, W. Zigman, and W. Silverman. Successful Aging in a 70-Year-Old Man With Down Syndrome: A Case Study. *Intellect. Dev. Disabil.*, 46(3):215–228, 2008.

[135] I. I. Kruman, R. P. Wersto, F. Cardozo-Pelaez, L. Smilenov, S. L. Chan, F. J. Chrest, R. Emokpae, M. Gorospe, and M. P. Mattson. Cell Cycle Activation Linked to Neuronal Cell Death Initiated by DNA Damage. *Neuron*, 41(4):549–561, 2004.

[136] I. V. Kurochkin. Insulin-degrading enzyme: embarking on amyloid destruction. *Trends Biochem. Sci.*, 26(7):421–5, jul 2001.

[137] M. Kurt, D. Davies, M. Kidd, K. Duff, S. Rolph, K. Jennings, and D. Howlett. Neurodegenerative Changes Associated with β-Amyloid Deposition in the Brains of Mice Carrying Mutant Amyloid Precursor Protein and Mutant Presenilin-1 Transgenes. *Exp. Neurol.*, 171(1):59–71, 2001.

[138] C. Laske, E. Stransky, N. Hoffmann, W. Maetzler, G. Straten, G. W. Eschweiler, and T. Leyhe. Macrophage colony-stimulating factor (M-CSF) in plasma and CSF of patients with mild cognitive impairment and Alzheimer's disease. *Curr. Alzheimer Res.*, 7(5):409–14, aug 2010.

[139] J. E. Lauckner, J. B. Jensen, H.-Y. Chen, H.-C. Lu, B. Hille, and K. Mackie. GPR55 is a cannabinoid receptor that increases intracellular calcium and inhibits M current. *Proc. Natl. Acad. Sci. U. S. A.*, 105(7):2699–704, feb 2008.

[140] B. Laursen, A. Mørk, N. Plath, U. Kristiansen, and J. F. Bastlund. Cholinergic degeneration is associated with increased plaque deposition and cognitive impairment in APPswe/PS1dE9 mice. *Behav. Brain Res.*, 240:146–152, 2013.

[141] T. Lawrence and G. Natoli. Transcriptional regulation of macrophage polarization: enabling diversity with identity. *Nat. Rev. Immunol.*, 11(11):750–761, 2011.

[142] E. Levy-lahad, W. Wasco, P. Poorkaj, D. M. Romano, J. Oshima, W. H. Pettingell, C.-e. Yu, P. D. Jondro, S. D. Schmidt, K. Wang, A. C. Crowley, Y.-h. Fu, S. Y. Guenette, D. Galas, E. Nemens, E. M. Wijsman, T. D. Bird, G. D. Schellenberg, and R. E. Tanzi. Candidate Gene for the Chromosome 1 Familial Alzheimer ' s Disease Locus. *Science (80-.).*, 269:973–977, 1995.

[143] Y. Li and J. Kim. Neuronal expression of CB2 cannabinoid receptor mRNAs in the mouse hippocampus. *Neuroscience*, 311(October):253–267, dec 2015.

[144] Y. Li and J. Kim. CB2 Cannabinoid Receptor Knockout in Mice Impairs Contextual Long-Term Memory and Enhances Spatial Working Memory. *Neural Plast.*, 2016:1–14, dec 2016.

[145] S. Liebscher and M. Meyer-Luehmann. A peephole into the brain: Neuropathological features of Alzheimer's disease revealed by in vivo two-photon imaging. *Front. Psychiatry*, 3(APR):1–11, 2012.

[146] G. P. Lim, F. Yang, T. Chu, P. Chen, W. Beech, B. Teter, T. Tran, O. Ubeda, K. H. Ashe, S. A. Frautschy, and G. M. Cole. Ibuprofen suppresses plaque pathology and inflammation in a mouse model for Alzheimer's disease. *J. Neurosci.*, 20(15):5709–14, aug 2000.

[147] Q.-R. Q.-R. Liu, C.-H. C.-H. Pan, A. Hishimoto, C.-Y. C.-Y. Li, Z.-X. Z.-X. Xi, A. Llorente-Berzal, M.-P. M.-P. Viveros, H. Ishiguro, T. Arinami, E. S. Onaivi, and G. R. Uhl. Species differences in cannabinoid receptor 2 (CNR2 gene): identification of novel human and rodent CB2 isoforms, differential tissue expression and regulation by cannabinoid receptor ligands. *Genes. Brain. Behav.*, 8(5):519–30, jul 2009.

[148] K. J. Livak and T. D. Schmittgen. Analysis of Relative Gene Expression Data Using Real-Time Quantitative PCR and the 2-$\Delta\Delta$CT Method. *Methods*, 25(4):402–408, dec 2001.

[149] J. Löffler and G. Huber. Beta-amyloid precursor protein isoforms in various rat brain regions and during brain development. *J. Neurochem.*, 59(4):1316–24, 1992.

[150] A. London, M. Cohen, and M. Schwartz. Microglia and monocyte-derived macrophages: functionally distinct populations that act in concert in CNS plasticity and repair. *Front. Cell. Neurosci.*, 7(April):34, 2013.

[151] J. D. Luterman, V. Haroutunian, S. Yemul, L. Ho, D. Purohit, P. S. Aisen, R. Mohs, and G. M. Pasinetti. Cytokine gene expression as a function of the clinical progression of Alzheimer disease dementia. *Arch. Neurol.*, 57(8):1153–1160, 2000.

[152] T. Ma, M. A. Trinh, A. J. Wexler, C. Bourbon, E. Gatti, P. Pierre, D. R. Cavener, and E. Klann. Suppression of eIF2α kinases alleviates Alzheimer's disease–related plasticity and memory deficits. *Nat. Neurosci.*, 16(9):1299–1305, aug 2013.

[153] D. J. Mahad and R. M. Ransohoff. The role of MCP-1 (CCL2) and CCR2 in multiple sclerosis and experimental autoimmune encephalomyelitis (EAE), 2003.

[154] P. Mai, L. Tian, L. L. Yang, L. Wang, L. L. Yang, and L. Li. Cannabinoid receptor 1 but not 2 mediates macrophage phagocytosis by G(α)i/o /RhoA/ROCK signaling pathway. *J. Cell. Physiol.*, 230(7):1640–50, jul 2015.

[155] A. Mantovani, A. Sica, S. Sozzani, P. Allavena, A. Vecchi, and M. Locati. The chemokine system in diverse forms of macrophage activation and polarization. *Trends Immunol.*, 25(12):677–86, dec 2004.

[156] I. Manuel, E. G. de San Román, M. T. Giralt, I. Ferrer, and R. Rodríguez-Puertas. Type-1 Cannabinoid Receptor Activity During Alzheimer's Disease Progression. *J. Alzheimers. Dis.*, 2014.

[157] N. Maroof, S. Ravipati, M. C. Pardon, D. a. Barrett, and D. a. Kendall. Reductions in Endocannabinoid Levels and Enhanced Coupling of Cannabinoid Receptors in the Striatum are Accompanied by Cognitive Impairments in the AβPPswe/PS1ΔE9 Mouse Model of Alzheimer's Disease. *J. Alzheimers. Dis.*, 42(1):227–45, jan 2014.

[158] G. Marsicano, S. Goodenough, K. Monory, H. Hermann, M. Eder, A. Cannich, S. C. Azad, M. G. Cascio, S. O. Gutiérrez, M. van der Stelt, M. L. López-Rodriguez, E. Casanova, G. Schütz, W. Zieglgänsberger, V. Di Marzo, C. Behl, and B. Lutz. CB1 cannabinoid receptors and on-demand defense against excitotoxicity. *Science*, 302(5642):84–88, 2003.

[159] A. M. Martín-Moreno, B. Brera, C. Spuch, E. Carro, L. García-García, M. Delgado, M. a. Pozo, N. G. Innamorato, A. Cuadrado, M. L. de Ceballos, and M. L. D. Ceballos. Prolonged oral cannabinoid administration prevents neuroinflammation, lowers β-amyloid levels and improves cognitive performance in Tg APP 2576 mice. *J. Neuroinflammation*, 9(1):8, jan 2012.

[160] F. O. Martinez, A. Sica, A. Mantovani, and M. Locati. Macrophage activation and polarization. *Front. Biosci. a J. virtual Libr.*, 13(4):453–461, 2008.

[161] V. D. Marzo, N. Stella, A. Zimmer, V. Di Marzo, N. Stella, and A. Zimmer. Endocannabinoid signalling and the deteriorating brain. *Nat. Rev. Neurosci.*, 16(1):30–42, dec 2014.

[162] S. B. Matousek, S. Ghosh, S. S. Shaftel, S. Kyrkanides, J. A. Olschowka, and M. K. O'Banion. Chronic IL-1β-mediated neuroinflammation mitigates amyloid pathology in a mouse model of Alzheimer's disease without inducing overt neurodegeneration. *J. Neuroimmune Pharmacol.*, 7(1):156–64, mar 2012.

[163] L. a. Matsuda, S. J. Lolait, M. J. Brownstein, a. C. Young, and T. I. Bonner. Structure of a cannabinoid receptor and functional expression of the cloned cDNA. *Nature*, 346(6284):561–564, 1990.

[164] C. Mazzola, V. Micale, and F. Drago. Amnesia induced by β-amyloid fragments is counteracted by cannabinoid CB1 receptor blockade. *Eur. J. Pharmacol.*, 477(3):219–225, sep 2003.

[165] P. L. McGeer, E. McGeer, J. Rogers, and J. Sibley. Anti-inflammatory drugs and Alzheimer disease. *Lancet (London, England)*, 335(8696):1037, apr 1990.

[166] P. L. McGeer and E. G. McGeer. NSAIDs and Alzheimer disease: Epidemiological, animal model and clinical studies. *Neurobiol. Aging*, 28:639–647, 2007.

[167] P. L. McGeer, M. Schulzer, and E. G. McGeer. Arthritis and anti-inflammatory agents as possible protective factors for Alzheimer's disease: A review of 17 epidemiologic studies. *Neurology*, 47(2):425–432, aug 1996.

[168] D. McHugh, S. S. J. Hu, N. Rimmerman, A. Juknat, Z. Vogel, J. M. Walker, and H. B. Bradshaw. N-arachidonoyl glycine, an abundant endogenous lipid, potently drives directed cellular migration through GPR18, the putative abnormal cannabidiol receptor. *BMC Neurosci.*, 11:44, 2010.

[169] D. McHugh, D. Roskowski, S. Xie, and H. B. Bradshaw. Δ(9)-THC and N-arachidonoyl glycine regulate BV-2 microglial morphology and cytokine release plasticity: implications for signaling at GPR18. *Front. Pharmacol.*, 4:162, 2014.

[170] M. Mecha, A. Feliú, F. Carrillo-Salinas, a. Rueda-Zubiaurre, S. Ortega-Gutiérrez, R. G. de Sola, and C. Guaza. Endocannabinoids drive the acquisition of an alternative phenotype in microglia. *Brain. Behav. Immun.*, 49:233–245, 2015.

[171] R. Mechoulam, S. Ben-Shabat, L. Hanus, M. Ligumsky, N. E. Kaminski, A. R. Schatz, A. Gopher, S. Almog, B. R. Martin, and D. R. Compton. Identification of an endogenous 2-monoglyceride, present in canine gut, that binds to cannabinoid receptors. *Biochem. Pharmacol.*, 50(1):83–90, jun 1995.

[172] A. Michelucci, T. Heurtaux, L. Grandbarbe, E. Morga, and P. Heuschling. Characterization of the microglial phenotype under specific pro-inflammatory and anti-inflammatory conditions: Effects of oligomeric and fibrillar amyloid-beta. *J. Neuroimmunol.*, 210(1-2):3–12, 2009.

[173] A. Mildner, B. Schlevogt, K. Kierdorf, C. Bottcher, D. Erny, M. P. Kummer, M. Quinn, W. Bruck, I. Bechmann, M. T. Heneka, J. Priller, and M. Prinz. Distinct and Non-Redundant Roles of Microglia and Myeloid Subsets in Mouse Models of Alzheimer's Disease. *J. Neurosci.*, 31(31):11159–11171, aug 2011.

[174] A. Mildner, H. Schmidt, M. Nitsche, D. Merkler, U.-K. Hanisch, M. Mack, M. Heikenwalder, W. Brück, J. Priller, and M. Prinz. Microglia in the adult brain arise from Ly-6ChiCCR2+ monocytes only under defined host conditions. *Nat. Neurosci.*, 10(12):1544–53, dec 2007.

[175] C. D. Mills, K. Kincaid, J. M. Alt, M. J. Heilman, and A. M. Hill. M-1/M-2 Macrophages and the Th1/Th2 Paradigm. *J. Immunol.*, 164(12):6166–6173, jun 2000.

[176] R. Morris. Developments of a water-maze procedure for studying spatial learning in the rat. *J. Neurosci. Methods*, 11(1):47–60, may 1984.

[177] R. Mrak. Interleukin-1, neuroinflammation, and Alzheimer's disease. *Neurobiol. Aging*, 22(6):903–908, 2001.

[178] R. E. Mrak and W. S. T. Griffin. Glia and their cytokines in progression of neurodegeneration. *Neurobiol. Aging*, 26(3):349–354, mar 2005.

[179] L. Mucke, E. Masliah, G. Q. Yu, M. Mallory, E. M. Rockenstein, G. Tatsuno, K. Hu, D. Kholodenko, K. Johnson-Wood, and L. McConlogue. High-level neuronal expression of abeta 1-42 in wild-type human amyloid protein precursor transgenic mice: synaptotoxicity without plaque formation. *J. Neurosci.*, 20(11):4050–4058, 2000.

[180] J. Mulder, M. Zilberter, S. J. Pasquaré, A. Alpár, G. Schulte, S. G. Ferreira, A. Köfalvi, A. M. Martín-Moreno, E. Keimpema, H. Tanila, M. Watanabe, K. Mackie, T. Hortobágyi, M. L. de Ceballos, and T. Harkany. Molecular reorganization of endocannabinoid signalling in Alzheimer's disease. *Brain*, 134(Pt 4):1041–60, apr 2011.

[181] S. Munro, K. L. Thomas, and M. Abu-Shaar. Molecular characterization of a peripheral receptor for cannabinoids. *Nature*, 365(6441):61–65, 1993.

[182] P. J. Murray, J. E. Allen, S. K. Biswas, E. A. Fisher, D. W. Gilroy, S. Goerdt, S. Gordon, J. A. Hamilton, L. B. Ivashkiv, T. Lawrence, M. Locati, A. Mantovani, F. O. Martinez, J.-L. Mege, D. M. Mosser, G. Natoli, J. P. Saeij, J. L. Schultze, K. A. Shirey, A. Sica, J. Suttles, I. Udalova, J. A. van Ginderachter, S. N. Vogel, and T. A. Wynn. Macrophage Activation and Polarization: Nomenclature and Experimental Guidelines. *Immunity*, 41(1):14–20, jul 2014.

[183] G. Naert and S. Rivest. CC chemokine receptor 2 deficiency aggravates cognitive impairments and amyloid pathology in a transgenic mouse model of Alzheimer's disease. *J. Neurosci.*, 31(16):6208–20, apr 2011.

[184] A. C. Naj, G. Jun, G. W. Beecham, L.-S. Wang, B. N. Vardarajan, J. Buros, P. J. Gallins, J. D. Buxbaum, G. P. Jarvik, P. K. Crane, E. B. Larson, T. D. Bird, B. F. Boeve, N. R. Graff-Radford, P. L. De Jager, D. Evans, J. A. Schneider, M. M. Carrasquillo, N. Ertekin-Taner, S. G. Younkin, C. Cruchaga, J. S. K. Kauwe, P. Nowotny, P. Kramer, J. Hardy, M. J.

Huentelman, A. J. Myers, M. M. Barmada, F. Y. Demirci, C. T. Baldwin, R. C. Green, E. Rogaeva, P. St George-Hyslop, S. E. Arnold, R. Barber, T. Beach, E. H. Bigio, J. D. Bowen, A. Boxer, J. R. Burke, N. J. Cairns, C. S. Carlson, R. M. Carney, S. L. Carroll, H. C. Chui, D. G. Clark, J. Corneveaux, C. W. Cotman, J. L. Cummings, C. DeCarli, S. T. DeKosky, R. Diaz-Arrastia, M. Dick, D. W. Dickson, W. G. Ellis, K. M. Faber, K. B. Fallon, M. R. Farlow, S. Ferris, M. P. Frosch, D. R. Galasko, M. Ganguli, M. Gearing, D. H. Geschwind, B. Ghetti, J. R. Gilbert, S. Gilman, B. Giordani, J. D. Glass, J. H. Growdon, R. L. Hamilton, L. E. Harrell, E. Head, L. S. Honig, C. M. Hulette, B. T. Hyman, G. A. Jicha, L.-W. Jin, N. Johnson, J. Karlawish, A. Karydas, J. A. Kaye, R. Kim, E. H. Koo, N. W. Kowall, J. J. Lah, A. I. Levey, A. P. Lieberman, O. L. Lopez, W. J. Mack, D. C. Marson, F. Martiniuk, D. C. Mash, E. Masliah, W. C. McCormick, S. M. McCurry, A. N. McDavid, A. C. McKee, M. Mesulam, B. L. Miller, C. A. Miller, J. W. Miller, J. E. Parisi, D. P. Perl, E. Peskind, R. C. Petersen, W. W. Poon, J. F. Quinn, R. A. Rajbhandary, M. Raskind, B. Reisberg, J. M. Ringman, E. D. Roberson, R. N. Rosenberg, M. Sano, L. S. Schneider, W. Seeley, M. L. Shelanski, M. A. Slifer, C. D. Smith, J. A. Sonnen, S. Spina, R. A. Stern, R. E. Tanzi, J. Q. Trojanowski, J. C. Troncoso, V. M. Van Deerlin, H. V. Vinters, J. P. Vonsattel, S. Weintraub, K. A. Welsh-Bohmer, J. Williamson, R. L. Woltjer, L. B. Cantwell, B. A. Dombroski, D. Beekly, K. L. Lunetta, E. R. Martin, M. I. Kamboh, A. J. Saykin, E. M. Reiman, D. A. Bennett, J. C. Morris, T. J. Montine, A. M. Goate, D. Blacker, D. W. Tsuang, H. Hakonarson, W. A. Kukull, T. M. Foroud, J. L. Haines, R. Mayeux, M. A. Pericak-Vance, L. A. Farrer, and G. D. Schellenberg. Common variants at MS4A4/MS4A6E, CD2AP, CD33 and EPHA1 are associated with late-onset Alzheimer's disease. *Nat. Genet.*, 43(5):436–41, 2011.

[185] Y. Nakagawa and K. Chiba. Role of microglial m1/m2 polarization in relapse and remission of psychiatric disorders and diseases. *Pharmaceuticals (Basel).*, 7(12):1028–48, 2014.

[186] D. A. Nickerson, S. L. Taylor, S. M. Fullerton, K. M. Weiss, A. G. Clark, J. H. Stengård, V. Salomaa, E. Boerwinkle, and C. F. Sing. Sequence diversity and large-scale typing of SNPs in the human apolipoprotein E gene. *Genome Res.*, 10(10):1532–45, oct 2000.

[187] C. Nilsberth, a. Westlind-Danielsson, C. B. Eckman, M. M. Condron, K. Axelman, C. Forsell, C. Stenh, J. Luthman, D. B. Teplow, S. G. Younkin, J. Näslund, and L. Lannfelt. The 'Arctic' APP mutation (E693G) causes Alzheimer's disease by enhanced Abeta protofibril formation. *Nat. Neurosci.*, 4(9):887–893, 2001.

[188] A. Nimmerjahn. Resting Microglial Cells Are Highly Dynamic Surveillants of Brain Parenchyma in Vivo. *Science (80-.).*, 308(5726):1314–1318, may 2005.

[189] R. A. Nixon and A. M. Cataldo. Lysosomal system pathways: genes to neurodegeneration in Alzheimer's disease. *J. Alzheimers. Dis.*, 9(3 Suppl):277–289, 2006.

[190] R. A. Nixon and D.-S. Yang. Autophagy failure in Alzheimer's disease—locating the primary defect. *Neurobiol. Dis.*, 43(1):38–45, jul 2011.

[191] I. Ohsawa, C. Takamura, and S. Kohsaka. The amino-terminal region of amyloid precursor protein is responsible for neurite outgrowth in rat neocortical explant culture. *Biochem. Biophys. Res. Commun.*, 236(1):59–65, 1997.

[192] J. Ojala, I. Alafuzoff, S.-K. Herukka, T. van Groen, H. Tanila, and T. Pirttilä. Expression of interleukin-18 is increased in the brains of Alzheimer's disease patients. *Neurobiol. Aging*, 30(2):198–209, feb 2009.

[193] E. S. Onaivi, H. Ishiguro, J.-P. Gong, S. Patel, A. Perchuk, P. a. Meozzi, L. Myers, Z. Mora, P. Tagliaferro, E. Gardner, A. Brusco, B. E. Akinshola, Q.-R. Liu, B. Hope, S. Iwasaki, T. Arinami, L. Teasenfitz, and G. R. Uhl. Discovery of the presence and functional expression of cannabinoid CB2 receptors in brain. *Ann. N. Y. Acad. Sci.*, 1074:514–36, aug 2006.

[194] J. N. O'Neil, P. R. Mouton, Y. Tizabi, M. A. Ottinger, D. L. Lei, D. K. Ingram, and K. F. Manaye. Catecholaminergic neuronal loss in locus coeruleus of aged female dtg APP/PS1 mice. *J. Chem. Neuroanat.*, 34:102–107, 2007.

[195] R. Orihuela, C. a. McPherson, and G. J. Harry. Microglial M1/M2 polarization and metabolic states. *Br. J. Pharmacol.*, pages 1–17, 2015.

[196] W. B. O'Shaughnessy. On the Preparations of the Indian Hemp, or gunjah*. *Prov. Med. Surg. J.*, 5(122):343–347, 1843.

[197] P. Pacher and R. Mechoulam. Is lipid signaling through cannabinoid 2 receptors part of a protective system? *Prog. Lipid Res.*, 50(2):193–211, 2011.

[198] A. Parachikova, V. Vasilevko, D. H. Cribbs, F. M. LaFerla, and K. N. Green. Reductions in amyloid-beta-derived neuroinflammation, with minocycline, restore cognition but do not significantly affect tau hyperphosphorylation. *J. Alzheimers. Dis.*, 21(2):527–42, 2010.

[199] D. a. Patten, M. Germain, M. a. Kelly, and R. S. Slack. Reactive oxygen species: Stuck in the middle of neurodegeneration. *J. Alzheimer's Dis.*, 20(SUPPL.2):S357–67, 2010.

[200] V. H. Perry. A revised view of the central nervous system microenvironment and major histocompatibility complex class II antigen presentation. *J. Neuroimmunol.*, 90(2):113–21, 1998.

[201] J. R. Piro, D. I. Benjamin, J. M. Duerr, Y. Pi, C. Gonzales, K. M. Wood, J. W. Schwartz, D. K. Nomura, and T. a. Samad. A dysregulated endocannabinoid-eicosanoid network supports pathogenesis in a mouse model of Alzheimer's disease. *Cell Rep.*, 1(6):617–23, jun 2012.

[202] A. Piyanova, E. Lomazzo, L. Bindila, R. Lerner, O. Albayram, T. Ruhl, B. Lutz, A. Zimmer, and A. Bilkei-Gorzo. Age-related changes in the endocannabinoid system in the mouse hippocampus. *Mech. Ageing Dev.*, 150:55–64, sep 2015.

[203] M. Popović, M. Caballero-Bleda, I. Kadish, and T. Van Groen. Subfield and layer-specific depletion in calbindin-D28K, calretinin and parvalbumin immunoreactivity in the dentate gyrus of amyloid precursor protein/presenilin 1 transgenic mice. *Neuroscience*, 155(1):182–191, jul 2008.

[204] J. Povova, P. Ambroz, M. Bar, V. Pavukova, O. Sery, H. Tomaskova, and V. Janout. Epidemiological of and risk factors for Alzheimer's disease: a review. *Biomed. Pap. Med. Fac. Univ. Palacky. Olomouc. Czech. Repub.*, 156(2):108–14, 2012.

[205] S. M. Prescott and P. W. Majerus. Characterization of 1,2-diacylglycerol hydrolysis in human platelets. Demonstration of an arachidonoyl-monoacylglycerol intermediate. *J. Biol. Chem.*, 258(2):764–769, 1983.

[206] M. Prinz and A. Mildner. Microglia in the CNS: immigrants from another world. *Glia*, 59(2):177–87, feb 2011.

[207] M. Prinz and J. Priller. Tickets to the brain: role of CCR2 and CX3CR1 in myeloid cell entry in the CNS. *J. Neuroimmunol.*, 224(1-2):80–4, jul 2010.

[208] M. Prinz and J. Priller. Microglia and brain macrophages in the molecular age: from origin to neuropsychiatric disease. *Nat. Rev. Neurosci.*, 15(5):300–12, may 2014.

[209] M. Prinz, J. Priller, S. S. Sisodia, and R. M. Ransohoff. Heterogeneity of CNS myeloid cells and their roles in neurodegeneration. *Nat. Neurosci.*, 13(10):1227–1235, sep 2011.

[210] R. a. Puffenbarger, a. C. Boothe, and G. a. Cabral. Cannabinoids inhibit LPS-inducible cytokine mRNA expression in rat microglial cells. *Glia*, 29(1):58–69, 2000.

[211] J. Puoliväli, J. Wang, T. Heikkinen, M. Heikkilä, T. Tapiola, T. van Groen, and H. Tanila. Hippocampal Aβ42 Levels Correlate with Spatial Memory Deficit in APP and PS1 Double Transgenic Mice. *Neurobiol. Dis.*, 9(3):339–347, 2002.

[212] L. Qin, Y. Liu, C. Cooper, B. Liu, B. Wilson, and J.-S. Hong. Microglia enhance β-amyloid peptide-induced toxicity in cortical and mesencephalic neurons by producing reactive oxygen species. *J. Neurochem.*, 83(4):973–983, nov 2002.

[213] W. Q. Qiu, D. M. Walsh, Z. Ye, K. Vekrellis, J. Zhang, M. B. Podlisny, M. R. Rosner, A. Safavi, L. B. Hersh, and D. J. Selkoe. Insulin-degrading enzyme regulates extracellular levels of amyloid beta-protein by degradation. *J. Biol. Chem.*, 273(49):32730–8, dec 1998.

[214] R. Radde, T. Bolmont, S. A. Kaeser, J. Coomaraswamy, D. Lindau, L. Stoltze, M. E. Calhoun, F. Jäggi, H. Wolburg, S. Gengler, C. Haass, B. Ghetti, C. Czech, C. Hölscher, P. M. Mathews, and M. Jucker. Abeta42-driven cerebral amyloidosis in transgenic mice reveals early and robust pathology. *EMBO Rep.*, 7(9):940–6, sep 2006.

[215] B. G. Ramírez, C. Blázquez, T. Gómez del Pulgar, M. Guzmán, and M. L. de Ceballos. Prevention of Alzheimer's disease pathology by cannabinoids: neuroprotection mediated by blockade of microglial activation. *J. Neurosci.*, 25(8):1904–13, feb 2005.

[216] R. G. Ramsay and T. J. Gonda. MYB function in normal and cancer cells. *Nat. Rev. Cancer*, 8(7):523–534, 2008.

[217] A. Rappert, K. Biber, C. Nolte, M. Lipp, A. Schubel, B. Lu, N. P. Gerard, C. Gerard, H. W. G. M. Boddeke, and H. Kettenmann. Secondary lymphoid tissue chemokine (CCL21) activates CXCR3 to trigger a Cl- current and chemotaxis in murine microglia. *J. Immunol.*, 168(7):3221–3226, 2002.

[218] L. T. Remington, A. a. Babcock, S. P. Zehntner, and T. Owens. Microglial recruitment, activation, and proliferation in response to primary demyelination. *Am. J. Pathol.*, 170(5):1713–1724, 2007.

[219] D. a. Rizzieri. MDS: Unraveling the mystery. *Blood*, 120(25):4906–4908, 2012.

[220] E. I. Rogaev, R. Sherrington, E. a. Rogaeva, G. Levesque, M. Ikeda, Y. Liang, H. Chi, C. Lin, K. Holman, and T. Tsuda. Familial Alzheimer's disease in kindreds with missense mutations in a gene on chromosome 1 related to the Alzheimer's disease type 3 gene., 1995.

[221] J. Rogers. The Inflammatory Response in Alzheimer's Disease. *J. Periodontol.*, 79(8s):1535–1543, 2008.

[222] J. Rogers, N. R. Cooper, S. Webster, J. Schultz, P. L. McGeer, S. D. Styren, W. H. Civin, L. Brachova, B. Bradt, and P. Ward. Complement activation by beta-amyloid in Alzheimer disease. *Proc. Natl. Acad. Sci. U. S. A.*, 89(November):10016–10020, 1992.

[223] L. E. Rojo, J. a. Fernández, A. a. Maccioni, J. M. Jimenez, and R. B. Maccioni. Neuroinflammation: Implications for the Pathogenesis and Molecular Diagnosis of Alzheimer's Disease. *Arch. Med. Res.*, 39(1):1–16, 2008.

[224] E. A. Romero-Sandoval, R. Horvath, R. P. Landry, and J. a. DeLeo. Cannabinoid receptor type 2 activation induces a microglial anti-inflammatory phenotype and reduces migration via MKP induction and ERK dephosphorylation. *Mol. Pain*, 5:25, may 2009.

[225] A. D. Roses. Apolipoprotein E alleles as risk factors in Alzheimer's disease. *Annu. Rev. Med.*, 47(1):387–400, feb 1996.

[226] E. B. Russo, H.-E. Jiang, X. Li, A. Sutton, A. Carboni, F. del Bianco, G. Mandolino, D. J. Potter, Y.-X. Zhao, S. Bera, Y.-B. Zhang, E.-G. Lu, D. K. Ferguson, F. Hueber, L.-C. Zhao, C.-J. Liu, Y.-F. Wang, and C.-S. Li. Phytochemical and genetic analyses of ancient cannabis from Central Asia. *J. Exp. Bot.*, 59(15):4171–4182, 2008.

[227] E. Ryberg, N. Larsson, S. Sjögren, S. Hjorth, N. O. Hermansson, J. Leonova, T. Elebring, K. Nilsson, T. Drmota, and P. J. Greasley. The orphan receptor GPR55 is a novel cannabinoid receptor. *Br. J. Pharmacol.*, 152(7):1092–1101, 2007.

[228] K. Rygiel. Novel strategies for Alzheimer's disease treatment: An overview of anti-amyloid beta monoclonal antibodies. *Indian J. Pharmacol.*, 48(6):629–636, 2016.

[229] M. Sastre, T. Klockgether, and M. T. Heneka. Contribution of inflammatory processes to Alzheimer's disease: Molecular mechanisms. *Int. J. Dev. Neurosci.*, 24(2-3):167–176, 2006.

[230] J. Saura, J. M. Tusell, and J. Serratosa. High-yield isolation of murine microglia by mild trypsinization. *Glia*, 44(3):183–189, 2003.

[231] J. R. Savinainen, S. M. Saario, and J. T. Laitinen. The serine hydrolases MAGL, ABHD6 and ABHD12 as guardians of 2-arachidonoylglycerol signalling through cannabinoid receptors. *Acta Physiol.*, 204(2):267–276, 2012.

[232] A. Savonenko, G. M. Xu, T. Melnikova, J. L. Morton, V. Gonzales, M. P. Wong, D. L. Price, F. Tang, A. L. Markowska, and D. R. Borchelt. Episodic-like memory deficits in the APPswe/PS1dE9 mouse model of Alzheimer's disease: Relationships to β-amyloid deposition and neurotransmitter abnormalities. *Neurobiol. Dis.*, 18(3):602–617, 2005.

[233] A. V. Savonenko, T. Melnikova, Y. Wang, H. Ravert, Y. Gao, J. Koppel, D. Lee, O. Pletnikova, E. Cho, N. Sayyida, A. Hiatt, J. Troncoso, P. Davies, R. F. Dannals, M. G. Pomper, and A. G. Horti. Cannabinoid CB2 Receptors in a Mouse Model of Aβ Amyloidosis: Immunohistochemical Analysis and Suitability as a PET Biomarker of Neuroinflammation. *PLoS One*, 10(6):e0129618, 2015.

[234] T. Schilling and C. Eder. Amyloid-β-induced reactive oxygen species production and priming are differentially regulated by ion channels in microglia. *J. Cell. Physiol.*, 226(12):3295–3302, dec 2011.

[235] A.-C. Schmöle, R. Lundt, S. Ternes, Ö. Albayram, T. Ulas, J. L. Schultze, D. Bano, P. Nicotera, J. Alferink, and A. Zimmer. Cannabinoid receptor 2 deficiency results in reduced neuroinflammation in an Alzheimer's disease mouse model. *Neurobiol. Aging*, 36(2):710–9, feb 2015.

[236] R. E. Schultes. Marihuana. The first twelve thousand years. *J. Ethnopharmacol.*, 5:115–116, 1982.

[237] C. Schulz, E. G. Perdiguero, L. Chorro, H. Szabo-Rogers, N. Cagnard, K. Kierdorf, M. Prinz, B. Wu, S. E. W. Jacobsen, J. W. Pollard, J. Frampton, K. J. Liu, and F. Geissmann. A Lineage of Myeloid Cells Independent of Myb and Hematopoietic Stem Cells. *Science (80-.).*, 336(6077):86–90, apr 2012.

[238] D. J. Selkoe. The Molecular Pathology of Alzheimer's Disease. *Neuron*, 6:487–498, 1991.

[239] A. Serrano-Pozo, M. L. Mielke, T. Gómez-Isla, R. a. Betensky, J. H. Growdon, M. P. Frosch, and B. T. Hyman. Reactive glia not only associates with plaques but also parallels tangles in Alzheimer's disease. *Am. J. Pathol.*, 179(3):1373–1384, 2011.

[240] K. A. Seta and R. A. Roth. Overexpression of Insulin Degrading Enzyme: Cellular Localization and Effects on Insulin Signaling. *Biochem. Biophys. Res. Commun.*, 231(1):167–171, 1997.

[241] S. S. Shaftel, W. S. T. Griffin, and M. K. O'Banion. The role of interleukin-1 in neuroinflammation and Alzheimer disease: an evolving perspective. *J. Neuroinflammation*, 5:7, 2008.

[242] S. S. Shaftel, S. Kyrkanides, J. A. Olschowka, J.-n. H. Miller, R. E. Johnson, and M. K. O. Banion. Sustained hippocampal IL-1b overexpression mediates chronic neuroinflammation and ameliorates Alzheimer plaque pathology. *J. Clin. Invest.*, 117(6), 2007.

[243] R. Sherrington, E. I. Rogaev, Y. Liang, E. a. Rogaeva, G. Levesque, M. Ikeda, H. Chi, C. Lin, G. Li, K. Holman, T. Tsuda, L. Mar, J. F. Foncin, a. C. Bruni, M. P. Montesi, S. Sorbi, I. Rainero, L. Pinessi, L. Nee, I. Chumakov, D. Pollen, A. Brookes, P. Sanseau, R. J. Polinsky, W. Wasco, H. a. Da Silva, J. L. Haines, M. a. Perkicak-Vance, R. E. Tanzi, a. D. Roses, P. E. Fraser, J. M. Rommens, and P. H. St George-Hyslop. Cloning of a gene bearing missense mutations in early-onset familial Alzheimer's disease., 1995.

[244] S. Shi, D. Liang, Y. Chen, Y. Xie, Y. Wang, L. Wang, Z. Wang, and Z. Qiao. Gx-50 reduces β-amyloid-induced TNF-α, IL-1β, NO, and PGE 2 expression and inhibits NF-κB signaling in a mouse model of Alzheimer's disease. *Eur. J. Immunol.*, 46(3):665–676, mar 2016.

[245] K. Shirotani, D. Edbauer, S. Prokop, C. Haass, and H. Steiner. Identification of distinct gamma-secretase complexes with different APH-1 variants. *J. Biol. Chem.*, 279(40):41340–41345, 2004.

[246] A. Sica and A. Mantovani. Macrophage plasticity and polarization : in vivo veritas. *J Clin Invest*, 122(3):787–795, 2012.

[247] A. R. Simard, D. Soulet, G. Gowing, J.-P. Julien, and S. Rivest. Bone marrow-derived microglia play a critical role in restricting senile plaque formation in Alzheimer's disease. *Neuron*, 49(4):489–502, 2006.

[248] M. Solas, P. T. Francis, R. Franco, and M. J. Ramirez. CB2 receptor and amyloid pathology in frontal cortex of Alzheimer's disease patients. *Neurobiol. Aging*, 34(3):805–8, mar 2013.

[249] A. Spooren, K. Kolmus, G. Laureys, R. Clinckers, J. De Keyser, G. Haegeman, and S. Gerlo. Interleukin-6, a mental cytokine. *Brain Res. Rev.*, 67(1-2):157–183, jun 2011.

[250] B. M. Stein, S. Keshav, N. Harris, and S. Gordon. Interleukin 4 Potently Enhances Murine Macrophage Mannose Receptor Activity: A Marker of Alternative Immunologic Macrophage Activation By Michael Stein, Satish Keshav, Neil Harris,* and Siamon Gordon. *J. Exp. Med.*, 176(July):287–292, 1992.

[251] R. a. Stelzmann, H. N. Schnitzlein, and F. R. Murtagh. An English translation of Alzheimer's 1907 paper, 'uber eine eigenartige erkankung der hirnrinde'. *Clin. Anat.*, 8(6):429–431, 1995.

[252] A. Stempel, A. Stumpf, H.-Y. Zhang, T. Özdoğan, U. Pannasch, A.-K. Theis, D.-M. Otte, A. Wojtalla, I. Rácz, A. Ponomarenko, Z.-X. Xi, A. Zimmer, and D. Schmitz. Cannabinoid Type 2 Receptors Mediate a Cell Type-Specific Plasticity in the Hippocampus. *Neuron*, 90(4):795–809, 2016.

[253] T. Sugiura, S. Kondo, A. Sukagawa, S. Nakane, A. Shinoda, K. Itoh, A. Yamashita, and K. Waku. 2-Arachidonoylglycerol: a possible endogenous cannabinoid receptor ligand in brain. *Biochem. Biophys. Res. Commun.*, 215(1):89–97, oct 1995.

[254] I. Svízenská, P. Dubový, and A. Sulcová. Cannabinoid receptors 1 and 2 (CB1 and CB2), their distribution, ligands and functional involvement in nervous system structures–a short review. *Pharmacol. Biochem. Behav.*, 90(4):501–11, oct 2008.

[255] R. H. Swerdlow, J. M. Burns, and S. M. Khan. The Alzheimer's disease mitochondrial cascade hypothesis: Progress and perspectives. *Biochim. Biophys. Acta - Mol. Basis Dis.*, 1842(8):1219–1231, aug 2014.

[256] R. H. Swerdlow and S. M. Khan. A "mitochondrial cascade hypothesis" for sporadic Alzheimer's disease. *Med. Hypotheses*, 63(1):8–20, jan 2004.

[257] H. Takahashi, I. Brasnjevic, B. P. F. Rutten, N. Van Der Kolk, D. P. Perl, C. Bouras, H. W. M. Steinbusch, C. Schmitz, P. R. Hof, and D. L. Dickstein. Hippocampal interneuron loss in an APP/PS1 double mutant mouse and in Alzheimer's disease. *Brain Struct. Funct.*, 214(2-3):145–160, mar 2010.

[258] P. Thériault, A. ElAli, and S. Rivest. The dynamics of monocytes and microglia in Alzheimer's disease. *Alzheimers. Res. Ther.*, 7(1):1–10, 2015.

[259] R. M. Tolón, E. Núñez, M. R. Pazos, C. Benito, A. I. Castillo, J. A. Martínez-Orgado, and J. Romero. The activation of cannabinoid CB2 receptors stimulates in situ and in vitro beta-amyloid removal by human macrophages. *Brain Res.*, 1283:148–154, aug 2009.

[260] Y. Tomidokoro, Y. Harigaya, E. Matsubara, M. Ikeda, T. Kawarabayashi, T. Shirao, K. Ishiguro, K. Okamoto, S. G. Younkin, and M. Shoji. Brain Ab amyloidosis in APPsw mice induces accumulation of presenilin-1 and tau. *J. Pathol.*, 194(4):500–506, 2001.

[261] T. Town, V. Nikolic, and J. Tan. The microglial "activation" continuum: from innate to adaptive responses. *J. Neuroinflammation*, 2:24, oct 2005.

[262] M.-E. Tremblay, B. Stevens, a. Sierra, H. Wake, a. Bessis, and a. Nimmerjahn. The Role of Microglia in the Healthy Brain. *J. Neurosci.*, 31(45):16064–16069, nov 2011.

[263] P. R. Turner, K. O'Connor, W. P. Tate, and W. C. Abraham. Roles of amyloid precursor protein and its fragments in regulating neural activity, plasticity and memory. *Prog. Neurobiol.*, 70(1):1–32, 2003.

[264] M. Uchigashima, M. Narushima, M. Fukaya, I. Katona, M. Kano, and M. Watanabe. Subcellular arrangement of molecules for 2-arachidonoyl-glycerol-mediated retrograde signaling and its physiological contribution to synaptic modulation in the striatum. *J. Neurosci.*, 27(14):3663–3676, 2007.

[265] E. A. van der Wal, F. Gómez-Pinilla, and C. W. Cotman. Transforming growth factor-beta 1 is in plaques in Alzheimer and Down pathologies. *Neuroreport*, 4(1):69–72, 1993.

[266] D. van Rossum and U. K. Hanisch. Microglia. *Metab Brain Dis*, 19(3-4):393–411, 2004.

[267] D. K. Vassilatis, J. G. Hohmann, H. Zeng, F. Li, J. E. Ranchalis, M. T. Mortrud, A. Brown, S. S. Rodriguez, J. R. Weller, A. C. Wright, J. E. Bergmann, and G. A. Gaitanaris. The G protein-coupled receptor repertoires of human and mouse. *Proc. Natl. Acad. Sci. U. S. A.*, 100(8):4903–8, apr 2003.

[268] K. Vekrellis, Z. Ye, W. Q. Qiu, D. Walsh, D. Hartley, V. Chesneau, M. R. Rosner, and D. J. Selkoe. Neurons regulate extracellular levels of amyloid beta-protein via proteolysis by insulin-degrading enzyme. *J. Neurosci.*, 20(5):1657–65, mar 2000.

[269] S. Vepsäläinen, M. Hiltunen, S. Helisalmi, J. Wang, T. van Groen, H. Tanila, and H. Soininen. Increased expression of Aβ degrading enzyme IDE in the cortex of transgenic mice with Alzheimer's disease-like neuropathology. *Neurosci. Lett.*, 438(2):216–220, jun 2008.

[270] D. Vernet, J. J. Bonavera, R. S. Swerdloff, N. F. Gonzalez-Cadavid, and C. Wang. Spontaneous Expression of Inducible Nitric Oxide Synthase in the Hypothalamus and Other Brain Regions of Aging Rats ¹. *Endocrinology*, 139(7):3254–3261, jul 1998.

[271] L. Verret, E. O. Mann, G. B. Hang, A. M. Barth, I. Cobos, K. Ho, N. Devidze, E. Masliah, A. C. Kreitzer, I. Mody, L. Mucke, and J. J. Palop. Inhibitory Interneuron Deficit Links Altered Network Activity and Cognitive Dysfunction in Alzheimer Model. *Cell*, 149(3):708–721, apr 2012.

[272] J. Vinet, H. R. van Weering, A. Heinrich, R. E. Kalin, A. Wegner, N. Brouwer, F. L. Heppner, N. van Rooijen, H. W. Boddeke, and K. Biber. Neuroprotective function for ramified microglia in hippocampal excitotoxicity. *J. Neuroinflammation*, 9(1):27, jan 2012.

[273] J. Wan, A. K. Y. Fu, F. C. F. Ip, H.-K. Ng, J. Hugon, G. Page, J. H. Wang, K.-O. Lai, Z. Wu, and N. Y. Ip. Tyk2/STAT3 signaling mediates beta-amyloid-induced neuronal cell death: implications in Alzheimer's disease. *J. Neurosci.*, 30(20):6873–6881, 2010.

[274] S. Wang, R. Wang, L. Chen, D. A. Bennett, D. W. Dickson, and D.-S. Wang. Expression and functional profiling of neprilysin, insulin-degrading enzyme, and endothelin-converting enzyme in prospectively studied elderly and Alzheimer's brain. *J. Neurochem.*, 115(1):47–57, oct 2010.

[275] K. Westin, P. Buchhave, H. Nielsen, L. Minthon, S. Janciauskiene, and O. Hansson. CCL2 Is Associated with a Faster Rate of Cognitive Decline during Early Stages of Alzheimer's Disease. *PLoS One*, 7(1):e30525, jan 2012.

[276] T. M. Westlake, a. C. Hewlett, T. I. Bonner, L. a. Matsuda, and M. Herkenham. Cannabinoid receptor binding and messenger RNA expression in human brain: An in vitro receptor autoradiography and in situ hybridization histochemistry study of normal aged and Alzheimer's brains. *Neuroscience*, 63(3):637–652, 1994.

[277] K. S. Williamson, S. P. Gabbita, S. Mou, M. West, Q. N. Pye, W. R. Markesbery, R. V. Cooney, P. Grammas, U. Reimann-Philipp, R. a. Floyd, and K. Hensley. The nitration product 5-nitro-gamma-tocopherol is increased in the Alzheimer brain. *Nitric Oxide*, 6(2):221–7, 2002.

[278] O. Wirths, H. Breyhan, A. Marcello, M. C. Cotel, W. Brück, and T. a. Bayer. Inflammatory changes are tightly associated with neurodegeneration in the brain and spinal cord of the APP/PS1KI mouse model of Alzheimer's disease. *Neurobiol. Aging*, 31(5):747–757, 2010.

[279] H. M. Wisniewski, M. Barcikowska, and E. Kida. Phagocytosis of beta/A4 amyloid fibrils of the neuritic neocortical plaques. *Acta Neuropathol.*, 81(5):588–590, 1991.

[280] K. E. Wisniewski, H. M. Wisniewski, and G. Y. Wen. Occurrence of Neuropathological Changes and Dementia of Alzheimer ' s Disease in Down' s Syndrome. *Ann. Neurol.*, 17(3):278–282, 1985.

[281] J. Wu, B. Bie, H. Yang, J. J. Xu, D. L. Brown, and M. Naguib. Activation of the CB(2) receptor system reverses amyloid-induced memory deficiency. *Neurobiol. Aging*, 34(3):791–804, mar 2013.

[282] T. Wyss-Coray. Inflammation in Alzheimer disease: driving force, bystander or beneficial response? *Nat. Med.*, 12(09):1005–1015, nov 2006.

[283] J. Xue, S. V. Schmidt, J. Sander, A. Draffehn, W. Krebs, I. Quester, D. DeNardo, T. D. Gohel, M. Emde, L. Schmidleithner, H. Ganesan, A. Nino-Castro, M. R. Mallmann, L. Labzin, H. Theis, M. Kraut, M. Beyer, E. Latz, T. C. Freeman, T. Ulas, and J. L. Schultze. Transcriptome-Based Network Analysis Reveals a Spectrum Model of Human Macrophage Activation. *Immunity*, 40(2):274–288, 2014.

[284] M. Yamamoto, M. Horiba, J. L. Buescher, D. Huang, H. E. Gendelman, R. M. Ransohoff, and T. Ikezu. Overexpression of Monocyte Chemotactic Protein-1/CCL2 in β-Amyloid Precursor Protein Transgenic Mice Show Accelerated Diffuse β-Amyloid Deposition. *Am. J. Pathol.*, 166(5):1475–1485, may 2005.

[285] M. Yamamoto, T. Kiyota, M. Horiba, J. L. Buescher, S. M. Walsh, H. E. Gendelman, and T. Ikezu. Interferon-gamma and tumor necrosis factor-alpha regulate amyloid-beta plaque

deposition and beta-secretase expression in Swedish mutant APP transgenic mice. *Am. J. Pathol.*, 170(2):680–92, feb 2007.

[286] M. Yamanaka, T. Ishikawa, A. Griep, D. Axt, M. P. Kummer, and M. T. Heneka. PPARγ/RXRα-induced and CD36-mediated microglial amyloid-β phagocytosis results in cognitive improvement in amyloid precursor protein/presenilin 1 mice. *J. Neurosci.*, 32(48):17321–31, nov 2012.

[287] J. Yao, R. W. Irwin, L. Zhao, J. Nilsen, R. T. Hamilton, and R. D. Brinton. Mitochondrial bioenergetic deficit precedes Alzheimer's pathology in female mouse model of Alzheimer's disease. *Proc. Natl. Acad. Sci. U. S. A.*, 106(34):14670–14675, 2009.

[288] H. Yin, A. Chu, W. Li, B. Wang, F. Shelton, F. Otero, D. G. Nguyen, J. S. Caldwell, and Y. A. Chen. Lipid G protein-coupled receptor ligand identification using beta-arrestin PathHunter assay. *J. Biol. Chem.*, 284(18):12328–38, may 2009.

[289] F. Zhang and L. Jiang. Neuroinflammation in Alzheimer ' s disease. *Neuropsychiatr. Dis. Treat.*, 11:243–256, 2015.

[290] H.-Y. Zhang, M. Gao, Q.-R. Liu, G.-H. Bi, X. Li, H.-J. Yang, E. L. Gardner, J. Wu, and Z.-X. Xi. Cannabinoid CB2 receptors modulate midbrain dopamine neuronal activity and dopamine-related behavior in mice. *Proc. Natl. Acad. Sci.*, 111(46):E5007–E5015, 2014.

[291] W. Zhang, J. Hao, R. Liu, Z. Zhang, G. Lei, C. Su, J. Miao, and Z. Li. Soluble Aβ levels correlate with cognitive deficits in the 12-month-old APPswe/PS1dE9 mouse model of Alzheimer's disease. *Behav. Brain Res.*, 222(2):342–350, 2011.

[292] X. Zhu, G. Perry, P. I. Moreira, G. Aliev, A. D. Cash, K. Hirai, and M. a. Smith. Mitochondrial abnormalities and oxidative imbalance in Alzheimer disease. *J. Alzheimers. Dis.*, 9:147–153, 2006.

[293] P. M. Zygmunt, J. Petersson, D. A. Andersson, H.-h. Chuang, M. Sørgård, V. Di Marzo, D. Julius, and E. D. Högestätt. Vanilloid receptors on sensory nerves mediate the vasodilator action of anandamide. *Nature*, 400(6743):452–457, jul 1999.